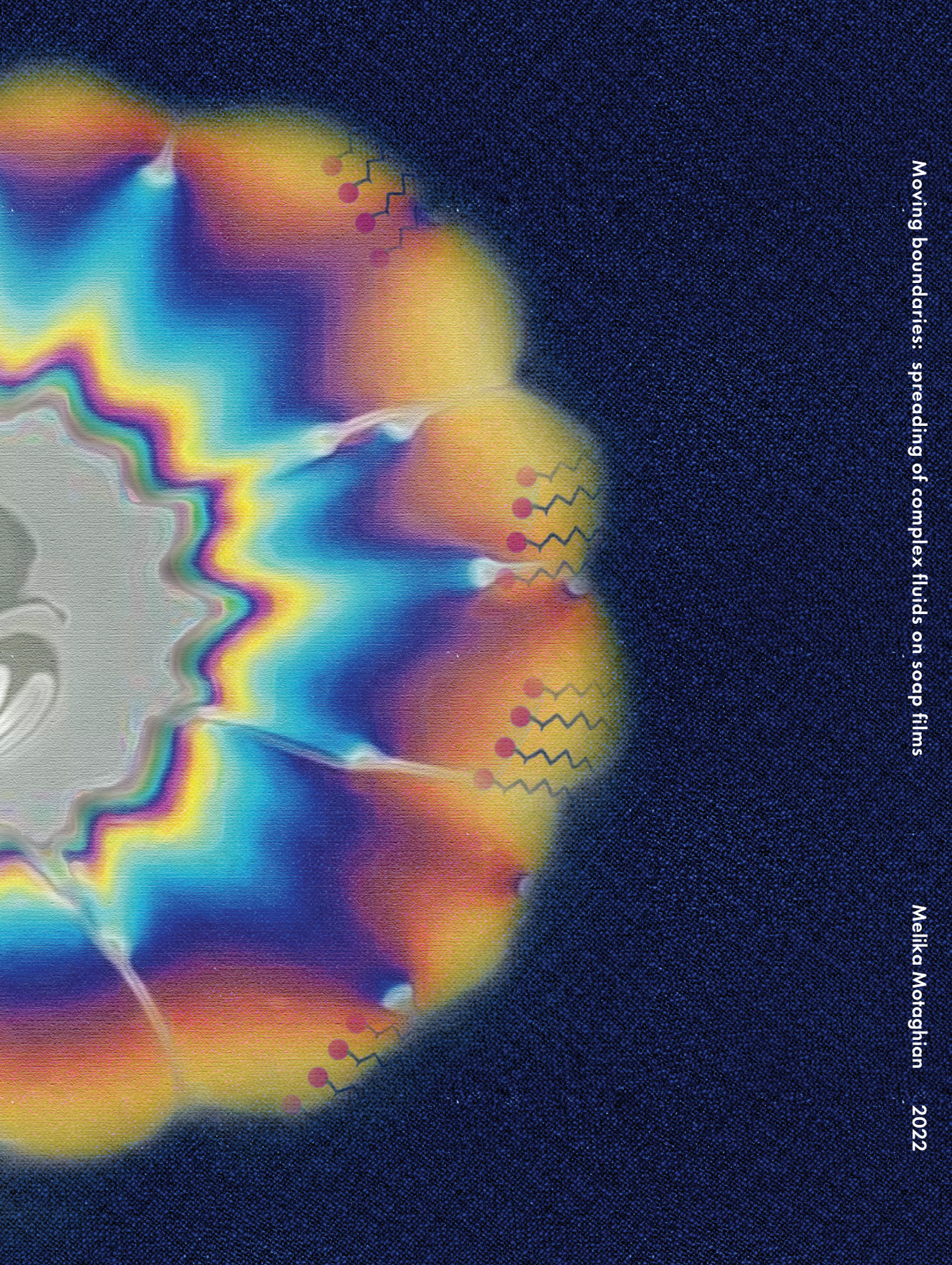

Moving boundaries: spreading of complex fluids on soap films

Melika Motaghian 2022

Moving boundaries

Spreading of complex fluids on soap films

Melika Motaghian

Propositions:

1. Tanner's law applies to spreading along liquid-liquid interfaces.
   (This thesis)

2. Elastic response of a polymeric liquid can cause symmetry breaking during the spreading of liquid film.
   (This thesis)

3. The statement "gender equality leads to economic growth" can be argued to be an extension of the work of Duflo. (E. Duflo, "Women Empowerment and Economic Development, " J. Econ. Lit., vol. 50, no. 4, pp. 1051–1079, 2012)

4. The lack of a systematic method to check the result of experimental data should have been mentioned by S. L. George and M. Buyse as a reason for endangering science. (S. L. George and M. Buyse, "Data fraud in clinical trials," *Clin. Investig. (Lond).*, vol. 5, no. 2, pp. 161–173, 2015)

5. Science, art and philosophy are evolutionary advantages to survive better.

6. Human beings are similar to quantum particles: upon observation they collapse into one of their eigen states.

7. Inaccessibility to science promotes the harmful gap that already exists between societies.

Propositions belonging to the thesis, entitled

`Moving boundaries: spreading of complex fluids on soap films´

Melika Motaghian
Wageningen, 4 July 2022

Moving boundaries

Spreading of complex fluids on soap films

Melika Motaghian

Thesis committee

Promotor

Prof. Dr. E. van der Linden
Professor of Physics and Physical Chemistry of Foods
Wageningen University & Research

Co-promotor

Dr. M. Habibi
Associate professor, Physics and Physical Chemistry of Foods
Wageningen University & Research

Other members

Prof. Dr. J. van der Gucht, Wageningen University & Research
Prof. Dr. RGM van der Sman, Wageningen University & Research
Dr. M.B.J. Meinders, Wageningen University & Research
Dr. M. Jalaal, University of Amsterdam

This research was conducted under the auspices of graduate school VLAG (Advanced Studies in Food Technology, Agrobiotechnology, Nutrition and Health Sciences).

Moving boundaries

Spreading of complex fluids on soap films

Melika Motaghian

Thesis

submitted in fulfilment of the requirements for the degree of doctor

at Wageningen University

by the authority of the Rector Magnificus,

Prof. Dr A.P.J. Mol,

in the presence of the

Thesis Committee appointed by the Academic Board

to be defended in public

on Monday 4 July 2022

at 1:30 p.m. in the Omnia Auditorium.

Melika Motaghian

Moving boundaries: spreading of complex fluids on soap films, 146 Pages.

PhD thesis, Wageningen University, Wageningen, the Netherlands (2022)

With references, with summary in English

ISBN: 978-94-6447-228-8

DOI: https://doi.org/10.18174/569736

Contents

Chapter 1

General Introduction

1.1 Surface phenomena; wetting and spreading

Our lives are full of droplets, large and small. The spreading of these droplets on various surfaces, solid or liquid, plays a vital role in many natural processes as well as numerous industrial applications[1–3]. When we breathe in, the inhaled air gets moisturized by the lining fluid that spreads over our lungs[4,5]. Water crawls up in a strong glass of wine and forms the familiar tears of wine. Hummingbird uses capillary forces to drink water[6]. Similar to plants , to take up water from the roots to the leaves on their branches. When we spray pesticides, we hope the droplets spread over the leaves to protect them instead of bouncing back and falling into the soil. On the contrary, when the raindrops hit our window pane, we would like them to roll down and not leave a water stain. Shampooing our hair and washing the dishes with soap or more subtle processes such as cleaning delicate silicon wafers or coating with high precision are a few examples of many everyday procedures which rely majorly on the wetting and spreading behavior of fluids on different surfaces. In Fig. 1.1, some of these manifestations are shown.

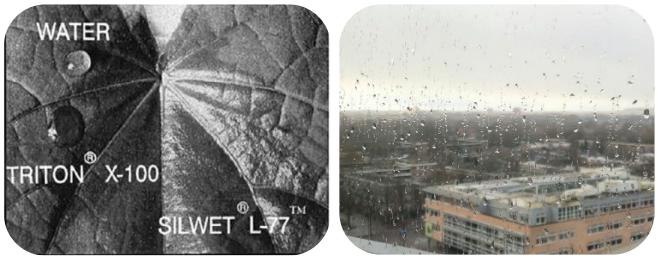

Fig. 1.1: Some manifestations of wetting and spreading phenomena in practice. Left: addition of even minute amounts of surface-active components can dramatically change the behavior of a droplet after deposition on a surface. In this picture a droplet of water is shown in comparison with two droplets containing surfactant (Triton X 100 and Silwet L77) deposited on a Lotus leaf. The droplet containing Silwet spreads and fully covers the surface, whereas droplets of water and Triton solution only show partial wetting. Courtesy of [7], copy right journal of Advances in colloid and interface science. Right: rain drops on a window.

A question that arises is how to tame the spreading behavior of liquids once they are brought into contact with other surfaces? The discipline of capillarity, which is the study of deformable interfaces between two liquids or a liquid and solid or gas, was first founded in the 19th century by Simon de Laplace

and Thomas Young. The competition between the intermolecular cohesion force between the molecules of a liquid, and the adhesion force between its molecules and the molecules of the adjacent phases, causes the interfacial tension that defines the shape and the destiny of a droplet. For instance, after deposition of a drop on a solid surface, depending on the interfacial tensions involved, three scenarios are possible: non-wetting, partial wetting, and complete wetting, which can be well predicted using Young's law[8]. In Fig. 1.2, these three scenarios and the forces at the contact line for the case of partial wetting are illustrated.

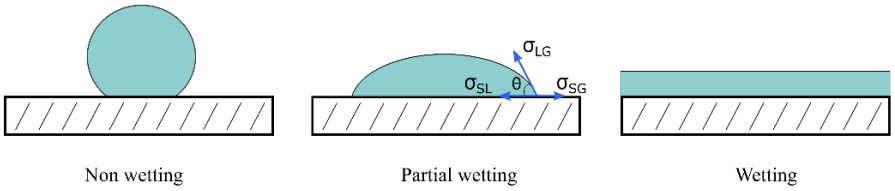

Fig. 1.2: Three possible wetting scenarios after deposition of a droplet on a solid surface. In the middle the interfacial tensions at the contact line is illustrated for partial wetting. For a stable contact line according to the Young's law $\sigma_{SG} = \sigma_{SL} + \sigma_{LG}\cos\theta$, where the σ_{SG} is the solid-gas surface tension σ_{SL} and σ_{LG} are the interfacial tensions between the liquid and the solid and air, respectively.

Near a century later, Zisman studied the interaction of various alkaline and solid surfaces to define the onset of complete wetting[9]. A decade later, in the 1970s, Tanner, an aerospace engineer, studied the wetting scenario and the forces governing the spreading of liquids on solid surfaces and modeled the spreading dynamics[10]. In parallel, the spreading along the liquid-liquid interfaces was also the center of scientists' attention, in particular, with the pioneering work of Marangoni, explaining the surface flows in fluids due to the gradient of surface tension. When he was experimenting with different fluids at Tuileries gardens in Paris, he noticed that when two liquids are brought into contact, the one with the lower surface tension spreads and covers the surface. It is energetically more favorable for a system to have a surface with lower surface tension, he explained. In the following decades, the influence of several factors on the spreading along liquid-liquid interfaces was

thoroughly investigated, including viscosity[11], miscibility/immiscibility[12], depth of the liquid[13] substrate and the presence of surface-active agents[14].

Although the scientific endeavors in the past century have shed light on many aspects of the spreading phenomenon, the diversity of the influential parameters and the various system conditions have impeded a comprehensive view in many cases, especially the spreading of complex fluids. Hence, the field of spreading and wetting is still a developing field, nowadays with a focus on bridging the gap between the simplified lab systems and complicated real-life problems. In practice, fluids are often multi-component, containing molecules of different sizes and different chemical compositions. The presence of multiple components in a liquid can influence its spreading behavior from two aspects; firstly, the intermolecular interactions in a liquid can influence the liquid's bulk properties, such as viscosity and viscoelasticity, and consequently affect the flow behavior of the solution. Secondly, the interaction of each component with the neighboring surfaces can significantly influence the interfacial tension, which in turn alters the spreading dynamics.

In this thesis, we have employed a unique geometry to study the spreading behavior of various fluids. In our experimental set-up, we deposit a droplet of multi-component liquid on a soap film and study the following spreading behavior using a high-speed camera. In **Chapter 2**, we provide pieces of evidence that after the deposition, the droplet does not stay on the top of the soap film but forms a new film in the center of the initial film and spreads. Thereby, this specific geometry allows us to minimize the contact area between the droplet and the adjacent phases (i.e., the soap film) to only a circular rim, placing the focus only on the spreading behavior of the droplet. One should note that in the time scales of our experiments, even for the slowest cases, the Péclet number (a dimensionless number calculated from the ratio of the advection rate to diffusion rate in a desired system) was orders of magnitude larger than 1, hence the effect of diffusion between the droplet and the soap film could be neglected.

Furthermore, in this scenario, because the droplet is suspended in the air and is not constrained by fixed boundaries, it is not subject to high shear forces induced by no-slip boundary conditions. In the absence of strong shear viscous forces, retarding the driving force of the surface tension gradient, of course, the spreading can being accelerated further. As such, mainly in **Chapter 2** and **Chapter 3**, we have observed notably faster spreading dynamics compared to what has been reported in previous studies for similar spreading liquids. In these cases, we were able to observe the unleashed effect of inertia in the spreading problem, which to the best of our knowledge, was not studied before.

In the schematic presented in Fig. 1.3, the cross-section view of the position of the droplet and the soap film in our experimental set-up is illustrated. A typical soap film is generated by dipping a concentric cylinder into a surfactant solution, then a droplet of desired liquid was gently deposited on the soap film using a glass capillary. Since in many cases the spreading was relatively fast and took place in only a few seconds, a high-speed camera was used to record the evolution of the radius of the droplet in time.

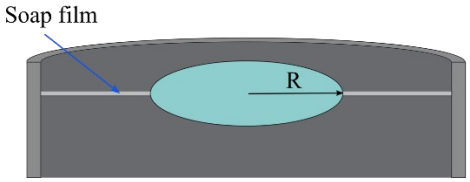

Fig. 1.3: Schematic cross section view of a droplet deposited on a soap film. In our set up the diameter of the concentric cylinder holding the soap film was 40 mm, unless otherwise stated. Thickness of the soap film was on average 12 ± 2 μm, whereas a typical droplet had initial radius of a few millimeter. Radius of the spreading, depicted with an arrow, was monitored using a high speed camera.

This set-up also provides a good medium to study the extensional flow of complex liquids, especially those containing large molecules such as polymers or proteins. The presence of the aforementioned components in a solution usually imposes a strong shear thinning behavior to the solution[15,16] which can

obscure the extensional properties. Among the current approaches to study the extensional flow of polymeric or biological solutions, two methods are more popular: microfluidic cross shape channels[17] and the neck thinning process of the liquid bridge formed between two pulled apart plates. However, each method has its own advantages and disadvantages. In the microfluidic approach, although the flow rates are very controllable and the streamlines can be visualized using microscopy, the shear-thinning effect strongly exists and need to be corrected. Additionally, the interaction of the solution with the walls of the channel can influence the flow properties. In the case of two parallel plates, the effect of solid boundaries is minimized only to the two ends of the liquid bridge, nevertheless, the extensional flow is one-dimensional and the range of applicable extensional rate is limited.

In our suggested experimental set-up, however, the two-dimensional extensional flow of a liquid sheet can be addressed and the effect of interaction with the neighboring solid or liquid surfaces is negligible. However, there are also limitations. For instance, in order to study the high extensional rates, the surface tension of the droplet needs to be considerably lower than the soap film which may require the addition of surfactants to the droplet.

1.2 Early modelling steps

The first steps towards modeling the spreading dynamics occurred in the late 1970s. Tanner[10] assumed that during the spreading of viscous droplets of silicon oil on a solid surface, the surface tension gradient as the driving force is resisted by viscous forces in the droplet. By neglecting the effect of gravity and numerically solving the Navier-Stokes equation, Tanner proved that the radius of a circular spreading droplet (R) will grow in time with a power-law manner with an exponent of 0.1 ($R \sim t^{0.1}$). His mostly theoretical work, explained the result of many previous observations[18,19] and some others that followed later[20–22]. However, many recent studies on the surfactant solutions showed some surfactants, namely super spreaders, exhibit markedly faster spreading with dynamics which do not follow Tanner's power-law model[23–

[25]. The reason behind the fast spreading of super spreaders is therefore still an open question.

Modeling of the liquid-liquid spreading, on the other hand, seemed to be even more challenging. The experimental study of the spreading of various oil droplets on different liquid baths dates back to the 1920s. Although all the studies agreed on the power-law growth of the radius of the spreading droplet, a great discrepancy could be observed in the reported spreading exponents. In 1976, Huh et. al[11] proposed the surface tension gradient should be scaled with the viscous forces resisting the spreading, both in the droplet and in the liquid substrate. In the cases that the viscosity of one of the liquids can be neglected (for instance the viscosity of the droplet compared to the liquid substrate) the scaling argument will be as follows:

$$\nabla\sigma \sim \eta \frac{\partial u_x}{\partial z} \tag{1.1}$$

where $\nabla\sigma$ is the surface tension gradient between the two liquids, η viscosity of the liquid substrate and u_x the velocity of the spreading front. Depending on the shape of the velocity profile in the viscous boundary layer, the solution of the resulting differential equation leads to power-law functions ($R \sim t^{\alpha}$) with different exponents. One of the key parameters in shaping the viscous boundary layer is the depth of the liquid substrate. In a deep bath, the velocity applied on the surface can slowly diffuse towards the solid surface at the bottom, while in a thin film a sharp linear decline will take place. The exponential decay in the first case, results[11,26] in $R \sim t^{3/4}$. while the linear decline[27] leads to $R \sim t^{1/2}$. In the schematic shown in Fig. 1.4, the viscous boundary layer in both cases is illustrated.

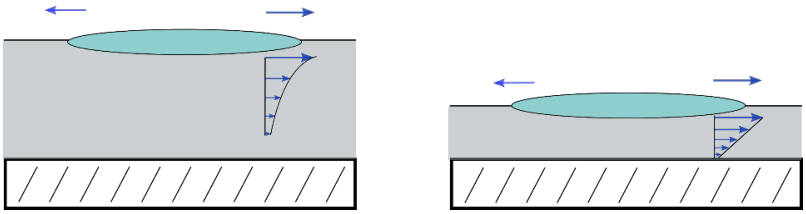

Fig. 1.4: Schematic view of a droplet spreading on deep liquid bath (left) and thin liquid substrate (right). The shape of velocity profile in the viscous boundary layer is depicted with arrows in the lower liquid phase. Liquid are considered to be immiscible and the effect of viscosity in the droplet is neglected.

Although the power-law behavior seems to be robust in many spreading problems, the exponent alpha is shown to be very sensitive to the boundary condition and geometry. Furthermore, the presence of surfactants can add to the complexity of the modeling, since their adsorption kinetics and diffusion in both phases need to be taken into account as well.

It should be noted that in these systems, the effect of viscosity cannot be neglected. Furthermore, because of the large contact area between the droplet and the lower liquid bath, in the presence of surfactants, the effect of diffusion will not be negligible. In a very recent study Doedhar et. al[28] showed that for the spreading of an oil droplet on a deep water bath, the addition of surfactant to the water bath can dramatically affect the spreading dynamics. A range of spreading exponent from 2/3 to 1, increasing by increment of the surface tension gradient, was observed. They suggested that the change of the spreading exponent is due to the transition from Laplace spreading regime, where spreading is governed by the Laplace pressure inside the droplet to the Marangoni regime, where surface tension gradient becomes the dominant governing force.

1.3 Surfactants and spreading

Surface active agents are molecules composed of a hydrophilic head group and a hydrophobic tail. When present in an aqueous medium, they travel to

the interface in order to extend their hydrophobic tail out of the water based environment. By increasing the concentration of surfactants, more and more surfactant molecules go to the interface. After saturation of the interface, increasing the concentration will result in the formation of micelles in the bulk. The critical concentration above which the micelles are being formed in the solution is known as the critical micellar concentration (CMC)[29]. The presence of surfactants at the interface, lowers the interfacial tension and facilitates the spreading. However, above the CMC, increasing the concentration of surfactant leads only to an insignificant decrease of the surface tension of the solution. The value of the critical micellar concentration and the shape of the micelles formed in the solution depends majorly on the molecular composition of each surfactant and in particular, the size and the geometry of the hydrophobic tail and the hydrophilic head group.

Surfactants are the basic ingredients of detergents and are also used in many agricultural, pharmaceutical, hair/skincare and food products, mainly to adjust the surface properties or as emulsifiers. However, the presence of surfactants at the interface can dramatically add to the complexity of the spreading problem, especially in the processes involving rapid spreading. During the spreading, a new surface is being created. In theory, instantly after the creation of a new surface from a surfactant solution, the surface tension of the new surface is equal to the surface tension of the solvent. As time passes, the surfactant molecules travel from bulk to the interface and lower the surface tension. This process which is in most cases diffusion-driven, imparts a strong time dependency on the surface tension of the surfactant solutions, especially at short time scales (order of milliseconds). Therefore, the equilibrium values of the surface tension cannot be a good representative of the surface properties of the surfactant solutions at short timescales, in particular, for the rapid spreading problems.

Throughout this thesis, we have used the bubble pressure surface tensiometry method to measure the dynamic surface tension of our samples in time scales as short as a few milliseconds. In this method, a capillary is submerged into the bulk of a liquid (e.g. surfactant solution) to form a gas bubble, while the pressure inside the bubble is monitored using a pressure cage. By continuously

injecting gas into the bubble, the curvature of the bubble at the tip of the capillary increases (radius of the spherical cap, R, decreases). Based on the Laplace equation, for the pressure inside a bubble ($p = \frac{2\sigma}{R}$; p: the inner pressure of the bubble, σ: the surface tension of the surrounding liquid and R: radius of the bubble) by decreasing R, the pressure inside the bubble increases. The pressure reaches its maximum when the radius of the bubble equals the radius of the capillary. At this maximum pressure point, by knowing the radius of the capillary and measuring the pressure inside the bubble, using the pressure cage, the surface tension of the liquid can be calculated using the Laplace equation. By repeating the experiment at different rates, the surface tension of the liquid can be measured for bubbles of different ages. In the schematic presented in Fig. 1.5, the submerged capillary and the evolution of the gas bubble are shown. Using this method allowed us to measure the surface tension of the solutions containing surfactants at time scales comparable to the time scales of our experiments.

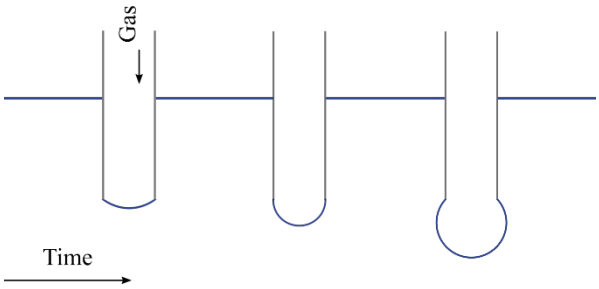

Fig. 1.5: Evolution of a gas bubble in a maximum bubble pressure surface tensiometry set up. By injecting more gas the radius of the curvature of the film at the tip of the capillary decreases until the bubble becomes a hemispherical cap with a radius equal to the radius of the capillary (middle), at this state the pressure inside the bubble reaches its maximum. By injecting more gas the pressure drops and the bubble leaves the capillary.

Although the spreading behavior of pure liquids has been studied thoroughly in the past century[14,24,28,30,31], the spreading dynamics of surfactant solutions has faced important challenges in the past decades. Rafai. et. al[32] showed that a droplet of an aqueous solution of Trisiloxane Silwet (a nonionic surfactant

commonly used in agriculture) spreads on the surface of polydimethylsiloxane (PDMS) with dynamics much faster than what Tanner proposed for spreading on the solid surfaces. Rafai reported that the radius of a droplet of Trisiloxane solution grows in time in a power-law manner, however, they observed the spreading exponent increased by increasing the concentration of the surfactants in the droplet, ranging from 0.05 to 1. Later, the mentioned rapid spreading behavior was also observed for some other surfactants such as AOT.

Compared to the spreading on solid surfaces, studying the spreading dynamics of surfactant solutions along the liquid-liquid interfaces is more challenging. In such a system the affinity of the surfactant to each phase and its adsorption mechanism in each liquid phases should be taken into account. In a recent study, Deodhar et. al[28] investigated the spreading of an oil droplet on a deep bath of surfactant solution. Interestingly they also observed that increasing the surface tension difference between the droplet and the liquid results in a range of exponents. In **Chapter 2** we observed a similar trend that by increasing the surface tension difference between the soap film and the droplet, the spreading exponent grows from 0.1 for negative values of $\Delta\sigma$ to approximately 1 for large positive$\Delta\sigma$.

Although there is an extensive body of experimental and theoretical work on the spreading of surfactant solutions, the effect of molecular interactions on the spreading dynamics in a liquid-liquid system where surfactants are present in both liquids, seems to be lacking. These systems are commonly faced in nature and industry, therefore, in **Chapter 3** of this thesis, we studied how the interaction of different surfactants at the molecular level can influence the spreading dynamics. Our experimental set-up allows us to neglect the effect of diffusion and the effect of adsorption kinetics between the two liquids, since surfactants cannot travel from one phase to another. We have kept the surface tension gradient constant and have changed the type of surfactant in the involving liquids to see how it affects the spreading dynamics. Strikingly the type of surfactant can have a considerable influence on the spreading dynamics, which is more pronounced when the surface tension gradient is not relatively large.

Our findings urge future studies to investigate the effect of the molecular structure of the surfactants on the Marangoni spreading and keep in mind that the value of the surface tension might not be fully representative of the surface properties. Furthermore, the fast decay of surface tension at the first few milliseconds should also be considered when studying rapid spreading problems.

1.4 Free surface flows and instabilities

Hydrodynamic instabilities comprise a sophisticated and essential part of fluid mechanics. To study the flow instabilities, first, one needs to delineate the boundaries of the stable state. Per definition, a system is stable if it is resistant to a small disturbance introduced to it, and if it can restore its initial state afterwards. In contrast, in unstable systems small disturbances can grow and lead to catastrophic changes in the overall state of the system and the initial state cannot be recovered naturally. Many fluid systems can undergo instabilities; opening the tap in the morning to wash our hands and see the stream of water breaking up into droplets, is maybe one of our many daily encounters to flow instabilities. Stability or instability of fluids' flow can also be very crucial in many industrial applications. For instance, in the processes involved spreading that full coverage of a surface is required (for example, printing, coating, cleaning, and oil recovery) instabilities are undesired and are needed to be prevented. On the contrary, in some microfluidic systems, turbulences can be employed to mix the liquids at microscale where a stirring mechanism cannot be available. Therefore, understanding the nature of the instabilities and the triggering parameters, is substantial to modify the resulting state of a system as it is desired.

Boundary conditions and bulk properties play essential roles in promoting or hindering flow instabilities. For the free surface flows, the surface properties of the liquid are influential in the boundary conditions. The addition of multiple components to a liquid can affect both the surface and the bulk

properties and add to the complexity of flow dynamics[33]. For instance, the presence of even minute amounts of polymers in a solution leads to a positive normal force response of the solution to an applied shear[34]. This in turn dramatically alters the breakup dynamics of the solution and triggers the formation of beads and blisters on the liquid column during the breakup. The presence of surfactants also can lead to destabilization of a spreading front of a surfactant solution on a thin liquid film.

One should note that in practice, fluids are often multi-component containing large molecules and surface-active agents. Flow behavior of these multi-component fluids is of great importance to many technological applications. In **Chapter 4** of this thesis, we have focused on the free surface spreading of such liquids containing polymers and surfactants. We observed a novel instability in the spreading of polymer-surfactant solutions when the concentration of polymer surpasses a critical level. Interestingly, in a confined system like Hele-Shaw cell this instability cannot be observed.

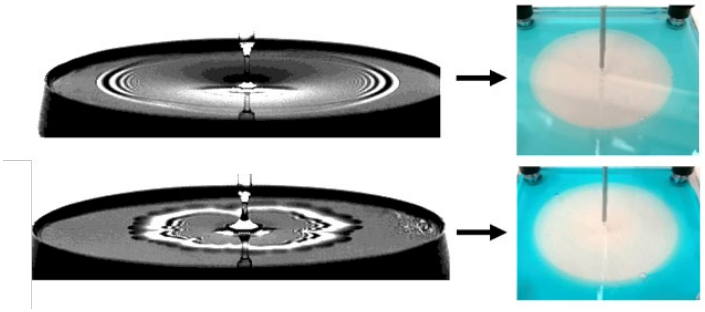

Fig 1.6: Comparison of free surface spreading of polymer-surfactant solution with its propagation in a Hele-Shaw cell. In the left column spreading of PEO-SDS solution is demonstrated on soap film, below and above critical concentration. Above the critical concentration spreading front is no longer circular. In the right column the same solutions are injected into a Hele-Sha cell prefilled with the same surfactant solution as in the soap film. Spreading front remains stable.

In Fig. 1.6 a comparison is made for both systems. For spreading on the soap films the spreading front destabilizes at high concentration of polymer whereas in a Hele-Shaw cell the same droplet propagates with a stable front at the same polymer concentration. One should note that the instabilities we

observed here are fundamentally different than Saffman-Taylor[35] instabilities as in the latter is observed when a thinner liquid is injected in a more viscous medium.

1.5 Rheology and tribology

As previously mentioned, the bulk properties of a complex liquid can significantly influence its spreading behavior. In **Chapter 5** of this thesis, we took a closer look at the interaction of polymers and surfactants and their influence on flow behavior. To do so, a rheometer equipped with a cone plate geometry was used to measure different rheological properties of the various polymer-surfactant solutions. In Fig. 1.7 (right) the schematic view of a cone plate geometry is shown. To simplify the problem polyethylene oxide (PEO) was used, which is a simple linear water soluble polymer, in combination with different surfactants. The concentration of surfactants was several times that of CMC, since we were interested in studying the interactions between micelles and the polymers, especially their influence on the entanglement of the polymers.

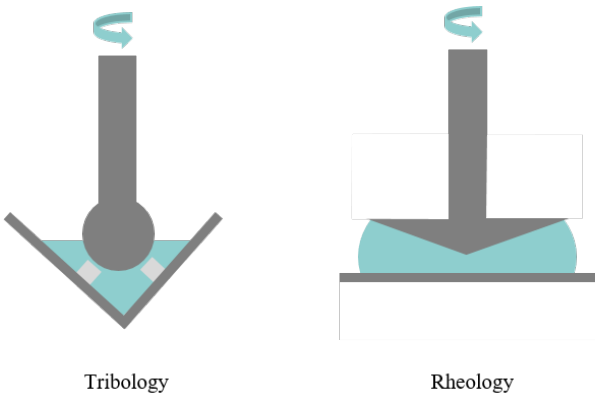

Fig. 1.7: Schematic view of a tribology set-up with ball on the pins geometry (left) and the cone-plate geometry of the rheometer.

Although the interaction of polymer surfactants has been the topic of research for decades, a comprehensive study where all rheological aspects of the polymer solutions with different surfactants could be compared seemed lacking. In **Chapter 5**, we provide a detailed and systematic rheological characterization of the polymer-surfactant samples using various methods including shear viscosity measurement to probe the shear thinning behavior, amplitude sweeps to determine the limits of the linear viscoelastic regime, small amplitude oscillatory shear (SAOS) for measuring the viscoelastic response within the linear regime and, large amplitude oscillatory shear (LAOS) for the viscoelastic response of the samples under large deformations. The large deformations are especially relevant to the spreading situation since during the spreading a droplet of liquid undergoes large deformations. To have a good overview of surfactants and the type and nature of the interactions with the polymer, we have chosen surfactants with different polarity states.

To extend our knowledge on the film formation and better understanding of polymer-surfactant solutions near surfaces, we have also studied the tribological behavior of the samples. A “ball on the pins” geometry was used to study the friction behavior of the solutions at different sliding speeds (Fig. 1.7, left). We show that when using polymer-surfactant solutions as a lubricant, the interaction of solutions with the solid surface can dominate the lubrication behavior and the affinity of the surfactants and the polymers with the solid surface, should be taken into account.

1.6 Thesis aim and out-line

In this thesis, we aim to investigate the spreading behavior of complex liquids once they are deposited on a soap film. We made use of a unique geometry, which allowed us to probe the spreading dynamics of liquids in the absence of solid or deep liquid boundaries. In this system, the spreading liquid is not subjected to high shear forces induced by no-slip boundary conditions, therefore, considerably faster dynamics can be observed compared to the

spreading on solid or liquid surfaces. Additionally, since the viscous forces are not dominant, the effect of inertia can be investigated.

Soap films can provide a good medium to study the planar spreading of various liquids. They can also be employed to create thin films of complex liquids such as polymeric solutions in less than a few milliseconds without high shearing forces, which is inevitable in methods such as electrospinning. The first step toward that goal, however, is to fully understand the mechanisms involved in the spreading on soap films. Since the configuration of "a drop on a soap" is considered novel in the field of spreading, we have dedicated this thesis to study the influence of various parameters and mechanisms governing the spreading in this geometry. Throughout the thesis, we start from simplified systems where droplets contain only surfactants, before moving towards more complicated liquids containing a high concentration of polymers and surfactants. We cover the most important influential parameters on the spreading and provide constituent models to understand and predict the effect of each parameters separately.

In **Chapter 2** we have focused on the influence of surface tension gradient on the spreading dynamics, therefore the droplets consisted of a simple surfactant solution with a viscosity similar to water. The surfactant used in the droplet and the soap film were kept the same or very similar in the molecular structure. We also studied the effect of the volume of the droplet and the size of the soap film on the spreading dynamics.

In **Chapter 3** we investigated the effect of molecular interactions between the surfactants present in the droplet and the soap film on the spreading dynamics. To do so we prepared an ensemble of liquids with similar macroscopic parameters such as viscosity (all similar to water), surface tension and volume and we only varied the type of the surfactant. Our results suggest that these microscopic interactions are not negligible especially when the surface tension gradient is not considerably large.

The effect of viscosity and viscoelasticity of polymer-surfactant solutions on the spreading dynamics is investigated in **Chapter 4**. We observed a novel hydrodynamic instability in the spreading front when the concentration of the

polymer surpassed the entanglement concentration. We explain that the enhanced elastic response of the polymeric network is in charge of the observed instability.

In **Chapter 5** we take a closer look at the influence of polymer-surfactant interactions on the rheological behavior of highly concentrated polymer-surfactant solutions. We provide a detailed overview of several rheological parameters of polymer solutions in combination with various surfactants with different ionic states. We also examined the lubrication properties of such systems.

References:

1. Bergeron, V., Bonn, D., Martin, J. Y. & Vovelle, L. Controlling droplet deposition with polymer additives. *Nature* **405**, 772–775 (2000).

2. Shahidzadeh, N. *et al.* Effect of Wetting on Gravity Drainage in Porous Media. *Transp. Porous Media* **52**, 213–227 (2003).

3. Jung, S., Hoath, S. D. & Hutchings, I. M. The role of viscoelasticity in drop impact and spreading for inkjet printing of polymer solution on a wettable surface. *Microfluid. Nanofluidics* **14**, 163–169 (2013).

4. Levy, R., Hill, D. B., Forest, M. G. & Grotberg, J. B. Pulmonary Fluid Flow Challenges for Experimental and Mathematical Modeling. *Integr. Comp. Biol.* **54**, 985–1000 (2014).

5. Bull, J. L. *et al.* Surfactant-Spreading and Surface-Compression Disturbance on a Thin Viscous Film. *J. Biomech. Eng.* **121**, 89–98 (1999).

6. Kim, W., Peaudecerf, F., Baldwin, M. W. & Bush, J. W. M. The hummingbird's tongue: a self-assembling capillary syphon. *Proc. R. Soc. B Biol. Sci.* **279**, 4990–4996 (2012).

7. Lee, K. S., Ivanova, N., Starov, V. M., Hilal, N. & Dutschk, V. Kinetics of wetting and spreading by aqueous surfactant solutions. *Adv. Colloid Interface Sci.* **144**, 54–65 (2008).

8. Young, T. III. An essay on the cohesion of fluids. *Philos. Trans. R. Soc. London* **95**, 65–87 (1805).

9. Fox, H. W. & Zisman, W. A. The spreading of liquids on low energy surfaces. I. polytetrafluoroethylene. *J. Colloid Sci.* **5**, 514–531 (1950).

10. Tanner, L. H. The spreading of silicone oil drops on horizontal surfaces. *J. Phys. D. Appl. Phys.* **12**, 1473–1484 (1979).

11. Huh, C., Inoue, M. & Mason, S. G. Uni-directional spreading of one liquid on the surface of another. *Can. J. Chem. Eng.* **53**, 367–371 (1975).

12. Roché, M. *et al.* Marangoni flow of soluble amphiphiles. *Phys. Rev. Lett.* **112**, 1–5 (2014).

13. Ewoldt, R. H., Hosoi, A. E. & McKinley, G. H. New measures for characterizing nonlinear viscoelasticity in large amplitude oscillatory shear.

J. Rheol. (N. Y. N. Y). **52**, 1427–1458 (2008).

14. Tang, X., Dong, J. & Li, X. A comparison of spreading behaviors of Silwet L-77 on dry and wet lotus leaves. *J. Colloid Interface Sci.* **325**, 223–227 (2008).

15. Ebagninin, K. W., Benchabane, A. & Bekkour, K. Rheological characterization of poly(ethylene oxide) solutions of different molecular weights. *J. Colloid Interface Sci.* **336**, 360–367 (2009).

16. Ryder, J. F. & Yeomans, J. M. Shear thinning in dilute polymer solutions. *J. Chem. Phys.* **125**, 194906 (2006).

17. Haward, S. J. Microfluidic extensional rheometry using stagnation point flow. *Biomicrofluidics* **10**, 43401 (2016).

18. Huh, C. & Scriven, L. E. Hydrodynamic model of steady movement of a solid/liquid/fluid contact line. *J. Colloid Interface Sci.* **35**, 85–101 (1971).

19. Hoffman, R. L. A study of the advancing interface. I. Interface shape in liquid—gas systems. *J. Colloid Interface Sci.* **50**, 228–241 (1975).

20. Blake, T. D. The physics of moving wetting lines. *J. Colloid Interface Sci.* **299**, 1–13 (2006).

21. Croll, A. B. & Dalnoki-Veress, K. Spreading of diblock copolymer droplets: A probe of polymer micro-rheology. *Eur. Phys. J. E* **29**, 239–244 (2009).

22. Courbin, L., Bird, J. C., Reyssat, M. & Stone, H. A. Dynamics of wetting: from inertial spreading to viscous imbibition. *J. Phys. Condens. Matter* **21**, 464127 (2009).

23. Kovalchuk, N. M., Sagisaka, M., Osaki, S. & Simmons, M. J. H. Superspreading performance of branched ionic trimethylsilyl surfactant Mg(AOTSiC)2. *Colloids Surfaces A Physicochem. Eng. Asp.* **604**, 125277 (2020).

24. Nikolov, A. D. *et al.* Superspreading driven by Marangoni flow. *Adv. Colloid Interface Sci.* **96**, 325–338 (2002).

25. Zhang, Y., Zhang, G. & Han, F. The spreading and superspeading behavior of new glucosamide-based trisiloxane surfactants on hydrophobic foliage. *Colloids Surfaces A Physicochem. Eng. Asp.* **276**, 100–106 (2006).

26. Bergeron, V. & Langevin, D. Monolayer Spreading of Polydimethylsiloxane Oil on Surfactant Solutions. *Phys. Rev. Lett.* **76**, 3152–3155 (1996).

27. Jensen, O. E. & Grotberg, J. B. Insoluble surfactant spreading on a thin viscous film: Shock evolution and film rupture. *J. Fluid Mech.* **240**, 259–288 (1992).

28. Deodhar, S., Thampi, S. P. & Basavaraj, M. G. Drops spreading on fluid surfaces: Transition from Laplace to Marangoni regime. *Phys. Rev. Fluids* **6**, 1–8 (2021).

29. Perger, T. M. & Bešter-Rogač, M. Thermodynamics of micelle formation of alkyltrimethylammonium chlorides from high performance electric conductivity measurements. *J. Colloid Interface Sci.* **313**, 288–295 (2007).

30. Afsar-Siddiqui, A. B., Luckham, P. F. & Matar, O. K. The spreading of surfactant solutions on thin liquid films. *Adv. Colloid Interface Sci.* **106**, 183–236 (2003).

31. Sharma, R. *et al.* Quasi-Immiscible Spreading of Aqueous Surfactant Solutions on Entangled Aqueous Polymer Solution Subphases. *ACS Appl. Mater. Interfaces* **5**, 5542–5549 (2013).

32. Rafaï, S., Sarker, D., Bergeron, V., Meunier, J. & Bonn, D. Superspreading: Aqueous Surfactant Drops Spreading on Hydrophobic Surfaces. *Langmuir* **18**, 10486–10488 (2002).

33. Goddard, E. D. Polymer/surfactant interaction—Its relevance to detergent systems. *J. Am. Oil Chem. Soc.* **71**, 1–16 (1994).

34. Bartolo, D., Boudaoud, A., Narcy, G. & Bonn, D. Dynamics of Non-Newtonian Droplets. *Phys. Rev. Lett.* **99**, 174502 (2007).

35. Saffman, P. G. & Taylor, G. I. The penetration of a fluid into a porous medium or Hele-Shaw cell containing a more viscous liquid. *Proc. R. Soc. London. Ser. A. Math. Phys. Sci.* **245**, 312–329 (1958).

Chapter 2

Rapid spreading of a droplet on a soap film

(This chapter has been published as: Motaghian, M, R Shirsavar, M Erfanifam, M Sabouhi, E van der Linden, H A Stone, D Bonn, and Mehdi Habibi. 2019. “Rapid Spreading of a Droplet on a Thin Soap Film.” Langmuir 35 (46): 14855–60. https://doi.org/10.1021/acs.langmuir.9b02274.)

Abstract:

We study the spreading of a droplet of surfactant solution on a thin suspended soap film as a function of dynamic surface tension and volume of the droplet. Radial growth of the leading edge (R) shows a power-law dependence on time with exponents ranging roughly from 0.1 to 1 for different surface tension differences ($\Delta\sigma$) between the film and the droplet. When the surface tension of the droplet is lower than the surface tension of the film ($\Delta\sigma>0$), we observe rapid spreading of the droplet with $R \sim t^{\alpha}$ where α ($0.4 < \alpha < 1$) is highly dependent on $\Delta\sigma$. Balance arguments assuming the spreading process is driven by Marangoni stresses versus inertial stresses yield $\alpha = 2/3$. When the surface tension difference does not favour spreading ($\Delta\sigma<0$), spreading still occurs but is slow with $0.1 < \alpha < 0.2$. This phenomenon could be used for stretching droplets in 2D and modifying thin suspended films.

2.1 Introduction

The dynamics of the spreading of a droplet over a solid or liquid surface is a phenomenon that has attracted much attention in the past decades[1,2]. Beside its relevance to many fields of technology[3,4], studying the dynamics of spreading can provide understanding of the various forces acting on an interface. It has been shown that depositing a droplet on a solid surface will initially result in the formation of a precursor film[5,6] with a molecular thickness[7], which decreases the spreading rate of the main droplet. However, Cazabat *et al*[8]. showed that spreading a droplet on a liquid substrate exhibits faster dynamics, and an even faster spreading has been observed in a drop-on-drop geometry[9].

In these previous studies on liquid-liquid spreading, the radius of the spreading front was shown to increase as a function of time according to a power law. The exponent of this power-law growth depends on physicochemical properties of both the spreading liquid and the substrate; e.g. surface energy, roughness[10], fluidity[11], miscibility[12], immiscibility[13], and the depth of the substrate for liquid substrates[8,14,15]. When capillary forces are driving the spreading of a drop on a solid substrate and inertial effects are negligible, a balance between viscous forces and capillary forces predicts a slow time evolution of the spreading front, $R \sim t^{1/10}$, known as Tanner's law[16–18].

When two different liquids are brought into contact with each other, it is often the difference in the surface tensions (Marangoni stress) that drives the spreading[19]. For spreading on a thin liquid substrate where the thickness of the film is much smaller than the radius of the spreading front, the lubrication approximation applies. Jensen *et al*[20]. have shown that when the viscous effects dominate the inertial effects, the width of a planar monolayer strip containing a fixed mass of surfactant spreads in time as $t^{1/3}$, and the radius of an axisymmetric monolayer droplet evolves as $t^{1/4}$. Numerical studies[21] also confirmed the exponent of 1/4 for spreading of a droplet on a rigid substrate.

Although spreading has been studied under various conditions, spreading a droplet on a soap film of a few micrometres thickness, suspended in the air,

hasn't been studied yet to the best of our knowledge. Here, we study a specific case of the droplet spreading on a liquid substrate: we deposit droplets of surfactant solution on a suspended thin soap film and document the spreading dynamics as a function of surface tension and droplet size using high-speed imaging. In contrast to our experimental system, thin liquid substrates studied in previous works[14] were at least a few millimetres thick, and in contact with a solid boundary, which causes significant viscous dissipation due to the no-slip boundary condition.

2.2 Material and Methods

To make a horizontal soap film, we used a concentric cylinder made of stainless steel with inner and outer diameters of 39.5 and 40.0 mm respectively. The concentric cylinder was dipped into sodium dodecyl sulphate (SDS) (Merck) solution to produce a horizontal soap film. Then a droplet of ammonium lauryl sulphate (ALS) (Fluka) solution or SDS solution was deposited on the soap film using a capillary tube. The average volume of the deposited droplets was 6±0.5 μL, although in one series of experiments, we varied the volume of the droplets to see how spreading depends on the droplet size. To vary the droplet size, capillary tubes with different diameters were used; for very small droplet sizes, the liquid was sprayed very close to the soap film. SDS solutions with molar concentrations of 0.005 M were used to make the initial soap films, and SDS solutions with concentrations of 0.005, 0.008, 0.01 and 0.02 M and ALS solutions with concentrations of 0.001, 0.002, 0.003, 0.005, 0.01, 0.04, 0.1 and 0.3 M were used for the droplets deposited on the soap film. The critical micelle concentrations (CMC) of ALS and SDS solutions at 25ºC are 0.0065 M[22] and 0.0082 M[23], respectively. For the deposited droplets, the concentrations of solutions corresponded to a range from 0.15 CMC to 46 CMC and 0.6 CMC to 2.4 CMC for ALS and SDS, respectively. Dynamic surface tensions of solutions were measured via maximum bubble pressure method using a Krüss BP50 bubble surface tensiometer. The thickness of the initial soap film was estimated indirectly from the speed of a traveling mechanical wave on the soap film using the

equation for wave speed on an elastic sheet under tension (see appendix A). After depositing an ALS droplet, the evolution of the deposited drop on the soap film was recorded using a high-speed camera (Phantom) at a rate of 4000 frames per second. To illuminate the surface of the soap film, we used a white light source with the incident and reflected angles of ~45º. The radius of the leading edge was measured by pixel counting on the frames.

2.3 Results and discussion

We focus on the spreading of a droplet on a suspended liquid film of a few microns thickness. This is different from other work on Marangoni spreading, where the minimum thickness of the liquid substrates[14] was typically about a few millimetres, and where the substrates were in contact with a solid boundary. Therefore, we expect the viscous dissipation in our system to be much smaller, which can lead to faster spreading. Furthermore, having a suspended soap film allows us to confine the liquid-liquid interface solely to a circular rim.

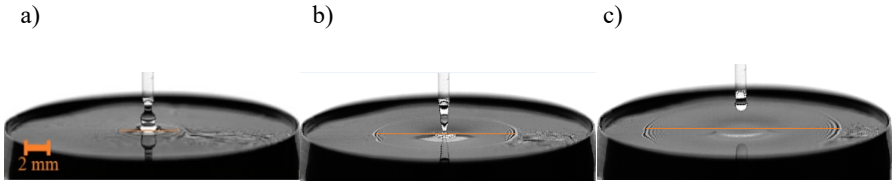

Fig. 2.1: Spreading a droplet of 0.3 M ALS on a soap film of 0.005 M SDS. Images from left to right show the instant of deposition and subsequent stretching of the droplet. From left to right, the images are taken at (a) 5, (b) 12 and (c) 24 ms after deposition.

To investigate the position of the droplet and the soap film during the course of spreading, we first made qualitative observations. Fig. 2.1 shows an example of spreading a droplet of 0.4 M ALS on a 0.005 M SDS soap film. In Fig. 2.2, spreading of a droplet of ALS 0.4 M on an SDS 0.005 M soap film is shown in which a fluorescent dye was added to the SDS solution. The sequence of images reveals that, after deposition of the droplet, a non-fluorescent circular film is formed in the centre, gradually growing and

pushing the fluorescent SDS soap film towards the edge of the container. The absence of fluorescence in the spreading film indicates that the ALS droplet is hardly contaminated by the initial soap film.

This qualitative observation is confirmed by calculating the ratio of advection rate to diffusion rate of our system. This ratio, the Peclet number, is given by $Pe=\frac{lu}{D}$ where l is a characteristic length of the system, u is the average flow velocity and D is the diffusion coefficient. By considering the size of the droplet (~1 mm) as the characteristic length, the lowest spreading speed (~0.1 m/s) and diffusion coefficient of $D\sim10^{-9}\ \mathrm{m^2 s^{-1}}$ (for a typical surfactant in water[24]), we arrive at a Peclet number significantly greater than 1, confirming that diffusion at the boundaries is negligible during the course of fast spreading.

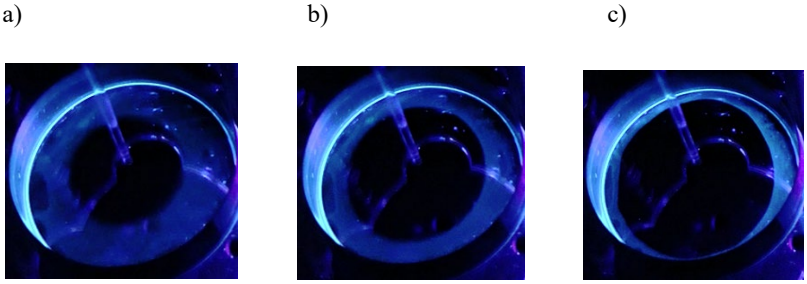

Fig. 2.2: Spreading of a droplet containing ALS 0.4 M on a soap film of SDS 0.005 M. A fluorescent dye (blue) is added to the initial SDS soap film. From left to right: the droplet (black circle) is stretched towards the edges of the container. The two liquids do not mix during spreading. From left to right images are taken at (a) 5, (b) 15 and (c) 30 ms after deposition of the droplet.

2.3.1 Effect of surface tension

Fig. 2.3 shows the dynamic surface tension for different concentrations of ALS and SDS as a function of the surface age measured using a bubble pressure surface tensiometer. To determine the effective surface tension difference ($\Delta\sigma$) between the droplets and the soap film in our experiments, we use the time-dependent data of Fig. 2.3. For the ALS droplet, we consider a characteristic time scale given by $\tau = {}^{L}/_{u}$ where u is the average speed of the spreading film and L is the maximum radius of the spreading film (~1 cm).

For the SDS substrate, in each experiment there was at least a few seconds between making the soap film and depositing the ALS droplet, therefore the surface tension of the SDS at 5 s (Fig. 2.3) is used to calculate Δσ.

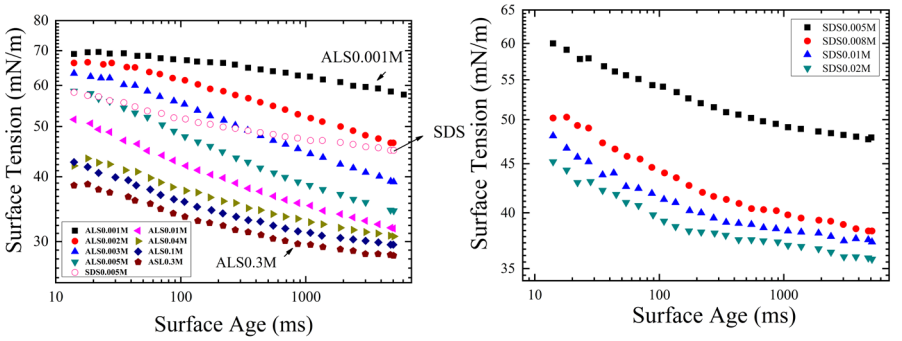

Fig. 2.3: Dynamic surface tension as a function of surface age for (left) different concentration of ALS solutions and 0.005 M SDS (open symbols) and (right) different concentrations of SDS solutions.

Taking this into account, the surface tension difference between droplets (ALS) and soap film (SDS) cover a wide range, from -19.4 mN/m for ALS 0.001 M to 6.3 mN/m for ALS 0.3 M.

In order to identify how surface tension regulates spreading, droplets with different concentrations of ALS and SDS (different surface tensions) were deposited on the soap film containing SDS 0.005 M. After the moment of deposition, the radius (R) of the leading front was measured as a function of time using high-speed imaging. The results are shown in Fig. 2.4 (left) and (right) for ALS and SDS droplets spreading on an SDS film, respectively. For the experiments where the radius of the leading front went beyond 1 cm, a cross-over regime is observed (open symbols in Fig. 2.4), probably due to boundary effects (the radius of the cylinder is 2 cm). After discarding the data points at and beyond the cross-over region, a clear power-law behaviour for R versus time is observed ($R \propto t^{\alpha}$). By fitting power-law functions to the closed-symbol data sets, we find exponents α ranging from 0.11 to 0.9 for different surface tension differences (Fig. 2.5 left). Power-law growth of

spreading fronts has been observed in many other spreading phenomena[8,12,14,25].

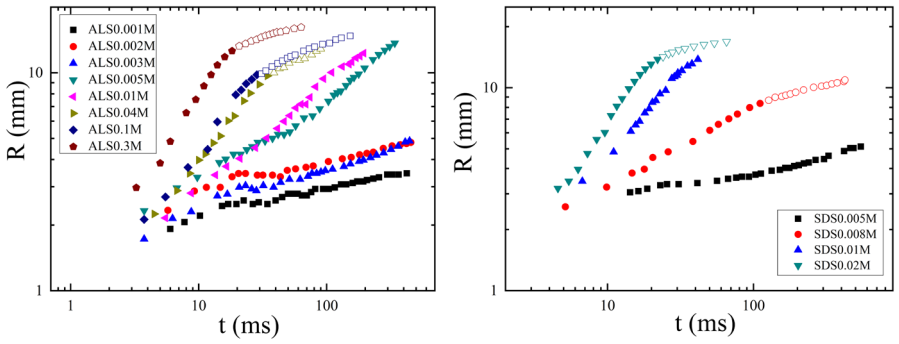

Fig. 2.4: Spreading radius versus time for droplets of (left) ALS and (right) SDS with different concentrations on a soap film of 0.005 M SDS. The open symbols show the cross-over regime due to the boundary effects. Error bars are smaller than the size of the symbols.

For droplets with low concentrations of ALS, where the surface tension of the droplets is larger than or equal to the surface tension of the soap film ($\Delta\sigma \leq 0$), a slow spreading regime was observed. Here the surface tension difference is not favourable for the spreading as the new stretched liquid film has a higher surface tension than the original film. For deposited droplets of ALS 0.001, 0.002, and 0.003 M, for which $\Delta\sigma$ = -19.4, -10.7, -3 mN/m, respectively, we obtain power-law exponents of 0.12±0.04, 0.14±0.04 and 0.19± 0.04, respectively (Fig. 2.5 left).

Fig. 2.6 shows the situation when the droplet and soap film are of the same composition and concentration: SDS 0.005 M. After deposition of the droplet, it forms a lens and spreads slowly (black squares in Fig. 2.4 right panel) with a power-law time dependence and an exponent of 0.15±0.04. This is in contrast with an earlier experimental work by Aarts *et al*[26]. for a three-dimensional configuration where coalescence of two droplets of the same liquid was studied and a linear dependence of radius on time (for early times) was measured, although the current work considers a system with surfactant molecules at the surface and a different surface geometry.

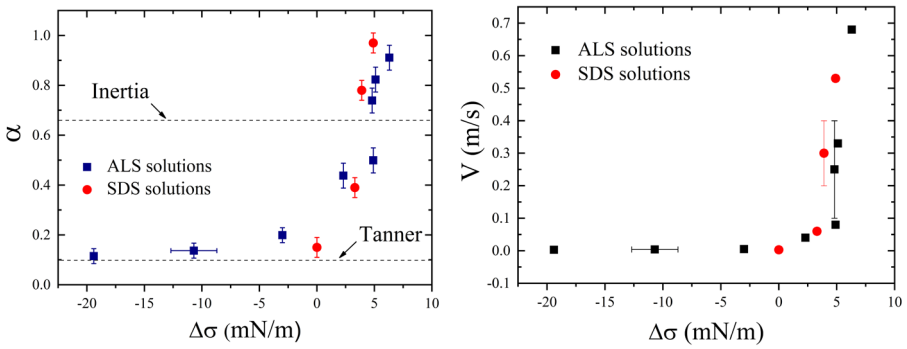

Fig. 2.5: (Left) Exponent α as a function of surface tension difference for deposited droplets with different concentrations of ALS and SDS on 0.005 M SDS soap film. α is calculated by a power-law fit to data in Fig. 2.4. (Right) Average spreading speed calculated by linear fits to the solid data points in Fig. 2.4. For the sake of clarity, only several typical error bars for the velocity and Δσ are shown.

When a drop of SDS solution spreads slowly on a film of the same liquid ($\Delta\sigma = 0$), there is a clear energetic reason due to lowering the total surface area. This slow spreading with small exponents may be explained by the regime of Tanner's law. In Tanner's regime, the driving force of spreading is due to capillary pressure induced by the curvature at the rim. We note that Tanner's law applies for spreading on a rigid boundary. If the surface exhibits slip then one might expect a slightly different result[27]. We have an almost similar situation for spreading a droplet on the same liquid film, where large curvatures are observed at the rim of the liquid lens. The exponent predicted by Tanner's law is shown by a horizontal dashed line on Fig. 2.5 (left); it is in agreement with the spreading exponents observed for ($\Delta\sigma$=0).

For droplets with larger surface tension with respect to the film ($\Delta\sigma$<0) we still see slow spreading dynamics with similar exponents ($\alpha < 0.2$). At first glance, it seems that the spreading should not occur due to higher surface tension of the final film. However, if we consider the very slow dynamics we can expect that the surface tension difference between the droplet and film rapidly decreases and reaches a uniform surface tension, which is lower than the original surface tension of the film surface, shortly after the coalescence. In particular, in the slow spreading regime the spreading speed is about 1

mm/s, so that it takes several seconds to spread about 1 cm. The data in Fig. 2.3 shows that the surface tension decreases considerably over this time scale so we anticipate that the surface tension everywhere becomes uniform in the slow spreading regime. Therefore, even in case of $\Delta\sigma<0$ the slow spreading continues with the Tanner-like dynamics discussed above.

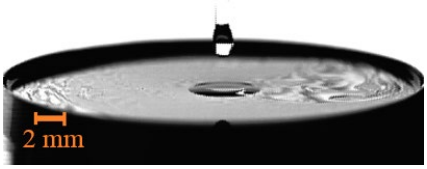

Fig. 2.6: A droplet of 0.005 M SDS is deposited on the same soap film. After deposition, a liquid lens is formed that spreads slowly in time. *R* as a function of time for this experiment is shown by black squares in Fig. 2.4 (right).

For the droplets with lower surface tension than the soap film ($\Delta\sigma > 0$), the exponent α strongly increases with increasing $\Delta\sigma$ (Fig. 2.5 left panel). Here the positive surface tension difference favours droplet spreading. Due to very fast stretching of the droplet, we expect a gradient of surface tension from the outside film toward the centre of the spreading droplet.

We estimate the average spreading speed by fitting a linear function to the data in Fig. 2.4 a and b. The results are shown as a function of $\Delta\sigma$ in Fig. 2.5 (right), ranging from 0.003 m/s for negative $\Delta\sigma$ to about 0.7 m/s for $\Delta\sigma$=6.3 mN/m. From the average spreading speed we determine an experimental time scale for the spreading. Using this time scale we obtain the dynamical surface tensions in Fig. 2.3.

In our system, we observe a range of exponents from $\alpha \sim 0.1$ to linear growth of the front radius ($\alpha \sim 1$). A similar range of spreading exponents was reported previously by Rafai *et al.*[28] in a completely different system consisting of a surfactant solution (Trisiloxan) spreading on a solid substrate where by increasing the concentration of surfactant α increased from 0.2 to 1. This wide range of exponents was associated with Marangoni effects.

2.3.2 Effect of droplet volume

In order to study the effect of the volume of the droplets on the spreading process, droplets with different diameters (D) were deposited on an SDS 0.005M film. We used ALS 0.04 M droplets for fast spreading and SDS 0.005 M droplets for slow spreading. Fig. 2.7 shows the radius of spreading as a function of time for droplets with different volumes deposited on the soap film in linear and logarithmic scale. We fit the time-dependencies with a power-law and find that the power-law exponent is roughly the same for all droplet volumes in each regime ($\alpha \sim 0.9$ for fast spreading and $\alpha \sim 0.11$. For the slow regime) as shown in Fig. 2.5 (left). Only for the smallest droplet of ALS, created by spraying, an exponent $\alpha = 0.8 \pm 0.05$ was obtained, which is slightly smaller than the other experiments in the fast regime. For the fast spreading experiments since the exponent α is close to unity, we can estimate the spreading speed from the slope of linear fits to the data points.

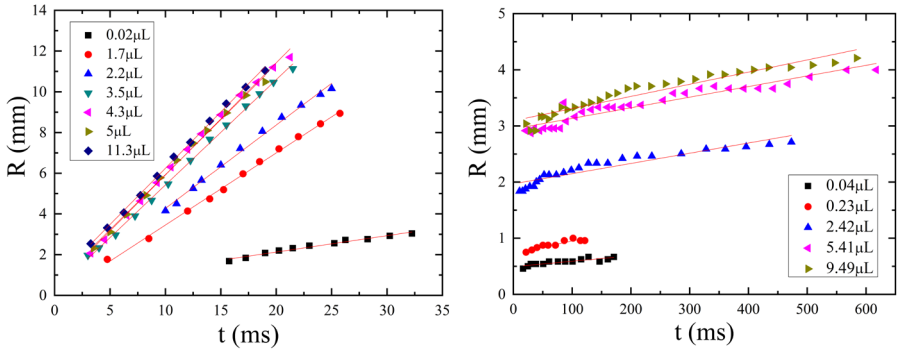

Fig. 2.7: Time evolution of spreading droplets with different volume on SDS soap films. (Right) Spreading of 0.04 M ALS droplets with different volumes on a 0.005 M SDS soap film (fast spreading). (Left) Spreading of 0.005 M SDS droplets with different volumes on a 0.005 M SDS soap film (Slow spreading). Error bars are smaller than the size of the symbols.

In Fig. 2.8 (right), the spreading speed is reported as a function of droplet diameter. By increasing the size of the droplets, the average speed of spreading increases slowly before reaching a plateau. The capillary length of the liquid ($L_c = \sqrt{\frac{\sigma}{\rho g}} \sim 2$ mm, where σ=41.2 mN/m is the dynamic surface tension of the

ALS 0.04 M), determines where the plateau starts. For the droplets with diameters smaller than the capillary length of the system, the average velocity grows linearly with increasing radius of the droplet (slope 1 in the log-log plot of Fig. 2.8 right). After that, the speed remains constant at 0.5±0.15 m/s. L_c is indicated in Fig. 2.8 (right) as a vertical dashed line. According to our results for the fast spreading, the volume of the spreading droplet does not affect the spreading exponent but the spreading speed can be influenced by the droplet volume when the diameter of the droplet is smaller than the capillary length of the liquid.

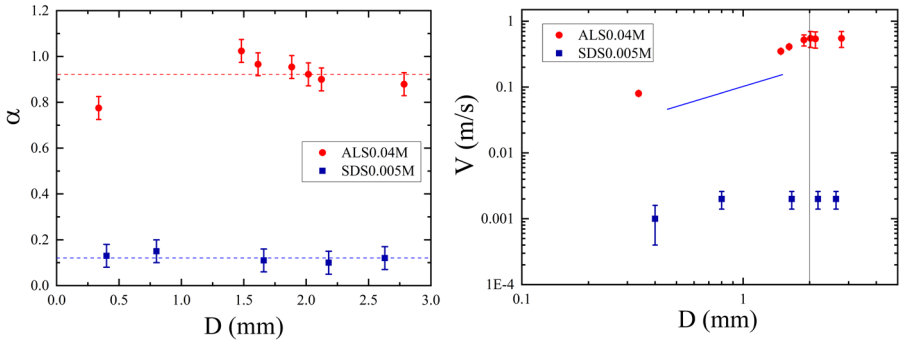

Fig. 2.8: (Right) Exponent α calculated by a power-law fit to the data in Fig. 2.7 as a function of the diameter of the droplets (D). The upper and lower horizontal dashed lines represent the average value of α for rapid and slow spreading, respectively.(left) Average spreading speed as a function of droplet size with logarithmic scales for fast (0.04 M ALS droplet on a soap film of 0.005 M SDS) and slow spreading (0.005 M SDS droplet on 0.005 M SDS soap film). The vertical dashed line illustrates the capillary length of the system. A blue line with slope one is shown as a guide to the eye.

For the slow spreading although the power law exponents are significantly smaller than unity ($\alpha \sim 0.11$) we still are able to linearly fit the time evolution data of Fig. 2.7 and estimate a spreading speed. The results are shown by square symbols in Fig. 2.8 (right) and indicate that the average spreading speed remains approximately constant with an increase of the volume of the droplet.

2.3.3 Scaling arguments

Bringing two miscible liquids into contact with each other will generate a gradient of surface tension and induces a flow known as a Marangoni-driven flow. The driving force in such flows is the tangential stress associated with gradients of surface tension at the interface which should be balanced by viscous stresses. Based on scaling the Marangoni stresses for viscosity-limited spreading on a deep bath (distance as a function of time), a spreading exponent of ¾ can be derived[13,29,30].

The Reynolds number ($Re = \frac{\rho u h}{\eta}$, with h the film thickness) of the system in the rapid spreading regime ($\Delta\sigma > 0$) is always larger than one, indicating that the inertial terms should be considered in the balance of stresses. In a first approximation, we ignore the viscous dissipation and balance the surface tension gradient by the inertial term: $|\nabla\sigma| \sim \rho u^2$ where $u \sim \dot{R}$ with a dot denoting the time derivative. The surface tension gradient term scales with the dynamic surface tension difference divided by the radius of the spreading front ($|\nabla\sigma| \sim \frac{\Delta\sigma}{R}$), so we arrive at $\frac{\Delta\sigma}{R} \sim \rho\dot{R}^2$ and hence $R \sim \left(\frac{\Delta\sigma}{\rho}\right)^{1/3} t^{2/3}$. The exponent 2/3 is within the range of exponents we observed for the fast spreading experiments as shown in Fig. 2.5a by a dashed line marked by "inertial".

2.4 Conclusions

Droplets will spread when deposited on a soap film. Spreading evolves as a function of time in a power-law manner with exponents ranging from about 0.1 to about 1 depending on the dynamic surface tension differences between the film and the droplet. Small spreading exponents with slow spreading dynamics occur when the surface tension of the droplet is greater than or equal to the surface tension of the film so that the tension difference does not favour spreading. This slow spreading regime resembles the Tanner's spreading on a solid substrate with exponent 0.1, as driven by capillary pressure at the rim.

By increasing the surface tension difference, the spreading exponent increases towards 1. In this regime, the spreading speed increases significantly with surface tension difference. Here, the driving mechanism is the Marangoni stress. By scaling the Marangoni stress with inertial terms, we can derive spreading exponents of $\alpha = 2/3$. Although this exponent is in the range of experimentally observed exponents for the fast spreading regime, however it does not explain the very fast spreading dynamics with exponents about one. This might be due to that fact that in our scaling argument we have simplified all the kinetics effects and surfactant absorption dynamics in a surface tension gradient.

We also find that the spreading speed depends on the size of the droplet in the fast spreading regime. The spreading speed depends linearly on the droplet size for drops smaller than the capillary length of the liquid, and remains constant for larger droplet sizes, however, the spreading exponent is not influenced by the droplet size. Our experimental results may help in understanding of the various forces acting on a droplet deposited on a liquid interface. Using a more detailed theoretical model in which the surfactant absorption kinetics is considered may elucidate all our experimental observations. In addition, our methodology can be used for stretching complex liquid droplets in 2D and therefore may have applications in modifying thin suspended films. For example, using this approach the effect of elongational viscosity on stretching a complex liquid droplet in 2D can be studied.

References:

1. Bonn, D., Eggers, J., Indekeu, J., Meunier, J. & Rolley, E. Wetting and spreading. *Rev. Mod. Phys.* **81**, 739–805 (2009).

2. Carrier, O. & Bonn, D. Chapter 1 - Liquid Spreading. in (ed. Brutin, D. B. T.-D. W. and E.) 3–13 (Academic Press, 2015). doi:https://doi.org/10.1016/B978-0-12-800722-8.00001-1.

3. Bergeron, V., Bonn, D., Martin, J. Y. & Vovelle, L. Controlling droplet deposition with polymer additives. *Nature* **405**, 772–775 (2000).

4. Javadi, A., Habibi, M., Taheri, F. S., Moulinet, S. & Bonn, D. Effect of wetting on capillary pumping in microchannels. *Sci. Rep.* **3**, 1412 (2013).

5. de Gennes, P. G. Wetting: statics and dynamics. *Rev. Mod. Phys.* **57**, 827–863 (1985).

6. Popescu, M. N., Oshanin, G., Dietrich, S. & Cazabat, A.-M. Precursor films in wetting phenomena. *J. Phys. Condens. Matter* **24**, 243102 (2012).

7. Cazabat, A. M., Gerdes, S., Valignat, M. P. & Villette, S. Dynamics of Wetting: From Theory to Experiment. *Interface Sci.* **5**, 129–139 (1997).

8. Fraaije, J. G. E. M. & Cazabat, A. M. Dynamics of spreading on a liquid substrate. *J. Colloid Interface Sci.* **133**, 452–460 (1989).

9. Koldeweij, R. B. J., van Capelleveen, B. F., Lohse, D. & Visser, C. W. Marangoni-driven spreading of miscible liquids in the binary pendant drop geometry. *Soft Matter* **15**, 8525–8531 (2019).

10. Cubaud, T., Fermigier, M. & Jenffer, P. Spreading of large drops on patterned surfaces. *Oil Gas Sci. Technol.* **56**, 23–31 (2001).

11. Rafai, S. Spreading of non-Newtonian fluids and surfactant solutions on solid surfaces. *Phys. A Stat. Mech. its Appl.* **358**, 58–67 (2005).

12. Santiago-Rosanne, M., Vignes-Adler, M. & Velarde, M. G. On the Spreading of Partially Miscible Liquids. *J. Colloid Interface Sci.* **234**, 375–383 (2001).

13. Camp, D. W. & Berg, J. C. The spreading of oil on water in the surface-tension

regime. *J. Fluid Mech.* **184**, 445–462 (1987).

14. Afsar-Siddiqui, A. B., Luckham, P. F. & Matar, O. K. The spreading of surfactant solutions on thin liquid films. *Adv. Colloid Interface Sci.* **106**, 183–236 (2003).

15. Wang, X., Bonaccurso, E., Venzmer, J. & Garoff, S. Deposition of drops containing surfactants on liquid pools: Movement of the contact line, Marangoni ridge, capillary waves and interfacial particles. *Colloids Surfaces A Physicochem. Eng. Asp.* **486**, 53–59 (2015).

16. Tanner, L. H. The spreading of silicone oil drops on horizontal surfaces. *J. Phys. D. Appl. Phys.* **12**, 1473–1484 (1979).

17. Cazabat, A. M. & Stuart, M. A. C. Dynamics of wetting: effects of surface roughness. *J. Phys. Chem.* **90**, 5845–5849 (1986).

18. Shiri, R., Najafi, A. & Habibi, M. Sampling moiré technique and the dynamics of a spreading droplet on a solid surface. *Meas. Sci. Technol.* **25**, 35305 (2014).

19. Hernández-Sánchez, J. F., Eddi, A. & Snoeijer, J. H. Marangoni spreading due to a localized alcohol supply on a thin water film. *Phys. Fluids* **27**, 32003 (2015).

20. Jensen, O. E. & Grotberg, J. B. Insoluble surfactant spreading on a thin viscous film: Shock evolution and film rupture. *J. Fluid Mech.* **240**, 259–288 (1992).

21. Gaver, D. P. & Grotberg, J. B. The dynamics of a localized surfactant on a thin film. *J. Fluid Mech.* **213**, 127–148 (1990).

22. Kang, K. H., Kim, H. U. & Lim, K. H. Effect of temperature on critical micelle concentration and thermodynamic potentials of micellization of anionic ammonium dodecyl sulfate and cationic octadecyl trimethyl ammonium chloride. *Colloids Surfaces A Physicochem. Eng. Asp.* **189**, 113–121 (2001).

23. Aguiar, J., Carpena, P., Molina-Bolívar, J. A. & Carnero Ruiz, C. On the determination of the critical micelle concentration by the pyrene 1:3 ratio method. *J. Colloid Interface Sci.* **258**, 116–122 (2003).

24. Price, H. C., Mattsson, J. & Murray, B. J. Sucrose diffusion in aqueous solution. *Phys. Chem. Chem. Phys.* **18**, 19207–19216 (2016).

25. Joos, P. & Pintens, J. Spreading kinetics of liquids on liquids. *J. Colloid Interface Sci.* **60**, 507–513 (1977).

26. Aarts, D. G. A. L., Lekkerkerker, H. N. W., Guo, H., Wegdam, G. H. & Bonn, D. Hydrodynamics of Droplet Coalescence. *Phys. Rev. Lett.* **95**, 164503 (2005).

27. HOWELL, P. D. & STONE, H. A. On the absence of marginal pinching in thin free films. *Eur. J. Appl. Math.* **16**, 569–582 (2005).

28. Rafaï, S., Sarker, D., Bergeron, V., Meunier, J. & Bonn, D. Superspreading: Aqueous Surfactant Drops Spreading on Hydrophobic Surfaces. *Langmuir* **18**, 10486–10488 (2002).

29. Hoult, D. P. Oil Spreading on the Sea. *Annu. Rev. Fluid Mech.* **4**, 341–368 (1972).

30. Fay, J. A. PHYSICAL PROCESSES IN THE SPREAD OF OIL ON A WATER SURFACE. *Int. Oil Spill Conf. Proc.* **1971**, 463–467 (1971).

Chapter 3

Surfactant-surfactant interaction dominating Marangoni spreading on a soap film

Abstract:

When spreading occurs along a liquid-liquid interface, presence of surfactants in one or both liquids can add to the complexity of the spreading dynamics. In this work, we systematically investigate the influence of the molecular structure of the surfactants on the Marangoni spreading. We studied the spreading behavior of various surfactant solutions with different molecular structures and ionic states while keeping the macroscopic parameters of the solutions such as surface tension and viscosity similar. To simplify the system and to remove the influence of adsorption kinetic of the surfactants in the liquid phases and also to remove the effect of diffusion, we have employed a unique configuration of "droplet on a soap film". Our results show that when the surface tension gradient between the droplet and the soap film is not significantly large, the molecular structures and microscopic interactions of the surfactants in the droplet and the soap film are no longer negligible and dramatically influence the spreading scenario.

3.1 Introduction

When two liquids come into contact, the one with the lower surface tension spreads and covers the free surface to minimize the surface energy. The so-called Marangoni spreading is prevalent in nature and plays a crucial role in many industrial applications such as manufacturing detergents[1], pesticides[2], cosmetics, and food products[3]. The general approach to study the dynamics of Marangoni spreading is to take the surface tension gradient as the driving force and scale it with the dissipative viscous term or inertial term, depending on the details of the system[4]. For pure liquids, the competition between the intermolecular cohesive and adhesive forces causes the tension exhibited by the interface which for pure liquids such as water or alcohol is constant in large time scales. However, the presence of even a minute amount of surface-active agents beside changing the initial value of the surface tension imparts time dependency to the surface properties[5] and dramatically changes the dynamics of the spreading.

Surfactants are amphiphilic molecules with a polar hydrophilic head group and a hydrophobic tail. In an aqueous solution, they migrate to the interface to extend their hydrophobic tail out of the water continuum[6]. This leads to a decrease of surface tension even at very low concentrations of surfactants. An extensive body of research has been dedicated to studying the influence of surfactants and their adsorption kinetics on the surface characteristics[7–10], especially due to the fact that many fluid systems in practice contain surface-active agents. For instance, many organic molecules have an amphiphilic nature, or in many applications, surfactants are used to alter the surface properties and foster liquid spreading.

In the past decades spreading and wetting in the presence of surfactants has attracted much attention[11–17]. Surfactants have diverse molecular structures, and their presence at the interface, beside weakening the surface tension, can change the surface chemistry. There are many examples in the past studies where the surface tension alone has failed to explain the spreading or wetting behavior of a surfactant solution[18–21]; therefore, the effect of the molecular structure and microscopic interaction of the surfactants had to be taken into

account as well. In spite of many other studies[13,22] indicating that the dynamics of liquid spreading is independent of the surface chemistry. The discrepancy lies in the diversity of the surface-active molecules and the complexity that they bring into the spreading process. Therefore, many aspects of the problem have remained unexplored, especially in the liquid-liquid spreading where surfactants are present at both liquid surfaces.

An intricate example is the spreading of surfactant solutions on suspended liquid films where both liquid phases contain surfactants. In our previous work[23], we have shown that when a droplet of surfactant solution is deposited on a soap film of a similar surfactant, it spreads and forms a new film in the center of the soap film. Depending on the initial surface tension difference between the two liquids, different spreading regimes were observed. When the droplet's surface tension was higher than the soap film ($\Delta\sigma = \sigma_{soap} - \sigma_{drop} < 0$), spreading was driven by the Laplace pressure induced by the curvature at the rim of the droplet, resulting in slow-spreading dynamics that was explained by Tanner's model[24]. In contrast, when the surface tension of the soap film was considerably higher than the droplet ($\Delta\sigma > 0$), spreading took place in a much faster manner.

We refer to the latter regime as the rapid spreading; in both regimes radius of the spreading region evolved in time according to a power-law function ($R \propto t^{\alpha}$) with the exponent α differentiating the slow and rapid regimes. For the slow spreading, the exponent α was close to 0.1, reciting Tanner's spreading law[24]. However, for the rapid spreading, α started from 0.4 and increased with the increment of $\Delta\sigma$. The maximum α for the system mentioned above was found to be 0.97. In that system the surface tension gradient was considered as the driving force of the spreading which was resisted by the inertial term; however, the effect of surfactant molecular structures and interactions was not investigated. The surfactants used in the droplet and the soap film were the same, or they had very similar and simple molecular structures with the same hydrophobic tail.

In this work, we systematically investigate the effect of surfactant-surfactant interactions and the surface charge on the Marangoni spreading on a soap film.

We use the same geometry of the previous study as it enables us to focus on the spreading dynamics in the absence of solid boundaries. We study a range of concentrations of various surfactants and deposit them on a soap film of SDS solution. We study the effect of molecular interaction and surface charge on the dynamics of the spreading beside the surface tension differences. Our results suggest that the interactions between the surfactants can shadow the effect of small surface tension gradients on the spreading. Therefore, our findings may help fine-tune the Marangoni flow dynamics to achieve desired spreading for applications that involve liquid-liquid spreading such as drug encapsulation and inkjet printing[25].

3.2 Experimental procedure and methods

To study the influence of surfactant charge on the Marangoni spreading we selected surfactants with various ionic states, including anionic, cationic and non-ionic surfactants. Solutions of three anionic surfactants: sodium dodecyl sulphate (SDS), ammonium lauryl sulphate (ALS) and dioctyl sulfosuccinate sodium salt (AOT), three cationic surfactants: Cetrimonium bromide (CTAB), trimethyloctylammonium bromide (OTAB), dodecyltrimethylammonium chloride (DTAC), and two non-ionic surfactants: Triton X100 and Silwet L77 were studied as working fluids. Aqueous solutions of the aforementioned surfactants were prepared at various concentrations by adding the required amount of powdered surfactant (or concentrated liquid in the case of ALS, Triton and Silwet) to Milli-Q water, and they were mixed overnight using a magnet stirrer. Concentrations were selected for each surfactant to keep the surface tension in a comparable range. The chemical composition and details of the hydrophobic parts of the surfactants are summarized in Table 3.1.

Table 3.1: Molecular structures and critical micellar concentrations of the surfactants with different ionic state.

	Surfactant	Molecular structure			CMC (mM)	Reference
		Hydrophilic tail	Polar head group	Released ion		
Anionic	SDS	$CH_3(CH)_{11}$	SO_4	Na^+	8	[26,27]
	ALS	$CH_3(CH)_{11}$	SO_4	NH_4^+	7	[28]
	AOT	$C_{19}H_{37}O_2$	$(SO_3)CO_2$	Na^+	2.6	[29,30]
Cationic	OTAB	$CH_3(CH)_7$	$N(CH3)_3$	Br^-	145	[31]
	CTAB	$CH_3(CH)_{15}$	$N(CH3)_3$	Br^-	1	[26,27]
	DTAC	$CH_3(CH)_{11}$	$N(CH3)_3$	Cl^-	22.6	[32,33]
Non-ionic	Triton X100	t-Oct-C6H4-(OCH2CH2)xOH, x= 9-10			0.22	[34]
	Silwet	C24H39N3O3Si3			0.14	[35,36]

Since the time scale involved in the spreading process is short, the dynamic surface tension (DST) of the solutions should be addressed rather than the equilibrium surface tensions. The dynamic surface tension of the solutions was measured using a Kruss maximum bubble pressure tensiometer. The bubble pressure method has been widely used to measure DST of the fast decaying surface tension of low viscous solutions at short time scales. In this method, a small capillary is submerged into the desired solution to induce a bubble while the pressure inside the bubble is monitored using a pressure cage[37]. By increasing the volume of the bubble at a certain rate, its radius of curvature decreases while the inside pressure increases. When the radius of the bubble equals the radius of the capillary, the inside pressure reaches its maximum. At the maximum pressure, the surface tension of the air-liquid interface can be calculated for a specific rate of volume change. With the help of this method, the dynamic surface tension can be measured for a range of timescales from 10 ms to several seconds.

The experimental set-up to study the spreading of surfactant solutions on the soap films is illustrated schematically in Fig. 3.1, left. In order to generate the soap film, a concentric cylinder (D=40 mm) was dipped into a solution of

0.01M SDS. Droplets of solutions of different surfactants were deposited on the soap film using a glass capillary. The following spreading was recorded using a Phantom V10 high-speed camera. The frames were image processed to track the radius of the spreading front in time. A typical spreading image is demonstrated in Fig. 3.1, right.

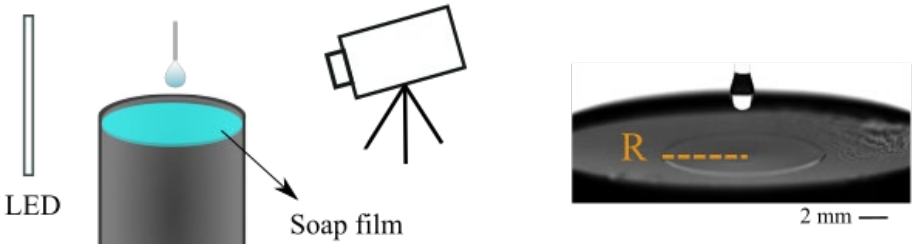

Fig. 3.1: (Right) schematic view of the experimental set-up. A droplet of surfactant solution is gently deposited on the soap film while a high-speed camera records the following spreading. (Left) spreading of a droplet of Triton X100 (c =20 CMC) on a soap film of 0.01 M SDS. The radius of the spreading front (R) is indicated with a dashed line.

To study the effect of the molecular structures and ionic state of different surfactants on the spreading dynamics in macroscopic scales, we chose various surfactants from three categories of anionic, nonionic and cationic. In each class, several surfactants with different molecular structures were selected. In the next section, we explain the experimental results of each category separately, then we compare and discuss the spreading behavior of surfactants with the different ionic states.

3.3 Experimental Results and Discussion

3.3.1 Anionic surfactant solutions:

SDS, ALS and AOT were chosen as anionic surfactants, based on their molecular structures. SDS and ALS have an identical amphiphilic structure composed of a sulfate hydrophilic head group attached to a hydrophobic tail consisting of 12 carbons. Upon dissolving in water, SDS releases sodium ions while ALS releases ammonium ions. Comparing the spreading behavior of

solutions of ALS and SDS with comparable surface tension can give us an insight into the influence of the released ion on the spreading.

AOT on the other hand has a very different molecular structure, in particular in the hydrophobic part. Two branched hydrophobic tails are attached to a polar sulphosuccinate head group in AOT. The polar head is comparable to that of SDS and ALS. However, the short and wide hydrophobic tail of AOT, makes it more surface-active and it can reduce the surface tension more significantly in comparison to SDS and ALS at the same concentrations. The difference in the tails of AOT in respect to the other two surfactants also explains its lower CMC (2.6 mM) compared to SDS or ALS (8 and 7 mM respectively). In Fig. 3.2 (top row) dynamic surface tension of three surfactant solutions with various concentrations is demonstrated. As it is expected, by increasing the concentration of the surfactant, the surface tension decreased for all the solutions. However, the reduction of surface tension was more significant at higher concentrations of AOT. In all graphs, the surface tension of the soap film, composed of 0.01 M SDS, is illustrated by hollow circles as a reference.

To study the spreading dynamics, droplets of the surfactant solutions were deposited on a soap film and the radius of the spreading front (R) was tracked in time. In Fig. 3.2 (bottom row), R is shown as a function of time for various concentrations of each surfactant on a logarithmic scale. It should be noted that the origin of time for the spreading experiments was the instant that the droplet contacted the soap film. Therefore, for the first few milliseconds, although the droplet was in contact with the soap film, it was not fully detached from the capillary. This has caused the deviation from the general trends in the spreading data points for the initial 10-20 milliseconds.

For all concentrations of SDS, the droplet formed a lens on the soap film and slowly spread in time. Power-law functions were fitted to the data series and exponent α was approximately 0.1 for all the series indicating that the spreading was in the slow regime (Tanner's law). ALS solutions with concentrations of 0.5, 1 and 2 CMC followed the same trend as of SDS

solutions, however, for the concentrations of 20 and 40 CMC ALS, rapid spreading was observed with exponents of 0.27 and 0.5 respectively.

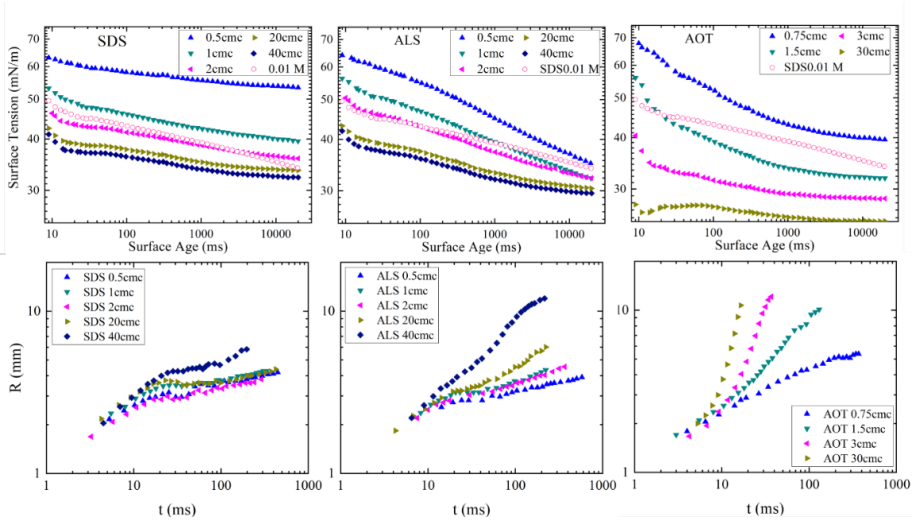

Fig. 3.2: (Top) Dynamic surface tension of various concentrations of SDS, ALS and AOT. (Bottom) Spreading radius of the same surfactant solutions on a soap film of SDS 0.01M.

As it can be seen from the graphs, spreading dynamics were substantially faster for AOT solutions. Rapid spreading was observed for all the selected concentrations. Even the 0.75 CMC AOT solution despite its larger surface tension than that of the soap film showed a rapid spreading. The exponent α increased from 0.5 for a concentration of 0.75 CMC to about 2 for 30 CMC.

In Fig. 3.3 (left) the dynamic surface tensions of SDS 40 CMC, ALS 20 CMC and AOT 3CMC solutions are presented as a function of time. These three solutions showed similar DST, especially after 500 ms with ALS having slightly lower surface tension than the others, however, the difference didn't surpass 2 mN/m even at 20 s where it was maximum.

At short time scales, from 10 ms to 500 ms, (comparable to the time scale of a typical spreading), AOT showed a higher surface tension than the others, starting from 54 mN/m at 10 ms and steeply decreasing to almost 34 mN/m at 500 ms. In contrast, ALS and SDS started with lower surface tension at 10 ms but with slower dynamics, they reached the same surface tension of AOT at

500 ms. Therefore, the surface tension differences between these solutions and the soap film were negligible, suggesting similar spreading dynamics based on the previous studies[23].

Surprisingly, the spreading radius in these three samples grew with different exponents of 0.18 and 0.27 and 1.32 respectively. Although the AOT solution had a smaller surface tension gradient with the soap film and even a negative surface tension difference for the time scales below 20 ms, it spread much faster than both SDS and ALS solutions. The exceptional spreading behavior of AOT has also been reported in previous studies of spreading on solid surfaces[38–40]. We know all these three surfactants have the same electric charge, however, AOT has two aliphatic tails and thus forms a thicker molecular chain. The unusual spreading of AOT indicates that the surfactant interactions should play a more important role than the surface tension differences in the spreading dynamics, specifically when the surface tension differences are not significant.

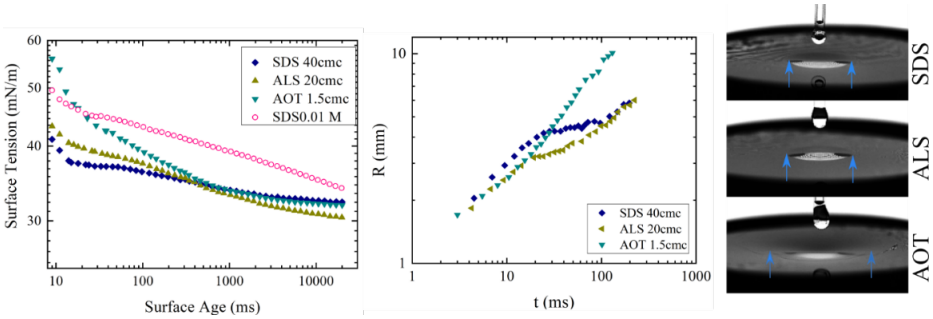

Fig 3.3: (Left) Dynamic surface tension of SDS 40 CMC, ALS 20 CMC and AOT 2 CMC solutions. At selected concentrations, the three solutions showed the most similarity in the surface tension behavior. (Middle) Evolution of the radius of spreading front as a function of time for the above solutions on a soap film of 0.01M SDS. Although the surface tension difference between AOT solution and the soap film is smaller than that of SDS and ALS before 500 ms, it spreads faster. Column of images on the right shows the droplet of the three surfactant solutions, 100 ms after deposition on the soap film. The arrows indicating the spreading front.

3.3.2 Non-ionic surfactant solutions:

For the non-ionic group of surfactants, we chose Silwet and Triton x100 which are widely used for industrial applications. Silwet is a commercial surfactant and known as a super spreader as it can readily spread on a variety of surfaces. It also has broad applications in the agriculture and pesticide industry to assist the spreading of aqueous solutions on hydrophobic surfaces of leaves[17]. Silwet molecules consist of a trisiloxane head group attached to a short hydrophobic tail. For instance, the size of the hydrophobic tail of Silwet (9.7 Å) is much shorter than the hydrophobic tail of SDS ($C_{12}H_{25}$ with a length of 15 Å) [41]. Triton on the other hand, is a common lab detergent and is often used for DNA extraction[42] and protein purification[43]. An aromatic circle connected to a polyethylene oxide chain plays the role of polar head group for Triton. Its hydrophobic tail has a branched structure consisting of 8 carbons.

The dynamic surface tension of these two surfactants at different concentrations is illustrated in Fig. 3.4 (left). As it can be seen, solutions containing Silwet have in general a lower surface tension compared to the solutions of Triton. The rate at which the surface tension decreases at the early times is also higher for Silwet solutions. By increasing the concentration to several CMC, the surface tension of the solutions converge to the same value at higher surface ages. At a time scale of 20 s, solutions of 70 and 700 CMC Silwet showed similar surface tensions about 20 mN/m, while surface tension of Triton solutions converged to 31 mN/m.

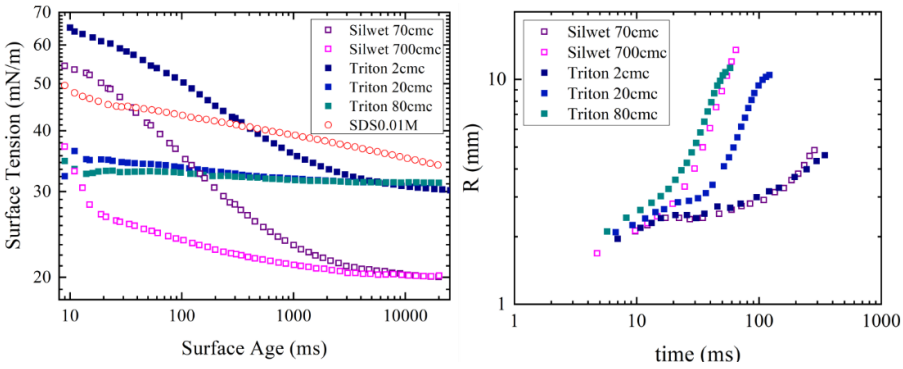

Fig. 3.4: (Left) Dynamic surface tension of two nonionic surfactant, Triton X100 and Silwet at various concentrations. (Right) Radius of the spreading front as a function of time for the non-ionic surfactant solutions on a soap film of 0.01M SDS.

In Fig. 3.4 (right) radius of the spreading fronts of droplets containing Silwet and Triton at various concentrations are demonstrated when they are deposited on a soap film of 0.01M SDS. For Triton at 2 CMC, the spreading dynamics were slow with a spreading exponent of 0.24, however, it was slightly faster than Tanner's regime. By increasing the concentration of Triton in the droplet, the surface tension difference between the droplet and the soap film increased and the spreading became faster. The spreading exponent for droplets of Triton 20 and 80 CMC was 1.1 and 1.2 respectively. Solutions of Silwet followed the same trend. For Silwet 70 CMC, the spreading exponent was 0.3 approximately matching the spreading of Triton 2 CMC. At a higher concentration of 700 CMC the surface tension difference was pronounced and the spreading exponent increased to 1.56. As it was mentioned for the anionic surfactants spreading, the first few milliseconds the droplet was still attached to the capillary, therefore, the initial data points were neglected during fitting power-law functions.

According to the spreading graph of Fig. 3.4, in the slow spreading regime, the evolution of the spreading front, for Silwet 70 CMC and Triton 2 CMC were closely similar. In the rapid spreading regime Silwet 700 CMC and triton 80 CMC were nearly identical. However, these solutions had very different

surface tensions. This clearly shows the influence of the size of the hydrophobic tail and the molecular interaction between hydrophobic parts of the two surfactants in the droplet and soap film could be dominant with respect to the effect of surface tension difference on the spreading dynamics on a soap film.

3.3.4 Cationic Surfactant solutions:

All cationic surfactants studied in this work consist of Trimethylamine as their polar head group and a hydrocarbon chain as their hydrophobic tail. This allows us to solely study how the structure of the hydrophobic tail of surfactants influences the spreading of the droplet on the soap film. The length of the hydrocarbon chain varied for each surfactant. OTAB with only 8 carbon in its hydrophobic tail, had the shortest hydrocarbon chain. DTAC and CTAB with 12 and 16 carbon respectively had relatively larger hydrophobic parts. In Table 1, the chemical composition and details of the molecular structure of the mentioned surfactants are presented.

Fig. 3.5 (left), shows the dynamic surface tension of aqueous solutions of the three cationic surfactants. Solutions containing OTAB and DTAC showed approximately constant surface tension within the time scales of measurements, except for 1 CMC DTAC which its surface tension dropped from 47 mN/m at 2 s to 37mN/m at 20 s. Solution of 0.1 CMC OTAB with a surface tension of 72 mN/m had the highest surface tension among cationic surfactant solutions. In contrast, 10 CMC DTAC solution has the lowest surface tension in the time window of 10 to 200 ms.

In the right panel of Fig. 3.5, the radius of spreading front of all four solutions is presented as a function of time. Although OTAB solution had a higher surface tension than the soap film it was the only solution that showed the rapid spreading with a spreading exponent of 0.49. OTAB also had a considerably higher critical micellar concentration compared to the rest of the surfactants studied here, indicating the lower affinity of the OTAB molecules

to each other and the higher potential energy that is needed for OTAB molecules to form micelles.

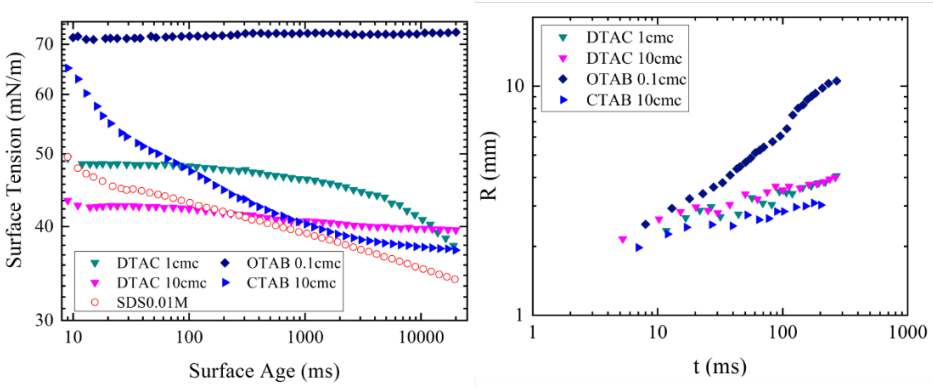

Fig. 3.5: (Left) Dynamic surface tension of Cationic surfactants. (Right) Evolution of the radius of the spreading front of cationic surfactant solutions as a function of time, when deposited on a soap film of 0.01M SDS.

Spreading of the rest of the cationic solutions was in the slow regime and was governed by Laplace pressure, with the spreading exponent of approximately 0.1. Oversight of the spreading exponent of cationic surfactant is presented in Fig. 3.6.

To have a closer look at the forces governing the spreading, first, the effective surface tension difference ($\Delta\sigma$) between the droplets and the soap film was needed to be determined. For the droplets, we considered a characteristic time scale given by $\tau = L/u$, where u is the average speed of the spreading film and L, the maximum radius of the spreading film for each experiment. For the SDS soap film, surface tension at 5 s was considered to calculate $\Delta\sigma$ since in our experiments there was on average a 5s gap between generating the soap film and deposition of the surfactants droplets.

Figure 6, shows the spreading exponent of all the surfactant solutions studied here as a function of $\Delta\sigma$. As it can be seen in the graph for droplets with $\Delta\sigma<0$ spreading exponent was scattered around 0.1 with a few exceptions and with increasing $\Delta\sigma$ to above zero the spreading dynamics were accelerated and α

increased sharply. The general trend observed here corroborates with the results reported in previous studies[23,44].

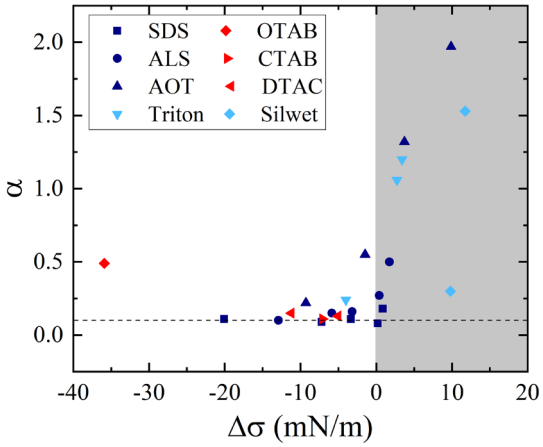

Fig. 3.6: The power-law exponent (α) for the spreading of droplets of various surfactant solutions deposited on a soap film of 0.01M SDS. In the grey region, surface tension difference is promoting

However, the deviations from the general trend that we observed here cannot be explained by solely considering the surface tension gradient. For instance, the spreading exponents for AOT solutions were in general higher than what the scaling laws predict. For AOT 0.75 and 1.5 CMC with $\Delta\sigma<0$, rapid spreading was observed and α was reported 0.22 and 0.55 respectively, suggesting that molecular interaction between AOT and SDS molecules were assisting Laplace pressure to accelerate the spreading and to dominate the effect of negative surface tension difference. For AOT solutions with $\Delta\sigma>0$, α were reported approximately 2 for the highest concentration of AOT which was significantly higher than what has been reported in the previous studies. The case of OTAB was even more intriguing. Solution of 0.1 CMC OTAB, showed a fast spreading with an exponent of 0.49 despite its strongly negative surface tension difference with the soap film. Triton and Silwet also showed rapid spreading for all the concentrations studied here. Although for lowest concentrations of Triton $\Delta\sigma$ was negative, the power-law exponent was higher than 0.1.

It can be concluded that although the surface tension difference between two surfactant solutions can outline the general trends of spreading (slow and rapid

regimes), it cannot precisely predict the onset of rapid spreading. Our results show for an accurate prediction of spreading behaviors of surfactant solutions, a thorough understanding of molecular interactions between surfactants at both liquid phases is required. In particular, when the surface tension difference between the two fluids is not significant, the effect of molecular interactions is emphasized and is needed to be considered. This study raises new questions and opens a new avenue for studying the liquid-liquid spreading in the presence of surfactants. These results might be useful for tuning the Marangoni flow dynamics to achieve desired spreading for applications in drug encapsulation and inkjet printing.

References:

1. Takenaka, Y., Sumino, Y. & Ohzono, T. Dewetting of a droplet induced by the adsorption of surfactants on a glass substrate. *Soft Matter* **10**, 5597–5602 (2014).

2. Bergeron, V., Bonn, D., Martin, J. Y. & Vovelle, L. Controlling droplet deposition with polymer additives. *Nature* **405**, 772–775 (2000).

3. Krebs, T., Schroën, C. G. P. H. & Boom, R. M. Coalescence kinetics of oil-in-water emulsions studied with microfluidics. *Fuel* **106**, 327–334 (2013).

4. de Gennes, P.-G., Brochard-Wyart, F. & Quéré, D. Transport Phenomena BT - Capillarity and Wetting Phenomena: Drops, Bubbles, Pearls, Waves. in (eds. de Gennes, P.-G., Brochard-Wyart, F. & Quéré, D.) 261–287 (Springer New York, 2004). doi:10.1007/978-0-387-21656-0_10.

5. Reduction of Surface and Interfacial Tension by Surfactants. *Surfactants and Interfacial Phenomena* 208–242 (2004) doi:https://doi.org/10.1002/0471670561.ch5.

6. Seymour, K. G. *Surfactants and Interfacial Phenomena*. *Journal of AOAC INTERNATIONAL* vol. 62 (1979).

7. Miller, R. On the solution of diffusion controlled adsorption kinetics for any adsorption isotherms. *Colloid Polym. Sci.* **259**, 375–381 (1981).

8. Miller, R., Hofmann, A., Hartmann, R., Halbig, A. & Schano, K.-H. Measuring dynamic surface and interfacial tensions. *Adv. Mater.* **4**, 370–374 (1992).

9. Miller, R., Wüstneck, R., Krägel, J. & Kretzschmar, G. Dilational and shear rheology of adsorption layers at liquid interfaces. *Colloids Surfaces A Physicochem. Eng. Asp.* **111**, 75–118 (1996).

10. Chapter 2 Thermodynamics and macro-kinetics of adsorption. in *Dynamics of Adsorption at Liquid Interfaces* (eds. Dukhin, S. S., Kretzschmar, G. & Miller, R. B. T.-S. in I. S.) vol. 1 30–67 (Elsevier, 1995).

11. Roché, M. *et al.* Marangoni flow of soluble amphiphiles. *Phys. Rev. Lett.* **112**, 1–5 (2014).

12. Nikolov, A. D. *et al.* Superspreading driven by Marangoni flow. *Adv. Colloid Interface Sci.* **96**, 325–338 (2002).

13. Bergeron, V. & Langevin, D. Monolayer Spreading of Polydimethylsiloxane Oil on Surfactant Solutions. *Phys. Rev. Lett.* **76**, 3152–3155 (1996).

14. Sauleda, M. L., Chu, H. C. W., Tilton, R. D. & Garo, S. Surfactant Driven Marangoni Spreading in the Presence of Predeposited Insoluble Surfactant Monolayers. (2021) doi:10.1021/acs.langmuir.0c03348.

15. Gaver, D. P. & Grotberg, J. B. The dynamics of a localized surfactant on a thin film. *J. Fluid Mech.* **213**, 127–148 (1990).

16. Ivanova, N. A., Kovalchuk, N. M., Sobolev, V. D. & Starov, V. M. Wetting films of aqueous solutions of Silwet L-77 on a hydrophobic surface. *Soft Matter* **12**, 26–30 (2015).

17. Tang, X., Dong, J. & Li, X. A comparison of spreading behaviors of Silwet L-77 on dry and wet lotus leaves. *J. Colloid Interface Sci.* **325**, 223–227 (2008).

18. Bera, B. *et al.* Antisurfactant (Autophobic) Behavior of Superspreader Surfactant Solutions. 13–17 (2021) doi:10.1021/acs.langmuir.1c00475.

19. Zhang, Y., Zhang, G. & Han, F. The spreading and superspeading behavior of new glucosamide-based trisiloxane surfactants on hydrophobic foliage. *Colloids Surfaces A Physicochem. Eng. Asp.* **276**, 100–106 (2006).

20. Kovalchuk, N. M., Sagisaka, M., Osaki, S. & Simmons, M. J. H. Superspreading performance of branched ionic trimethylsilyl surfactant Mg(AOTSiC)2. *Colloids Surfaces A Physicochem. Eng. Asp.* **604**, 125277 (2020).

21. Wang, X., Chen, L., Bonaccurso, E. & Venzmer, J. Dynamic wetting of hydrophobic polymers by aqueous surfactant and superspreader solutions. *Langmuir* **29**, 14855–14864 (2013).

22. Bera, B. *et al.* Counteracting Interfacial Energetics for Wetting of Hydrophobic Surfaces in the Presence of Surfactants. *Langmuir* **34**, 12344–12349 (2018).

23. Motaghian, M. *et al.* Rapid Spreading of a Droplet on a Thin Soap Film. *Langmuir* **35**, 14855–14860 (2019).

24. Tanner, L. H. The spreading of silicone oil drops on horizontal surfaces. *J. Phys. D. Appl. Phys.* **12**, 1473–1484 (1979).

25. Lohse, D. Fundamental Fluid Dynamics Challenges in Inkjet Printing. *Annu. Rev. Fluid Mech.* **54**, 349–382 (2021).

26. Ambrose, R. J. *Surfactants and interfacial phenomena—second edition, by Milton J. Rosen, John Wiley & Sons, Inc., New York, 1989, 431 pp. price: $49.95. Journal of Polymer Science Part C: Polymer Letters* vol. 27 (John Wiley & Sons, Ltd, 1989).

27. Aguiar, J., Carpena, P., Molina-Bolívar, J. A. & Carnero Ruiz, C. On the determination of the critical micelle concentration by the pyrene 1:3 ratio method. *J. Colloid Interface Sci.* **258**, 116–122 (2003).

28. Kang, K. H., Kim, H. U. & Lim, K. H. Effect of temperature on critical micelle concentration and thermodynamic potentials of micellization of anionic ammonium dodecyl sulfate and cationic octadecyl trimethyl ammonium chloride. *Colloids Surfaces A Physicochem. Eng. Asp.* **189**, 113–121 (2001).

29. Umlong, I. M. & Ismail, K. Micellization of AOT in aqueous sodium chloride, sodium acetate, sodium propionate, and sodium butyrate media: A case of two different concentration regions of counterion binding. *J. Colloid Interface Sci.* **291**, 529–536 (2005).

30. Das, D., Dey, J., Chandra, A. K., Thapa, U. & Ismail, K. Aggregation behavior of sodium dioctylsulfosuccinate in aqueous ethylene glycol medium. A case of hydrogen bonding between surfactant and solvent and its manifestation in the surface tension isotherm. *Langmuir* **28**, 15762–15769 (2012).

31. Mansour, O. T. *et al.* Assembly of small molecule surfactants at highly dynamic air-water interfaces. *Soft Matter* **13**, 8807–8815 (2017).

32. Šarac, B. & Bešter-Rogač, M. Temperature and salt-induced micellization of dodecyltrimethylammonium chloride in aqueous solution: A thermodynamic study. *J. Colloid Interface Sci.* **338**, 216–221 (2009).

33. Perger, T. M. & Bešter-Rogač, M. Thermodynamics of micelle formation of alkyltrimethylammonium chlorides from high performance electric conductivity measurements. *J. Colloid Interface Sci.* **313**, 288–295 (2007).

34. Tiller, G. E., Mueller, T. J., Dockter, M. E. & Struve, W. G. Hydrogenation of Triton X-100 eliminates its fluorescence and ultraviolet light absorption while preserving its detergent properties. *Anal. Biochem.* **141**, 262–266 (1984).

35. Han, F., Chen, Y., Zhou, Y. & Xu, B. A Surface Rheological Study of Silwet L-77 Surfactant at the Air/Water Interface. *J. Dispers. Sci. Technol.* **33**, 396–402 (2012).

36. Janků, J., Bartovská, L., Soukup, J., Jursík, M. & Hamouzová, K. Densitysity and surface tension of aqueous solutions of adjuvants used for tank-mixes

with pesticides. *Plant, Soil Environ.* **58**, 568–572 (2012).

37. Adamson Gast, Alice P., A. W. *Physical chemistry of surfaces*. (Wiley, 1997).

38. Afsar-Siddiqui, A. B., Luckham, P. F. & Matar, O. K. The spreading of surfactant solutions on thin liquid films. *Adv. Colloid Interface Sci.* **106**, 183–236 (2003).

39. Aytouna, M., Bartolo, D., Wegdam, G., Bonn, D. & Rafaï, S. Impact dynamics of surfactant laden drops: Dynamic surface tension effects. *Exp. Fluids* **48**, 49–57 (2010).

40. Stoebe, T., M. Hill, R., D. Ward, M. & Ted Davis, H. Enhanced Spreading of Aqueous Films Containing Ionic Surfactants on Solid Substrates. *Langmuir* **13**, 7276–7281 (1997).

41. Hill, R. M. Silicone (Siloxane) Surfactants. in (ed. Meyers, R. A. B. T.-E. of P. S. and T. (Third E.) 793–804 (Academic Press, 2003). doi:https://doi.org/10.1016/B0-12-227410-5/00690-6.

42. Lever, M. A. *et al.* A modular method for the extraction of DNA and RNA, and the separation of DNA pools from diverse environmental sample types . *Frontiers in Microbiology* vol. 6 476 (2015).

43. Yu, D. *et al.* Triton X-100 as an effective surfactant for the isolation and purification of photosystem I from Arthrospira platensis. *Photosynth. Res.* **120**, 311–321 (2014).

44. Deodhar, S., Thampi, S. P. & Basavaraj, M. G. Drops spreading on fluid surfaces: Transition from Laplace to Marangoni regime. *Phys. Rev. Fluids* **6**, 1–8 (2021).

Chapter 4

Interfacial instabilities in spreading of polymer solutions

(This chapter has been published as: Motaghian, Melika, Thiemo van Esbroeck, Erik van der Linden, and Mehdi Habibi. 2021. “Interfacial Instabilities in Marangoni-Driven Spreading of Polymer Solutions on Soap Films.” Journal of Colloid and Interface Science 612: 261–66. https://doi.org/10.1016/j.jcis.2021.12.168.)

Abstract:

Tuning and controlling the flow behavior of multi-component liquids has been a long-lasting struggle in various technological applications. Here, we studied Marangoni spreading of a polymer-surfactant ternary solution when deposited on a soap film with higher surface tension. The spreading front becomes unstable into a fingering pattern above the entanglement concentration of the polymer solution, indicating that the interplay between the elastic and interfacial properties drives the instability. Balancing these terms results in a critical length scale for the onset of the instability. To investigate the connection between the rheological characteristics of the samples and the origins of the instabilities, various rheological tests were performed. Elastic and loss modulus of the samples were measured within the linear viscoelastic regime. The spreading behavior of the solutions was studied using high-speed imaging techniques. At low concentrations of polymers, spreading dynamics are governed by surface tension gradient and viscous dissipation leading to a stable front growing linearly in time. However, above the entanglement concentration of polymers spreading front destabilizes into a daisy shape pattern suggesting the elastic forces dominating the spreading dynamics. We introduced a length scale that precisely predicts the onset of the instability.

4.1 Introduction

Spreading of a droplet over a solid or liquid surface is a sophisticated and omnipresent phenomenon in various fields of science and technology[1,2]. Ink-jet printing, spray coating, cleaning silicon wafers[3] and many other industrial applications rely majorly on the spreading behavior of liquids[4]. During spreading, a complex interplay takes place between surface tension gradients, viscous and inertial forces, leading to perplexing dynamics[5]. Moreover, boundary conditions and, in particular, high shear forces caused by solid boundaries dictate dramatic changes in the flow profile[6], especially in non-Newtonian fluids. To simplify the problem, previous studies have mainly focused on the spreading of single-component liquids or solutions with very low concentrations of polymer[7], often in the vicinity of a solid boundary. Thus physical aspects of the spreading of multicomponent droplets in the absence of the no-slip boundary condition have not been fully captured yet. However, free-surface flows are widespread in the industry, and fluids are often multicomponent, containing polymers and surface-active molecules. Microscopic interactions between these molecules can dramatically influence the flow behavior of the whole solution[8,9] and, in many cases, lead to instabilities[10–12]. Fragmentation[13–15], formation of beads, blisters[16,17], or large terminal drops[18] during the breakup of a polymer solution are instances of these instabilities. They are often undesired; therefore, a complete understanding of the dynamics of these instabilities is required to tune the flow and impede the instabilities.

In this study, we unravel a novel instability in the spreading of multi-component droplets containing high molecular weight polymer and surfactant on a thin soap film. When a droplet is deposited on a soap film, depending on its surface tension, it can spread and form a new film in the center of the soap film[19]. This unique geometry allows studying the spreading behavior in the absence of high shear viscous forces induced by the no-slip boundary condition. We observe that at relatively low polymer concentration, spreading takes place smoothly, and the leading edge remains perfectly circular. However, above a critical concentration (C_l), the spreading front is no longer

stable. Undulations emerge at the front line and form a daisy shape pattern. Fig. 4.1 (top row) shows the spreading front of two droplets below (left) and above (right) C_I.

We first discuss the experimental procedure, including the rheological characterization of our polymer-surfactant ternary solutions and the spreading dynamics. Then we continue with introducing the instability and the triggering parameters related to the critical concentration of polymers. We provide a scaling argument that predicts the onset of the instability.

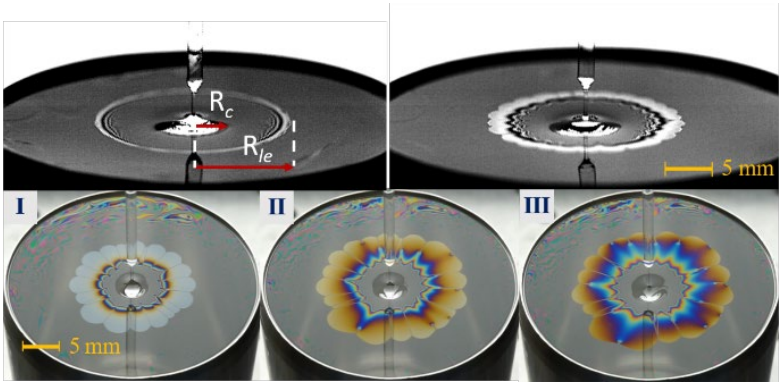

Fig. 4.1: (Top row) Droplets of PEO-SDS solution spread on soap films of 0.01 M SDS. Both droplets contain 0.3 M SDS. Concentrations of PEO (Mw ~ 2×10^6) solutions are 4 gr/L (left) and 14 gr/L (right). Above the critical concentration (right), the leading edge destabilizes into a daisy shape pattern. (Bottom row) Colored images of the unstable spreading front of PEO 12 gr/L. Images are 500 ms apart. The thickness of the advancing region is in the order of the wavelength of visible light and changes in the film thickness cause the rainbow patterns.

4.2 Experimental procedure

Polymer-surfactant solutions were prepared by slowly adding powdered polymer to the mixture of surfactant and Milli-Q water. Then they were placed on a rotator at low rotating speed for a day to ensure that mixing was homogenous and polymer chains were not broken due to the high shear rates of mixing flows. We studied various combinations of polymers and surfactants, including polyethylene oxide (PEO) different molecular weight

(0.3 – 4 $\times 10^6$ amu, 99%, Sigma Aldrich), polyacrylamide (PAM, Mw ~ 18 $\times 10^6$, 99% , Sigma Aldrich), sodium dodecyl sulfate (SDS, 98% , Sigma Aldrich), ammonium lauryl sulfate (ALS, 30% in H_2O, Sigma Aldrich), and dioctyl sulfosuccinate sodium salt (AOT, 97% , Sigma Aldrich). We use solutions of PEO 4 $\times 10^6$ amu and 0.3M SDS as an explanatory case; some details on the rest of the solutions can be found in SI.

Rheological properties of the solutions were studied using a stress-controlled rheometer (MCR 302, Anton Paar) equipped with a cone-plate geometry (diameter of 50mm and angel of 4˚). Shear viscosity of the samples was measured within the shear rates of 0.01 to 1000 1/s.

Amplitude sweep tests were performed on the solutions with the lowest and highest polymer concentration to determine the linear viscoelastic (LVE) region. 10% strain was then selected within LVE to perform the frequency sweep tests.

In order to measure the surface tension of the samples in a time scale relevant to that of the spreading experiments, we used Krüss BPT Mobile bubble pressure surface tensiometer. With this method, the dynamic surface tension of the solutions was measured in time scales as short as 10 ms. For highly concentrated samples, however, reaching10 ms time scale was not feasible due to the very high viscosity of the solution.

After characterization of the samples, droplets of polymer-surfactant solutions were gently deposited on a soap film of 0.01 M SDS. The following spreading was recorded with a Phantom high-speed camera (V710) at 4000 f/s. These video frames were image processed to track the radius of the spreading regions in time.

4.3 Results and discussion

4.3.1 Rheological characterization

Microscopic interactions between polymer strands can heavily influence the rheological properties of a polymer solution. Increasing the concentration highly promotes these interactions and, therefore causes different topological state transitions[20,21] such as non-entangled to entangled polymeric phase. The footprint of these phase transitions can be found in the rheological properties of the solution[22,23]. One approach is to study the shear viscosity of the solutions as the polymer concentration increases. In Fig. 4.2 shear viscosity of the samples containing 0.3M SDS and different concentrations of PEO is presented. All the samples showed a clear shear thinning behavior within the shear rates of 0.01 to 1000 1/s which became more pronounced with the increment of polymer concentration.

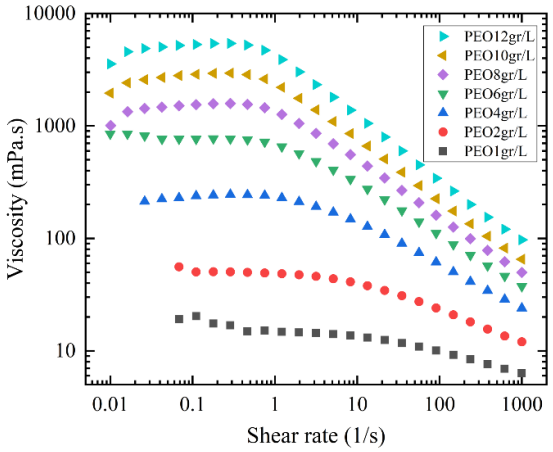

Fig. 4.2: Shear viscosity of the solutions containing different concentrations of PEO and 0.3M SDS.

Carreau-Yassuda model was fitted to the data sets to extract the zero shear viscosity (η_0). In Fig. 3, η_0 is presented for different concentrations of PEO of three different molecular weights (3×10^5, 2×10^6, and 4×10^6 amu) and polyacrylamide (PAM) with a molecular weight of 18×10^6 amu. The

concentration range in all of our polymer-SDS solutions is above c+ and the solutions are in a semi-dilute regime. Therefore, the change in the slope of the lines in Fig. 4.3 indicates the transition from non-entangled to entangled polymeric states.

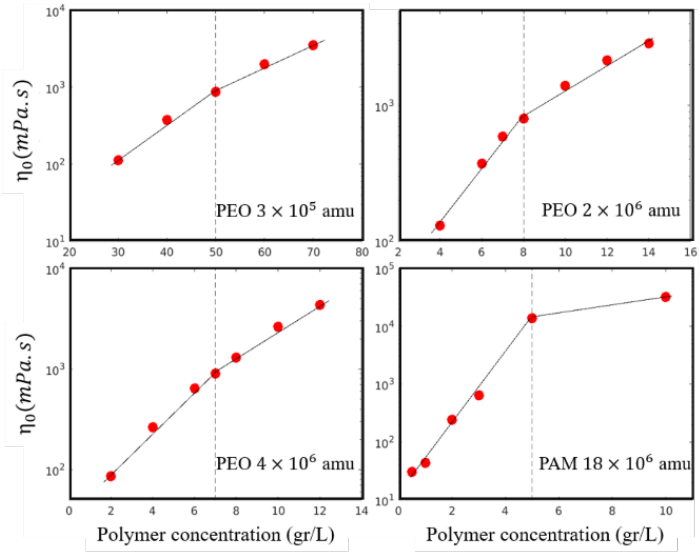

Fig. 4.3: Zero shear viscosity as a function of polymer concentration for different molecular weights of PEO and PAM. All the solutions contained 0.3M SDS. The dashed lines indicate the crossover concentration.

According to Fig. 4.3, the entanglement concentration (Ce) determined from the crossover concentration is 50, 8, and 7 gr/L for PEO 3×10^5 2×10^6, and 4×10^6 amu, respectively. For PAM 18×10^6 the pivot point occurs at 5gr/L. As it can be seen, by increasing the molecular weight of the polymer, the entanglement occurs at lower concentrations.

To characterize the viscoelastic properties of the samples, frequency sweep tests were performed within the linear viscoelastic regime. Elastic (G') and loss (G") modulus of the PEO (4×10^6 amu) solutions are presented In Fig. 4.4. By increasing the concentration of polymer, both G' and G" of the samples increased. As it is known for polymer solutions, at low frequencies, the loss modulus (G") of all samples was larger than the respective elastic modulus (G') and by increasing the frequency, G' grew and surpassed G".

Using the frequency at which G' and G" intersect, one can define a relaxation time (τ) for the system. For low polymer concentration, intersection of G' and G" could not be detected within our experimental range of frequency. Relaxation time was calculated by extrapolating the G' and G" to higher frequencies. The relaxation time of our samples varied from less than 8 ms for PEO 1 gr/L to 250 ms for PEO 12 gr/L.

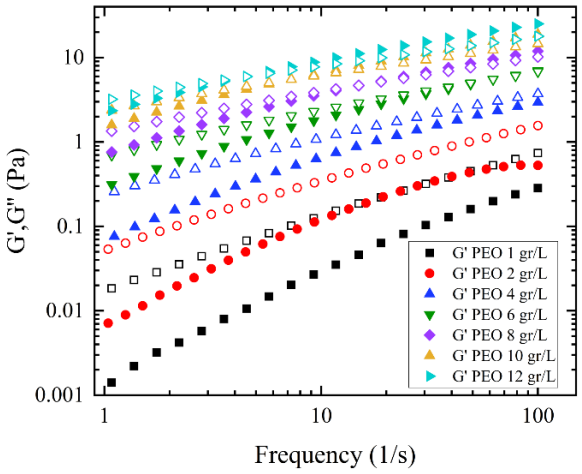

Fig. 4.4: Frequency sweep test of solutions containing 0.3M SDS and various concentrations of PEO 4×10^6 amu. Solid symbols represent the elastic modulus and open symbols of the same shape show related loss modulus.

4.3.3 Spreading dynamics and interfacial instabilities

To study the spreading dynamics, we deposit a droplet of polymer-surfactant solution on the soap film and track the spreading front in time. Although the droplet and the soap film are composed of miscible liquids, the Péclet number in all experiments is orders of magnitude smaller than one. Thus the mass diffusivity could be neglected during the course of spreading. In all our experiments, the droplet's surface tension is lower than the surface tension of the soap film. Therefore, after deposition, the droplet forms a new film in the

center of the soap film and spreads to the edges. This spreading area then divides into two regions (Fig. 4.1 top, left): a central region where the main body of the droplet rests (with radius R_c) and an advancing thin-film moving ahead (with radius R). R_c increases in time in a power-law manner with an exponent of 0.1±0.02 (data are shown in appendix B, Fig. B4), indicating this region spreads according to Tanner's law[19,24]. Here, the capillary pressure induced by the curvature at the rim of this region drives the spreading.

In the leading region, the thickness of the film is much smaller than the central region, resembling the precursor films introduced in the previous studies[3,25]. This thin region is in direct contact with the initial soap film; thus, the surface tension gradient dominates the spreading dynamics in this region. Fig. 4.5 demonstrates the growth of the radius of this region (R) in time for various concentrations of PEO (4×10^6 amu). Solid data points represent spreading with a perfectly circular (stable) front, while the open symbols represent experiments in which the spreading front becomes unstable.

After deposition, the radius of the droplet first grows slowly (lag phase) then, it evolves rapidly (second phase) until it is slowed down again by the boundary effects at the edge of the container. In the lag phase, there is no clear distinction between R and Rc; therefore, the precursor film is not formed yet. This phase often occurs at time scales smaller than the relaxation time of the solutions (τ), where the system mostly represents its solid-like behavior and thus, the growth of the radius of the droplet is slower.

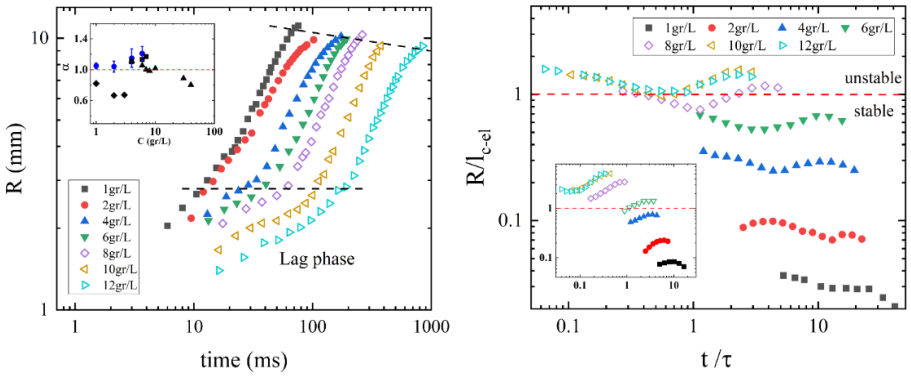

Fig. 4.5: (left) Radius of the advancing edge as a function of time for different concentrations of the polymer. Numbers in the legend indicate concentrations of PEO with 4×10^6 *amu*. Solid symbols represent stable spreading front while open symbols refer to unstable spreading fronts. Inset: exponent α is shown as a function of polymer concentration for the stable spreading of four polymer -SDS solutions: (● PEO 4×10^6 ■ PEO 2×10^6 ▲ PEO 3×10^5 ◆PAM 18×10^6 data points for PEO 4×10^6 is highlighted in blue) Error bars for α values illustrated for spreading of PEO 4×10^6 based on two series of spreading measurements. For the rest of the data points the error bar is smaller than ±0.1. (Right) R/l_{c-el} as a function of dimensionless time for various concentrations of PEO (4×10^6 amu) and 0.3 M SDS deposited on the soap film of 0.01 M SDS. Hollow symbols represent the unstable spreading experiments and the solid ones are the stable spreading. Inset: the same plot for an experiment with a soap film of 0.005 M SDS.

Power-law functions ($R \propto t^{\alpha}$) were fitted to the solid data sets (stable front) in the second region (between the dashed lines in Fig . 4.5 left), and exponent α is reported in the inset of Fig. 4.5 as a function of polymer concentration for different polymeric systems. With a good approximation, α is scattered around one. It is shown that balancing the surface tension gradient as the driving force of spreading with inertial terms in this system results in an exponent of 2/3[19]. However, the viscosity of our polymer solutions is often considerably high and the viscous dissipation is dominant with respect to the inertial term. Since the spreading film is suspended in the air, the velocity gradient through the thickness of the film is nearly zero. Therefore, the viscous dissipation acts only along the radius of the droplet. By scaling the viscous stress with the surface tension gradient, we will have $\eta \frac{V}{R} \propto \frac{\Delta\sigma}{R}$ where η is the viscosity of the spreading liquid and $\Delta\sigma$ is the surface tension difference. This will result in

$R \propto t$ thus α is equal to 1. The prefactor $\frac{\Delta\sigma}{\eta}$ has an order of magnitude of 0.1 to 0.01 m/s in our experiments. The good agreement of our scaling discussion with the experimental results of Fig. 4.5 (left) indicates that for the stable spreading of polymer solutions, the capillary driving force is balanced by the viscous dissipation in the growing thin film.

For PEO concentrations of 8 gr/L and higher, the spreading front is no longer stable, and after deposition of the drop, azimuthal undulations emerge on the leading edge (Fig. 4.1 right panel). This daisy shape front grows until it reaches the boundaries. The instability also occurs for different molecular weights of PEO and PAM and different combinations of polymer-surfactants when the polymer concentration is above a critical level. This critical concentration decreases by increasing the molecular weight of the polymer, and it is 8 for PEO of 4×10^6, 2×10^6, and 50 gr/L for PEO of 3×10^5 amu and 5 gr/L for PAM 18×10^6. Strikingly, these concentrations coincide precisely with the entanglement concentration (C_e) introduced in the previous section.

In order to check if the instability has a viscous origin or initiates due to shear thinning of the solutions, we have performed spreading experiments with a droplet of 30 wt% ALS in water on a soap film of 0.01 M SDS. The ALS solution has a zero shear viscosity of 42.9 Pa.s, high above the zero shear viscosity for the onset of instability in all our polymer samples, and shows a shear-thinning behavior similar to the polymer solutions. The spreading front of the ALS droplet remains perfectly stable (Fig. B7 appendix B) with a spreading exponent of α=1.1, indicating that instability is not derived by the viscosity or shear thinning. These observations suggest that the elastic properties of the liquid should govern the instability since, above the entanglement concentration, the elastic contribution dominates, owing to the liquid acting as a network of entangled springs.

Looking back at Fig. 4.5 (left), one can notice that the spreading of the droplets takes place in time scales comparable to the relaxation time of each sample, especially for the higher concentrations of polymer. Therefore, we expect the elastic response of the polymeric solution would be dominant in the spreading dynamics at high polymer concentrations. Balancing the elastic energy with

the surface energy in a stretching liquid film gives a capillary-elastic length scale:

$$\boldsymbol{l_{c-el}} \sim \frac{\boldsymbol{\sigma}}{\boldsymbol{G'(\omega)}} \tag{4.1}$$

with an order of magnitude between 1.5 mm to 28.7 m in our system. Since G' increases by increasing the frequency of applied deformations (ω), G' decreases in time and l_{c-el} increases when the polymer relaxes during the course of spreading. When the droplet radius during the spreading grows at a lower rate with respect to l_{c-el} , the spreading front can stay stable. On the other hand, if the growth of the spreading edge exceeds the growth of l_{c-el}, the leading edge becomes unstable. In Fig. 5 (right), we plot the dimensionless radius of spreading (R/ l_{c-el}) as a function of dimensionless time (t/τ). The solid symbols represent stable spreading, while the hollow symbols show unstable samples. The inset of Fig. 5 (right) shows the same plot for similar droplets deposited on a soap film of 0.005 M SDS, which has a higher initial surface tension than 0.1 M SDS solution. In both systems, R/l_{c-el} is an excellent predictor of the onset of instability. For the soap film of 0.005 M SDS, instabilities could be observed at slightly lower polymer concentration (6 gr/L).

When R grows faster than l_{c-el}, the system is susceptible to disturbances; thereby, any perturbation amplifies and grows into petals in the leading front. In the case of R/l_{c-el} < 1, on the other hand, small perturbations are damped, and the front remains circular. However, adding a minute amount of microparticles to the polymer solution triggers large long-lived disturbances in the leading front, promoting instability at concentrations lower than the critical concentrations (See appendix B, Fig. B8).

To investigate the effect of surfactant type on the onset of instability, we performed experiments with three different surfactants (0.3 M SDS, 0.5 M ALS, 8mM AOT) in PEO (4×10^6 amu) solutions. The critical concentration for the onset of instability for the systems containing SDS and ALS were relatively close with 8 and 7 gr/L, respectively. Surprisingly for the systems

of PEO-AOT, instability is observed at a much higher critical concentration of 18 gr/L. In addition, the viscosity of solutions of PEO-AOT is significantly lower than their counterpart with the same concentration of PEO and different surfactant (See appendix B, Fig. B5). The difference in the critical concentration for different surfactant systems lies in their different molecular structure and their interactions with the polymers in the solution. ALS and SDS have similar hydrophobic tails, and they interact with the hydrophobic portions of PEO similarly. The formation of mutual micelles between polymer strands acts as linkers and promotes the entanglement of strands[26]. AOT with a double tail, on the other hand, has a very different molecular structure. Because of its large molecular structure, AOT cannot readily form micelles to form linkers between the strands of the polymer; thus, it impedes the entanglement. Therefore, the structure of the surfactant can affect the onset of the instability by affecting the entanglement concentrations.

4.4 Conclusion

We studied the spreading dynamics of multicomponent droplets containing polymers and surfactants on a soap film and observed a novel interfacial instability during spreading at high concentrations of polymer. We found that the instability has an elastic origin and is governed by the interplay between the surface tension as the driving force of spreading and the elastic properties of the polymer solution responsible for the destabilization of the spreading front. A capillary-elastic length was introduced. compering the growth rate of mentioned capillary-elastic length to the growth rate of radius of the spreading droplet determined the onset of instability. The general spreading dynamics of the stable front below the critical concentration were discussed. The radius of the stable spreading front grew linearly in time and was explained by a viscous scaling argument.

The spreading of droplets on solid or liquid substrates has been extensively studied in the past[5,27,28] and it is well known that solid or liquid boundaries can

significantly influence the spreading behavior of liquids. The specific geometry that we have used in this work has allowed us to study the spreading behavior of multi-component liquids in the absence of solid boundaries. We observed that in this scenario, the elastic response of polymer-surfactant solution strongly influences the spreading behavior resulting in a novel interfacial instability. These results inspire more fundamental and theoretical studies of this novel instability and free surface multi-component systems in general for applications from 2D stretching of polymer films to coating by multi-component droplets or even indirect rheological probing of complex liquids.

References

1. Bergeron, V., Bonn, D., Martin, J. Y. & Vovelle, L. Controlling droplet deposition with polymer additives. *Nature* **405**, 772–775 (2000).

2. Gaver, D. P. & Grotberg, J. B. The dynamics of a localized surfactant on a thin film. *J. Fluid Mech.* **213**, 127–148 (1990).

3. Heslot, F., Fraysse, N. & Cazabat, A. M. Molecular layering in the spreading of wetting liquid drops. *Nature* **338**, 640–642 (1989).

4. Bolleddula, D. A., Berchielli, A. & Aliseda, A. Impact of a heterogeneous liquid droplet on a dry surface: application to the pharmaceutical industry. *Adv. Colloid Interface Sci.* **159**, 144–159 (2010).

5. Gennes, P.-G., Brochard-Wyart, F., Quéré, D., Reisinger, A. & Widom, B. Capillarity and Wetting Phenomena: Drops, Bubbles, Pearls, Waves. *Phys. Today - PHYS TODAY* **57**, 66–67 (2004).

6. Camp, D. W. & Berg, J. C. The spreading of oil on water in the surface-tension regime. *J. Fluid Mech.* **184**, 445–462 (1987).

7. Yamani, S. *et al.* Spectral Universality of Elastoinertial Turbulence. *Phys. Rev. Lett.* **127**, 74501 (2021).

8. De Gennes, P. G. Dynamics of Entangled Polymer Solutions. I. The Rouse Model. *Macromolecules* **9**, 587–593 (1976).

9. Seiffert, S. & Sprakel, J. Physical chemistry of supramolecular polymer networks. *Chem. Soc. Rev.* **41**, 909–930 (2012).

10. Keiser, L., Bense, H., Colinet, P., Bico, J. & Reyssat, E. Marangoni Bursting : Evaporation-Induced Emulsification of Binary Mixtures on a Liquid Layer. *Phys. Rev. Lett.* **074504**, 1–5 (2017).

11. Troian, S. M., Wu, X. L. & Safran, S. A. Fingering instability in thin wetting films. *Phys. Rev. Lett.* **62**, 1496–1499 (1989).

12. Habibi, M., Rahmani, Y., Bonn, D. & Ribe, N. M. Buckling of Liquid Columns. *Phys. Rev. Lett.* **104**, 74301 (2010).

13. Keshavarz, B., Houze, E. C., Moore, J. R., Koerner, M. R. & McKinley, G. H. Ligament Mediated Fragmentation of Viscoelastic Liquids. *Phys. Rev. Lett.* **117**, 154502 (2016).

14. Villermaux, E. & Bossa, B. Single-drop fragmentation determines size distribution of raindrops. *Nat. Phys.* **5**, 697–702 (2009).

15. Hoyt, J. W., Taylor, J. J. & Runge, C. D. The structure of jets of water and polymer solution in air. *J. Fluid Mech.* **63**, 635–640 (1974).

16. Deblais, A., Velikov, K. P. & Bonn, D. Pearling Instabilities of a Viscoelastic Thread. *Phys. Rev. Lett.* **120**, 194501 (2018).

17. Sattler, R., Wagner, C. & Eggers, J. Blistering Pattern and Formation of Nanofibers in Capillary Thinning of Polymer Solutions. *Phys. Rev. Lett.* **100**, 164502 (2008).

18. Clasen, C., Bico, J., Entov, V. M. & Mckinley, G. H. 'Gobbling drops': the jetting–dripping transition in flows of polymer solutions. *J. Fluid Mech.* **636**, 5–40 (2009).

19. Motaghian, M. *et al.* Rapid Spreading of a Droplet on a Thin Soap Film. *Langmuir* **35**, 14855–14860 (2019).

20. Feldman, D. The theory of polymer dynamics, by M. Doi and S. F. Edwards, the Clarendon Press, Oxford University Press, New York, 1986, 391 pp. Price: $78.50. *J. Polym. Sci. Part C Polym. Lett.* **27**, 239–240 (1989).

21. Deblais, A., Maggs, A. C., Bonn, D. & Woutersen, S. Phase Separation by Entanglement of Active Polymerlike Worms. *Phys. Rev. Lett.* **124**, 208006 (2020).

22. Ebagninin, K. W., Benchabane, A. & Bekkour, K. Rheological characterization of poly(ethylene oxide) solutions of different molecular weights. *J. Colloid Interface Sci.* **336**, 360–367 (2009).

23. Fall, A. & Bonn, D. Shear thickening of Laponite suspensions with poly(ethylene oxide). *Soft Matter* **8**, 4645–4651 (2012).

24. Tanner, L. H. The spreading of silicone oil drops on horizontal surfaces. *J. Phys. D. Appl. Phys.* **12**, 1473–1484 (1979).

25. Heslot, F., Cazabat, A. M. & Levinson, P. Dynamics of wetting of tiny drops: Ellipsometric study of the late stages of spreading. *Phys. Rev. Lett.* **62**, 1286–1289 (1989).

26. Dastyar, P., Salehi, M. S., Firoozabadi, B. & Afshin, H. Influences of Polymer–Surfactant Interaction on the Drop Formation Process: An Experimental Study. *Langmuir* **37**, 1025–1036 (2021).

27. Fraaije, J. G. E. M. & Cazabat, A. M. Dynamics of spreading on a liquid substrate. *J. Colloid Interface Sci.* **133**, 452–460 (1989).

28. Jensen, O. E. & Grotberg, J. B. Insoluble surfactant spreading on a thin viscous film: Shock evolution and film rupture. *J. Fluid Mech.* **240**, 259–288 (1992).

Chapter 5

Polymer-surfactant mixtures: Rheology and tribology

Abstract:

Mixtures of polymer and surfactants are widely used in many industrial applications such as food, hair and skincare and also as lubricants. Understanding the flow behavior and rheological response of such solutions under various conditions is crucial to optimize their production procedure and functionality. Here we provide a comprehensive rheological characterization of solutions containing a high molecular weight linear polymer (polyethylene oxide) in combination with various surfactants with different ionic states. Our study covered diverse rheological measurements including shear viscosity, amplitude and frequency sweep, and in particular large amplitude oscillatory shear test. Eventually, we also investigated the lubricating properties of the mentioned solutions to compare their functionality and film formation behavior as lubricants.

5.1 Introduction

The flow behavior of polymeric fluids exhibits intricate dynamics and has inspired many scientific works in the past decades. Moreover, rheological characterization of solutions containing synthetic or biological polymers is pertinent to many industrial applications. In the food industry polymers are widely used as thickening agents[1,2] or dispersants, in pharmaceutical applications they are used as controlled release agents or osmotic pressure enhancers. In surface technologies, polymers are used to preserve paints on surfaces or as lubricants for various surfaces. In many of mentioned applications polymers are present in multi-component solutions along with other ingredients. The molecular interactions between polymers and other ingredients often have significant macroscopic manifestation; therefore, a thorough understanding of the nature of these interactions and their macroscopic representation is required to engineer or optimize the functionality of a multi-component polymeric fluid.

In a solution, polymers take different morphologies depending on how their constituent building blocks interact with the solvent and with each other. For instance, partially hydrophobic polymers take a packed form in an aqueous solution to minimize the exposure of the hydrophobic parts to water continuum. However, if these building units are polarized or slightly charged they will be self-repellent and the final shape of the polymer will be defined by minimizing the free energy costs due to hydrophobicity or electrostatic repulsion. In such situations, the addition of salt or any free ions (i.e. change of pH) can dramatically influence the shape of the polymer. The free ions can screen the polymer charge/polarity locally and allow for further packing. In contrast, if amphiphilic molecules such as surfactants, are added to the polymer solution, the hydrophobic interaction between polymers and surfactants can result in the expansion of the polymer coil. The molecular-level shape transformation of polymer strands has a direct influence on the macroscopic parameters of the solution such as viscosity, shear-thinning and characteristic relaxation time.

An extensive experimental and theoretical body of work has been dedicated to studying the interaction of polymers and surfactants in an aqueous ternary solution[3–6]. In particular, polyethylene oxide (PEO) has been widely investigated because of its simple linear molecular structure[7], broad application in industry and its availability. PEO is a non-ionic polymer with high solubility in water and it is commercially available in a wide range of molecular weights. Physical properties of aqueous PEO solutions including shear[8] and extensional viscosity[8,9], conductivity, and surface tension have been studied in several seminal works and particularly from the perspective of drop formation and spreading behavior[10]. It was in 1950s that the interaction of PEO with surface-active molecules attracted attention because they vastly coexisted in detergent formulations[11]. The early work of Jones[3] showed that when sodium dodecyl sulphate (SDS), an anionic surfactant, is added to PEO solution, above the critical association concentration (CAC), SDS molecules bind to PEO strands and form complexations. The presence of these polymer-surfactant pairs increases the shear viscosity[12], characteristic relaxation time[9,12] and conductivity of the solution[13]. Later their influence on the extensional viscosity[12] of the solutions and drop formation process[14] were also studied.

Investigating the interaction of PEO with a variety of surfactants has shown that cationic and non-ionic surfactants form only weak associations with PEO molecules. For instance, the work of Nagarajan[15] illustrated that the bulky polar head of Triton X100, a well-known non-ionic surfactant, prevents interactions with PEO. It is energetically more favorable for Triton molecules to form micelles than to bind with PEO. In the cationic category cetyltrimethylammonium bromide (CTAB)[16] has been shown to barely interact with PEO as the changes in the rheological parameters of the PEO solutions after the addition of CTAB were negligible.

Although the influence of various surfactants on PEO solutions has been explored separately, a comprehensive study where the rheological parameters of the solutions can be quantitatively compared is still lacking. Furthermore, in previous studies, the rheological characterization of polymer-surfactant solutions was limited to shear viscosity or oscillatory measurements within

the linear viscoelastic regime. However, in practice, multi-component polymer solutions often undergo large deformations. For instance, in a previous work[17], we observed that during the spreading of polymer-surfactant solutions on a soap film, the enhanced elastic response of the polymeric network above the entanglement concentration of polymers, triggers instabilities on the spreading front. Although the emergence of the instabilities was not limited to one type of polymer or surfactant, the critical concentration for the onset of instability varied for different polymers and different combinations of polymer-surfactants. This stresses the importance of the elastic response of polymer-surfactant solutions, especially for the cases such as spreading and coating where large deformations are involved. Therefore, in this work, we study aqueous solutions of PEO and PEO in combination with three different surfactants: sodium dodecyl sulphate (SDS), Silwet L77 and Dodecyltrimethylammonium chloride (DTAC) (anionic, non-ionic and cationic respectively). We present a thorough rheological characterization of the solutions including shear viscosity, amplitude and frequency sweep and large amplitude oscillatory shear (LAOS) tests. In the last section, we investigate the lubricating properties of the mentioned solutions since polymer-surfactant solutions are often used as lubricants where they are subjected to large deformations. The rheological properties of such solutions can help better understand and modify their lubricant properties.

5.2 Material and Methods

Powdered polyethylene oxide (PEO) with a molecular weight of 4×10^6 amu was purchased from Sigma Aldrich. PEO solutions with concentrations of 1,5,10 and 15 gr/L were prepared by slowly adding the powdered polymer to Milli-Q water. The solutions were placed on a rotator with a low rotating speed for two days to ensure that polymers were homogeneously dissolved in water. Three surfactants: Sodium dodecyl sulphate (SDS) (Sigma Aldrich), Silwet L77 (Momentive) and Dodecyltrimethylammonium chloride (DTAC) (Sigma Aldrich) were selected to study their interactions with PEO. SDS as an anionic

surfactant, Silwet as a non-ionic and DTAC as a cationic surfactant. The required amount of surfactants was added to polymer solutions to have solutions with 0.1 M concentration of surfactant, irrespective of the concentration of polymer. The solutions were placed on the rotator again for complete mixing of surfactant and PEO solution. The concentration of 0.1 M of surfactants is chosen because it is several times the critical micellar concentration (CMC) of all the surfactants used in this study. CMC of SDS[18,19], Silwet[20,21] and DTAC[22,23] are 8, 0.14 and 22.6 mM respectively.

Rheological experiments were performed on the PEO or PEO-surfactant solutions using an Anton Paar 302 stress-controlled rheometer equipped with a cone-plate geometry with a diameter of 50 mm and a cone angle of 1 degree. Viscosity measurements were performed with an increasing shear rate from 0.01 to 1000 1/s. Frequency sweeps were performed at a constant amplitude of 10% strain, with a frequency range of 0.1-100. Amplitude sweeps encompassing short amplitude oscillatory shear (SAOS) and large amplitude oscillatory shear (LAOS) were performed at a constant frequency of 0.1 1/s. All rheological experiments were performed at 25ºC. Tribology measurements were performed with the same model of rheometer and Anton Paar "ball on the pins" tribology geometry.

5.3 Results and Discussion

5.3.1 Viscosity

Shear viscosity of the samples with different concentrations of PEO, with and without surfactants is presented in Fig. 5.1 on a logarithmic scale. Each panel illustrates the viscosity of the samples as a function of the shear rate for a fixed concentration of polymer. As it can be seen, in general, the viscosity of the solutions increases with the increment of PEO concentration as it has also been reported in previous works for aqueous solutions of PEO and also in combination of PEO and surfactants[24]. At all four concentrations, aqueous PEO and PEO-DTAC solutions were observed to have identical shear

viscosity curves. At the lowest concentration of PEO (1 gr/L), the solutions of PEO and PEO-DTAC had a viscosity of 2.4 mPa.s which remains approximately constant within the range of the measured shear rates.

However, PEO-Silwet and PEO-SDS solutions had nearly one order of magnitude higher viscosity at low shear rates and both solutions showed a mild shear thinning behavior at higher shear rates. Interaction of SDS and Silwet molecules with PEO strands leads to expansion of polymer coils which in turn results in increased viscosity as has been proven in previous works for the case of PEO-SDS[3,6,13,15]. By increasing the concentration of the PEO, the shear-thinning behavior was observed to have a higher slope. Especially for the higher concentrations of polymers, the viscosity curve can be separated into two regions: a plateau at low shear rates and the shear-thinning region where the viscosity declines with the increment of the shear rate. The critical shear rate at which the transition between the two regions occurred was observed to shift towards the lower shear rates when the concentration of PEO was increased.

Although the difference in the viscosity of the samples at low shear rates was pronounced at low concentrations of polymer (1 and 5 gr/L), the viscosity curves were more similar at high concentrations of polymer (10 and 15 gr/L). One possible reason can be the lower surfactant polymer ratio at higher concentrations of polymer since the concentration of surfactant is kept equal to 0.1 M for all the samples. Another possible reason is that at high concentrations of polymer the influence of polymer concentration on the viscosity is so pronounced that dominates the influence of polymer-surfactant interactions.

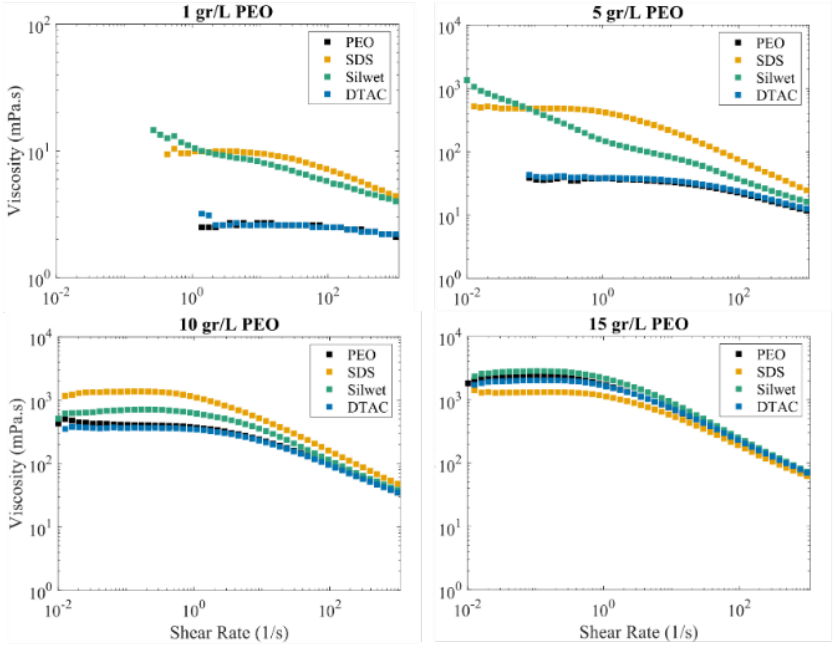

Fig. 5.1: Viscosity of aqueous PEO solution (black points, as a reference) and PEO solution with 0.1 M of three different surfactants: SDS, Silwet and DTAC. Each panel compares the viscosity of the polymer-surfactant solutions at fixed concentrations of polymer.

It should be noted that at the concentration of 15 gr/L of polymer, the solution of PEO-SDS interestingly showed the lowest viscosity compared to all the other polymer-surfactant solutions and also even lower than the aqueous PEO solution. To be sure about the reproducibility of the results the experiments were repeated several times and with two batches made separately. The data was well reproducible with error bars smaller than 0.5 mPa.s at any given shear rate.

5.3.2 Amplitude and frequency sweeps:

To evaluate the rheological response of the samples under large deformations and also to define the limits of the linear viscoelastic region (LVE), amplitude sweep tests were carried out on the samples at an angular frequency of 10 rad/s. The limits of LVE are defined by the region where the viscoelastic moduli of a system are independent of the applied strain. The elastic (G') and viscous (G'') moduli for PEO and PEO-surfactant solutions are reported in Fig. 5.2 as a function of applied strain. For the lowest concentration of PEO, because of the very low viscosity of the samples, the ratio of noise to signal was relatively high and the data points were scattered. For PEO concentrations of 5 gr/L and higher both G' and G'' showed a plateau at low strains. In the plateau region, the value of G'' was higher than G' for all the solutions indicating that all the samples showed a predominant viscous behavior, characterized also by $tan(\delta)$ greater than 1, with δ being the phase shift between strain and stress responses.

The plateau values of G' and G'' followed a trend similar to the viscosity data for different surfactants at fixed concentrations of polymer. Aqueous PEO and PEO-DTAC solutions displayed approximately identical elastic and viscous modulus across all the deformation ranges and at all PEO concentrations. PEO-SDS solution at PEO concentrations of 5 and 10 gr/L showed the highest plateau value. However, at a concentration of 15 gr/L PEO, similar to viscosity behavior, the plateau value of G' and G'' of PEO-SDS was similar to that of aqueous PEO or PEO-DTAC. For all the solutions by increasing the polymer concentration the onset of nonlinearity showed a shift towards lower deformations. Regarding the amplitude sweep diagrams in Fig. 5.2, 10% deformation was selected to conduct the frequency sweep tests since at this strain all the solutions were in the linear region.

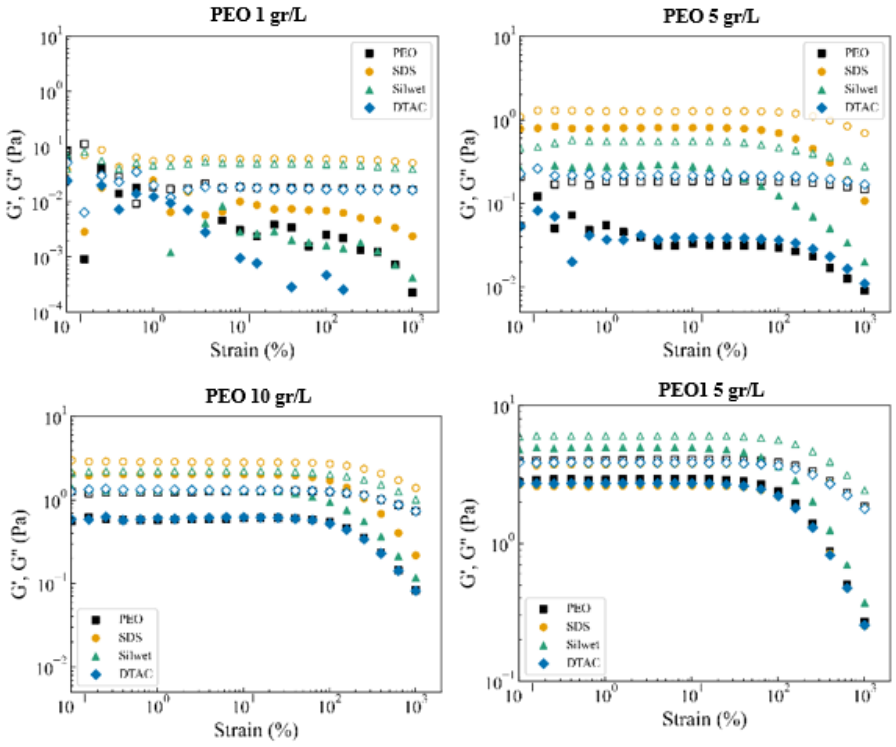

Fig. 5.2: Amplitude sweep tests of aqueous PEO solution and PEO solution with 0.1 M for three different surfactants: SDS, Silwet and DTAC. Each panel compares the G' and G'' of the polymer-surfactant solutions at a fixed concentration of polymer. Solid, open symbols with similar colors represent the elastic and viscous modulus of a solution respectively.

The result of frequency sweep tests is presented in Fig. 5.3. Similar to the amplitude sweep and viscosity data, by increasing the concentration of polymer the G' and G'' increases for all solutions at any given frequency. The only exception was PEO-SDS solution with 15 gr/L PEO which its G' and G'' curves were approximately similar to G' and G'' curves of PEO-SDS with 10 gr/L PEO. At higher concentrations of polymer, the crossover of G' and G'' curved was observed to occur at lower frequencies. As one expects, by

increasing the concentration of the polymer the characteristic time needed for entanglement-disentanglement of polymer strands increases.

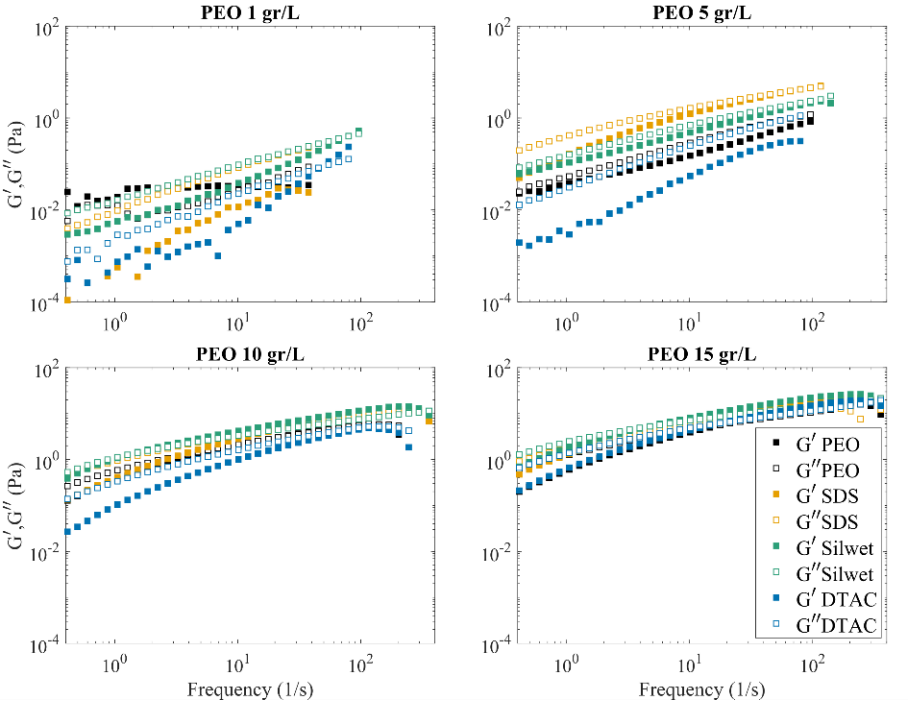

Fig. 5.3: Frequency sweep of aqueous PEO solution and PEO solution with 0.1 M of three different surfactants: SDS, Silwet and DTAC. Each panel compares the G' and G'' of the polymer-surfactant solutions at a fixed concentration of polymer. Solid symbols represent G' curves whereas open symbols represent G'' curves.

5.3.3 LAOS: Large amplitude oscillatory shear test

In many applications such as food, cosmetics, and detergents industry and also in the case of spreading instability (introduced in the previous chapter), polymer-surfactant solutions are subject to large deformations. As it was shown by the amplitude sweep tests in the previous section, these solutions exhibit nonlinear behaviour at relatively large strains. In a real-life situation where large deformations are involved, rheological measurements limited to only the linear viscoelastic region will no longer be able to fully represent the

properties of such polymeric systems. Therefore, a deeper understanding of the systems' elastic and viscous properties in the nonlinear viscoelastic (NLVE) region is required to predict and modify the behaviour of polymer-surfactant solutions in practical conditions.

Nevertheless, G' and G'' in the NLVE regime have an ambiguous physical meaning. One should note that the elastic and viscous moduli are obtained from the first harmonic compound of the stress response. In the linear regime, the first order harmonic in the Fourier spectrum of the stress response is significantly dominant and the effect of higher harmonics can be neglected. However, in the presence of nonlinearities, the contribution of higher harmonics is no longer negligible. One approach to have a better insight into the viscoelastic behaviour of a system in NLVE regime is to study the intracycle stress response of the system as a function of strain or strain rate[25,26]. By qualitatively comparing the shape and the size of the so-called elastic and viscous Lissajous plots one can have a deeper insight into the rheological behaviour of complex liquids within the NLVE region.

The elastic and viscous Lissajous plots of PEO and PEO surfactant solutions are presented in Fig. 5.4. For a concentration of 1gr/L of PEO, the stress signal was too weak to be analysed. Therefore, in both elastic and viscous Lissajous plots the rows represent only the concentrations of 5, 10 and 15 gr/L PEO (from top to down, respectively). As it is shown in Fig. 4.a. for the lowest concentration of PEO (5gr/L) at the lowest stain ($\gamma = 10.1\ \%$), the stress response is still weak and noisy. At a strain equal to 101%, solutions of PEO and mixtures of PEO with surfactants, all displayed an elliptical plot with the PEO-SDS solution having the largest elliptic curve. The shape and the size of the Lissajous plots contain information about the rheological response of the material under deformation. For instance, the Lissajous plot of purely elastic material will be a straight line whereas for purely viscous materials it will be a circle. An ellipsoidal stress response indicates that the material exhibits both elastic and viscous properties. The length of the ellipse corresponds to the size

of the G' and G'' at the regarded strain and the enclosed surface area by the elastic Lissajous plot is an indicator of the dissipated energy during a cycle.

The steep ellipsoidal shape of PEO-SDS corresponds to the large G' and $G''$of the PEO-SDS solutions compared to the other PEO-surfactant solutions. For PEO concentrations of 5 and 10 gr/L the same trends were observed and PEO-SDS showed the largest maximum stress at maximum strain compared to the rest. However, at a concentration of 15 gr/L of PEO the stress response of the PEO-Silwet was observed to reach the highest stress values, resulting in a larger surface area within the Lissajous curves. This is similar to what we observed with the previous measurements of different rheological parameters of these solutions. While most Lissajous curves showed an elliptical shape, characterized by having only a first harmonic contribution to the stress signal, some Lissajous started to show rhomboidal shapes at large strains.

Interestingly the solutions of PEO and PEO-DTAC showed identical Lissajous plots (they overlapped perfectly) for all the concentrations of polymer similar to the previous rheological parameters measured in this study. This demonstrates that the presence of DTAC in PEO solutions does not influence the rheological properties of PEO solutions even at large deformations.

By increasing the applied strain to 400% and 1010% the shape of the Lissajous plots starts to deviate from a perfect ellipse and the impact of higher harmonics become more pronounced, exhibiting a rhomboidal shape. This gradual transition can be observed for all the concentrations of polymer and also for all PEO-surfactant solutions. However, it is more pronounced at higher concentrations of polymer. The rhomboidal shape of these Lissajous indicates an initial (weak) elastic response, followed by a gradual yielding.

As a complement the viscous Lissajous plots where stress is plotted as a function of strain rate in one cycle of deformation are also presented in Fig. 5.4.b

(a)

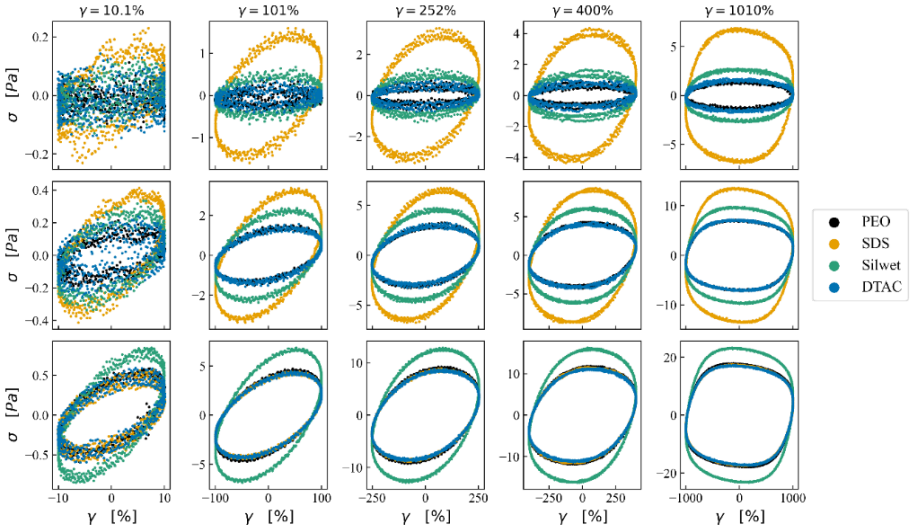

(b)

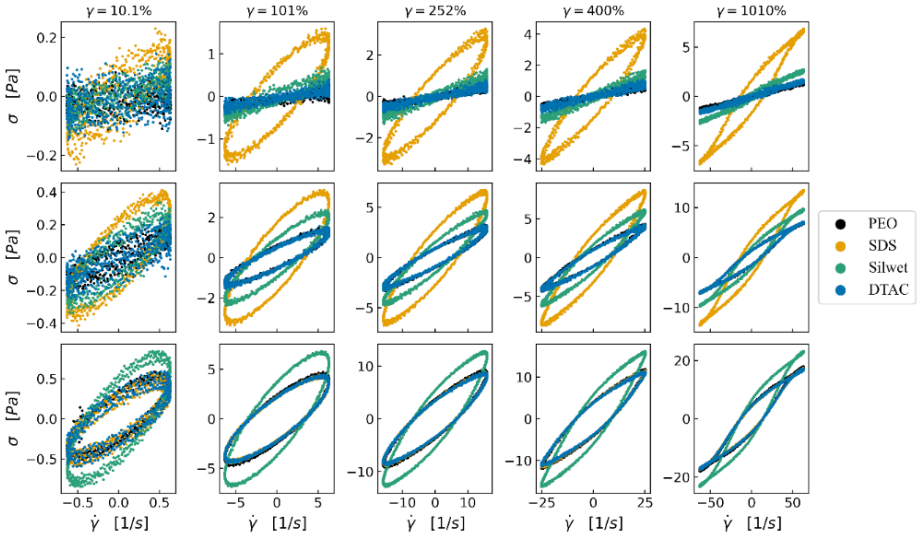

Fig. 5.4: Elastic (a) and viscous (b) Lissajous plots where stress is plotted as a function of strain and strain rate, respectively, for aqueous PEO solution and PEO solution with 0.1 M of three different surfactants: SDS, Silwet and DTAC at five different strains. In both series, rows correspond to PEO concentrations of 5, 10 and 15 gr/L from top to down, respectively.

5.4 Tribology

When two surfaces are sliding next to each other, to reduce the friction, one can add a lubricating fluid. Polymer solutions are widely used as lubricants in various fields of technology. The lubricating agent by forming a fluid film between the surfaces and keeping them apart reduces the friction. High molecular weight polymers are in particular good lubricating agents from two aspects: firstly because the addition of polymers to a solvent such as water increases the viscosity of the solution which in turn helps the formation of a more stale lubricating fluid film between surfaces. Secondly, high molecular weight polymers exhibit strong normal force responses while they are subject to high shear forces. The gap size between two sliding surfaces can be less than a millimetre in many practical situations for instance in our joints or engine parts of a car. Even a small sliding speed in such a small gap size results in high shear rates. When high molecular weight polymers are used as the lubricating fluid, at high shear rates the normal force response of the polymeric solution assists in keeping the surfaces apart, and therefore, reducing the friction. However, during the sliding process the polymeric solutions beside the large shear forces, are subject to large deformations. The flow behaviour and stability of polymeric fluid film under large deformation can have a serious impact on the frictional behaviour of the system.

Beside the rheological properties, the affinity of the lubricating solution to the surfaces can also play an important role in the lubrication process. It has been shown that the addition of surfactants to polymer solutions can enhance the lubricating properties of such solutions[27]. The presence of surfactants can improve surface coverage. Furthermore, the formation of polymer-surfactant complexes can result in a higher viscosity of the solution. However, it has been shown that the enhanced elastic response of a polymer-surfactant solution can trigger instabilities in the spreading of thin liquid films[17]. This has motivated us to study the lubricating behaviour of polymer surfactant

solutions where the rheological and interfacial properties of the solution and formation of stable liquid films play important roles.

In our tribology set-up a glass ball slides on three PDMS pins. While keeping the normal force constant, the sliding speed can vary within a broad range to measure the friction coefficient. In Fig. 5.5 the friction coefficient of aqueous solutions of PEO is presented as a function of sliding speed. As it can be seen by increasing the concentration of PEO from 1 to 10 gr/L, the friction coefficient at low sliding speeds decreases to almost half. However, the concentrations of 10 and 15 gr/L PEO demonstrate approximately similar frictional behaviour. By increasing the sliding speed the friction coefficient decreases for all the solutions. The slight increase of friction coefficient at high sliding speeds for all concentrations except for PEO is due to the hydraulic regime.

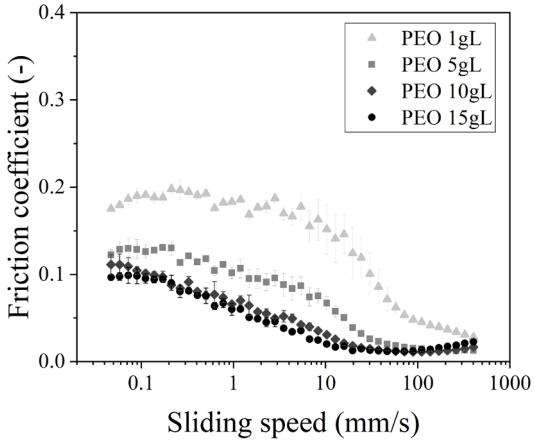

Fig. 5.5: Friction coefficient of PEO solutions as a function of sliding speed for different concentration of PEO.

To compare the frictional behaviour of polymer solutions with and without surfactants, we first have looked at the frictional behaviour of each surfactant separately. In Fig. 5.6 (left) friction coefficient of 0.1M solutions of SDS, Silwet and DTAC is presented. Although solutions of SDS and Silwet displayed similar behaviour, especially at low sliding speeds, DTAC had a

very high friction coefficient. Its friction was observed to be more than 0.4 at low sliding speeds and decreased to less than 0.1 at a sliding speed of 30 mm/s. On the right panel of Fig. 5.6 the friction coefficient is shown for solutions of 15gr/L PEO as a reference and solutions of 15 gr/L with 0.1M of surfactants. Although the frictional behaviour of all the solutions converged at high sliding speeds, they showed a marked difference at low speeds. The friction coefficient of PEO-SDS and PEO-Silwet was measured less than 0.1 at low speeds which mildly declined by increasing the sliding speed. PEO-DTAC solution, however, showed a large friction coefficient of 0.3 at the lowest sliding speed and sharply decreased to less than 0.1 at the speed of mm/s.

One should note that, as it was shown in the previous sections, the solutions of PEO and PEO-DTAC were observed to be rheologically identical. The significant difference in their frictional behaviour, therefore, is rooted in their affinity to the surface and how the presence of DTAC alters the interaction of PEO molecules with the surfaces involved in the friction.

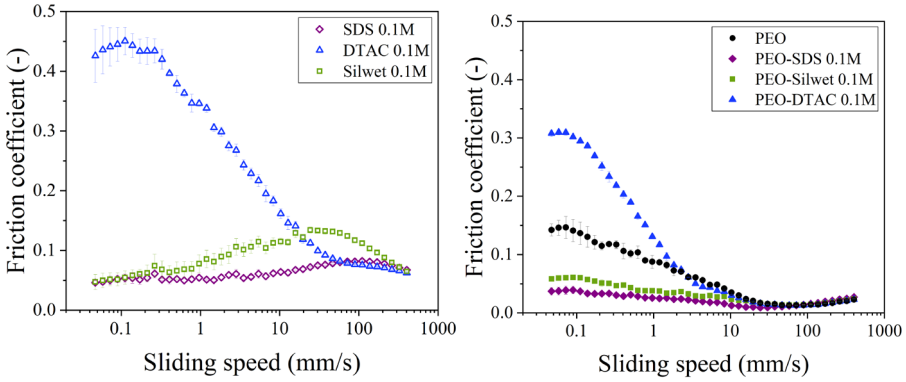

Fig 5.6: Friction coefficient of the (left) 0.1 M solutions of three surfactants; SDS, Silwet and DTAC (right) solution of 15gr/L PEO and solutions of 15gr/L PEO in combination with 0.1M of three surfactants (SDS, Silwet and DTAC).

5.5 Conclusion:

A thorough rheological characterization of PEO solutions of different concentrations with and without surfactants was provided. We have used various rheological methods including shear viscosity, amplitude and frequency sweep tests, and LAOS to probe the flow behavior and bulk properties of the solutions and quantitively compare the influence of various surfactants on the mentioned parameters. Three different surfactants; SDS, Silwet and DTAC as anionic, nonionic and cationic surfactants, respectively were selected to study their influence on the rheological parameters of the PEO solutions. At the concentrations of 1, 5 and 10 gr/L PEO, the solutions of PEO-SDS showed the strongest deviation from the pure PEO solution in all rheological tests due to the interaction of SDS molecules with PEO strands and formation of polymer-surfactant complexations. The interaction of molecules of Silwet with PEO appeared to have a weaker influence on the rheological properties compared to SDS at these concentrations. However, surprisingly at a concentration of 15 gr/L PEO viscosity of PEO-SDS solution was observed to be lower than the pure PEO solution. The same trend was observed in all rheological test for PEO-SDS solutions. In all the rheological measurements the solutions of PEO and PEO-DTAC were observed to have nearly identical behavior.

However, the friction behavior measured by tribology techniques was considerably different for PEO-DTAC solutions compared to the rest of the solutions. Frictional behavior of solutions of PEO 15gr/L with and without surfactants was investigated. Although SDS and Silwet were observed to enhance the lubricating properties of the PEO solution, the solution of PEO-DTAC showed a high friction coefficient. Especially, at low sliding speeds. Our results suggest that for polymer-surfactant solutions the surface properties of the solutions can dominate the lubricating dynamics.

This study showed that the polymer-surfactant system is more complex than what was expected and the molecular structure of the components and their concentrations can considerably change the bulk and surface properties of the solutions. These results bring forward new questions and suggest the need for

more detailed studies of such systems to understand the dynamics of surfactant-polymer interactions and their effect on the bulk rheology and formation of the lubricating films. For instance, the adsorption dynamics of polymers and surfactants on the surfaces need to be investigated or micelle formation in the present polymers and their interaction should be visualized to be able to suggest physical mechanisms predicting the bulk and surface properties. Our results are pertinent to many industrial applications such as food processing, hair and skincare where both polymer and surfactant are present or other multi-component systems with large deformation and nonlinear interface and nonlinear properties.

References:

1. Gupta, S. & Variyar, P. S. Chapter 12 - Guar Gum: A Versatile Polymer for the Food Industry. in *Handbook of Food Bioengineering* (eds. Grumezescu, A. M. & Holban, A. M. B. T.-B. for F. D.) 383–407 (Academic Press, 2018). doi:https://doi.org/10.1016/B978-0-12-811449-0.00012-8.

2. Katzbauer, B. Properties and applications of xanthan gum. *Polym. Degrad. Stab.* **59**, 81–84 (1998).

3. Jones, M. N. The interaction of sodium dodecyl sulfate with polyethylene oxide. *J. Colloid Interface Sci.* **23**, 36–42 (1967).

4. Bakshi, M. S., Sachar, S., Yoshimura, T. & Esumi, K. Association behavior of poly(ethylene oxide)–poly(propylene oxide)–poly(ethylene oxide) block copolymers with cationic surfactants in aqueous solution. *J. Colloid Interface Sci.* **278**, 224–233 (2004).

5. Fall, A. & Bonn, D. Shear thickening of Laponite suspensions with poly(ethylene oxide). *Soft Matter* **8**, 4645–4651 (2012).

6. Dastyar, P., Salehi, M. S., Firoozabadi, B. & Afshin, H. Influences of Polymer–Surfactant Interaction on the Drop Formation Process: An Experimental Study. *Langmuir* **37**, 1025–1036 (2021).

7. Tadokoro, H., Chatani, Y., Yoshihara, T., Tahara, S. & Murahashi, S. Structural studies on polyethers, [-(CH2)m-O-]n. II. Molecular structure of polyethylene oxide. *Die Makromol. Chemie* **73**, 109–127 (1964).

8. Ebagninin, K. W., Benchabane, A. & Bekkour, K. Rheological characterization of poly(ethylene oxide) solutions of different molecular weights. *J. Colloid Interface Sci.* **336**, 360–367 (2009).

9. Dinic, J., Zhang, Y., Jimenez, L. N. & Sharma, V. Extensional Relaxation Times of Dilute, Aqueous Polymer Solutions. *ACS Macro Lett.* **4**, 804–808 (2015).

10. Bergeron, V., Bonn, D., Martin, J. Y. & Vovelle, L. Controlling droplet deposition with polymer additives. *Nature* **405**, 772–775 (2000).

11. Goddard, E. D. Polymer/surfactant interaction—Its relevance to detergent systems. *J. Am. Oil Chem. Soc.* **71**, 1–16 (1994).

12. Martínez Narváez, C. D. V., Mazur, T. & Sharma, V. Dynamics and extensional rheology of polymer-surfactant association complexes. *Soft Matter* **17**, 6116–6126 (2021).

13. Minatti, E. & Zanette, D. Salt effects on the interaction of poly(ethylene oxide) and sodium dodecyl sulfate measured by conductivity. *Colloids Surfaces A Physicochem. Eng. Asp.* **113**, 237–246 (1996).

14. Dastyar, P., Salehi, M. S., Firoozabadi, B. & Afshin, H. Influences of Polymer-Surfactant Interaction on the Drop Formation Process: An Experimental Study. *Langmuir* **37**, 1025–1036 (2021).

15. Nagarajan, R. Thermodynamics of nonionic polymer—micelle association. *Colloids and Surfaces* **13**, 1–17 (1985).

16. Sharma, S. & Kamil, M. Studies on the Interaction Between Polyethylene Oxide and Cationic Gemini/Conventional Surfactants. *Indian Chem. Eng.* **60**, 72–87 (2018).

17. Motaghian, M., van Esbroeck, T., van der Linden, E. & Habibi, M. Interfacial instabilities in Marangoni-driven spreading of polymer solutions on soap films. *J. Colloid Interface Sci.* **612**, 261–266 (2021).

18. Ambrose, R. J. *Surfactants and interfacial phenomena—second edition, by Milton J. Rosen, John Wiley & Sons, Inc., New York, 1989, 431 pp. price: $49.95. Journal of Polymer Science Part C: Polymer Letters* vol. 27 (John Wiley & Sons, Ltd, 1989).

19. Aguiar, J., Carpena, P., Molina-Bolívar, J. A. & Carnero Ruiz, C. On the determination of the critical micelle concentration by the pyrene 1:3 ratio method. *J. Colloid Interface Sci.* **258**, 116–122 (2003).

20. Han, F., Chen, Y., Zhou, Y. & Xu, B. A Surface Rheological Study of Silwet L-77 Surfactant at the Air/Water Interface. *J. Dispers. Sci. Technol.* **33**, 396–402 (2012).

21. Janků, J., Bartovská, L., Soukup, J., Jursík, M. & Hamouzová, K. Densitysity and surface tension of aqueous solutions of adjuvants used for tank-mixes

with pesticides. *Plant, Soil Environ.* **58**, 568–572 (2012).

22. Šarac, B. & Bešter-Rogač, M. Temperature and salt-induced micellization of dodecyltrimethylammonium chloride in aqueous solution: A thermodynamic study. *J. Colloid Interface Sci.* **338**, 216–221 (2009).

23. Perger, T. M. & Bešter-Rogač, M. Thermodynamics of micelle formation of alkyltrimethylammonium chlorides from high performance electric conductivity measurements. *J. Colloid Interface Sci.* **313**, 288–295 (2007).

24. Ebagninin, K. W., Benchabane, A. & Bekkour, K. Rheological characterization of poly(ethylene oxide) solutions of different molecular weights. *J. Colloid Interface Sci.* **336**, 360–367 (2009).

25. Ewoldt, R. H., Hosoi, A. E. & McKinley, G. H. New measures for characterizing nonlinear viscoelasticity in large amplitude oscillatory shear. *J. Rheol. (N. Y. N. Y).* **52**, 1427–1458 (2008).

26. Ewoldt, R. H., Winter, P., Maxey, J. & McKinley, G. H. Large amplitude oscillatory shear of pseudoplastic and elastoviscoplastic materials. *Rheol. Acta* **49**, 191–212 (2010).

27. SUŁEK, M. W. & JEDYNAK, R. the Effect of the Formation of Polymer /Surfactant Complexes on Selected Tribological Properties of Their Aqueous Solutions. *Tribologia* **281**, 117–122 (2018).

Chapter 6

General discussion

6.1 Main findings:

In this thesis, we have studied the spreading behaviour of various liquids using a unique configuration of "droplet on a soap film". Since a soap film is a thin liquid sheet suspended in the air, it provides us with the advantage to study the spreading of a deposited droplet in the absence of solid or deep liquid boundaries. With four experimental chapters presented in this thesis, we aim to provide a deeper understanding of the influence of various parameters on the spreading dynamic in this specific configuration.

We started our work by clarifying the configuration of the droplet and the soap film. In **Chapter 2** we show that when a droplet is deposited on a soap film, it forms a new layer in the centre of the initial film and spread. This reduces the contact area between the droplet and the soap film to only a circular rim around the droplet. Considering the small contact area and the time scale of our experiments, even for the slowest spreading, we have shown that the Pe number is orders of magnitude larger than 1 and diffusion can be neglected. Therefore, the droplet is not contaminated by diffusion of surfactants from the soap film. The sequence of images in Fig. 6.1 shows a droplet on a soap film a few milliseconds after the deposition. In the first image, the incident of destabilization of the soap film can be seen which grows in the following frames and lead to the full rupture of the soap film. As it can be seen the well-defined boundary of the droplet and the soap film can be recovered after the rupture of the soap film and the droplet can be retrieved.

Fig. 6.1: Droplet of Silwet L77 (concentration of 80 CMC) deposited on the soap film of SDS 0.01M. after rupture of the soap film the droplet retracts due to its surface tension. These images substantiate that in system, during the spreading the droplet and the soap film do not mix and the droplet can be retrieved after the initial spreading by the puncture of the soap film. Using this configuration the extensional flow of liquids can be studied in the absence of high shear forces caused by solid or liquid substrates.

In the same chapter, we discuss the influence of one of the most important parameters in the spreading problem; The surface tension gradient. The effect of the volume of the droplet and the size of the soap film were also studied in this chapter.

In **Chapter 3**, we take a closer look at the importance of the molecular structure and the type of surfactants in the spreading problem. Therefore, we studied the spreading behaviour of an ensemble of surfactant solutions with very similar surface tension and viscosity but different molecular structures of surfactants. We show that when the surface tension gradient is not relatively large, the effect of interactions between surfactants in the droplet and the soap film becomes more pronounced.

In contrast with previous chapters where the droplet was composed of low viscous (similar to water) surfactant solution, in **Chapter 4**, we investigate the more complex multi-component liquids with high viscosities. To probe the effect of viscosity on the spreading, we added polymer to the droplet in different concentrations. We observed a novel instability in the spreading of polymer-surfactant solutions above the entanglement concentration of polymer. For the stable cases, we provide a model for evolution of the spreading area by scaling viscous forces with the surface tension gradient. It should be noted that the presence of polymers, beside increasing the viscosity, induces viscoelastic characteristics to the solution. We explain that the instabilities are triggered by the enhanced elastic response of the polymers after the entanglement concentration.

But how the interaction of polymer and surfactants can influence the rheological properties of the polymer-surfactant solutions? In **Chapter 5**, we provide a comprehensive overview of several rheological parameters of polymer solutions in combination with various surfactants. Eventually, we discuss the lubricating properties of polymer-surfactant solutions and we show how the surface affinity of the solutions can influence the film formation and tribological behaviour of such solutions. A schematic overview of the chapters is provided in Fig. 6.2.

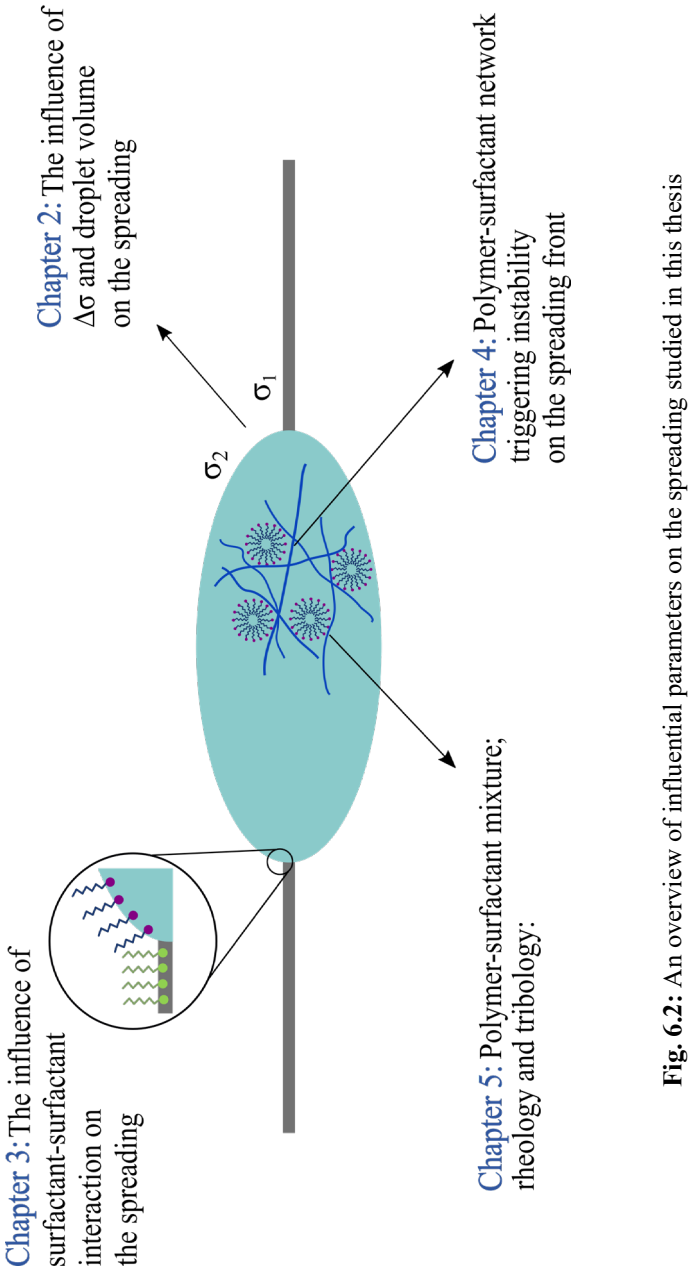

Fig. 6.2: An overview of influential parameters on the spreading studied in this thesis

6.2 Influential parameters in liquid spreading

6.2.1 Surface tension and the effect of inertia

Many parameters can influence the spreading of a droplet over different surfaces which we strive to control in many applications or experiments. Here, by the means of soap films, we are aiming to limit the varying parameters in each set of experiments, thus we can study the influence of each parameter separately. We started our journey by investigating the spreading behaviour of simple solutions. In **Chapter 2** we discussed the spreading behaviour of aqueous surfactant solutions with low viscosities similar to water. In such a system, Reynolds number was orders of magnitude larger than 1, therefore, the effect of viscosity was negligible. Additionally, the surfactants used in the experiments (SDS and ALS) had a simple molecular structure and the surfactants used in the droplet and the soap film were either the same or very similar. The influence of the surfactant-surfactant interaction thereby, could be dismissed.

By varying the concentration of the surfactant in the droplet we were able to change the magnitude of the surface tension gradient and study how it affects the evolution of the spreading front in time. We found that in all cases the radius of the spreading droplet grows in time with a power-law manner ($R \sim t^{\alpha}$). The exponent α however, displayed a strong dependency on the surface tension difference between the droplet and the soap film ($\Delta\sigma = \sigma_{soap} - \sigma_{drop}$). Interestingly, for the droplets with $\Delta\sigma < 0$ we still observed a spreading although it was relatively slow with $\alpha \sim 0.1$ which hadn't been reported before to the best of our knowledge. In this set up the surface tension difference was not favouring the spreading, however, on the contact line, Laplace pressure induced by the curvature at the rim of the droplet overweighs the hydrostatic pressure inside the soap film. The imbalanced pressure at the contact line causes a slow-spreading which follows Tanner's spreading law.

For the cases that the droplet had a lower surface tension than the soap film ($\Delta\sigma > 0$), the spreading was observed to be considerably faster with α

increasing from 0.4 to nearly 1 by the increment of $\Delta\sigma$. As it was explained in **Chapter 1**, a power-law behaviour is commonly observed in studies of spreading of a droplet on different surfaces[1–3] and a range of exponents has been suggested based on different scaling arguments. For liquid-liquid spreading the exponent of 1/2 for thin liquid substrates[4] and 3/4 for spreading on a deep liquid bath[5–7] are well known to the reader. Nevertheless, the aforementioned exponents are derived based on the scaling of the surface tension gradient with the viscous stress in both liquids. Therefore, they won't stay valid for our case here, with the inertia dominating the viscous effect. In **Chapter 2** we proposed to scale the surface tension gradient with the inertial term for our system as follows:

$$(\Delta\sigma/_R)\sim\rho u^2$$

Where R is the radius of the spreading droplet, ρ the density and u the characteristic velocity. This scaling argument results in $R\sim t^{2/3}$ which was within the range of the exponents we obtained experimentally. In **Chapter 3** we showed that this general trend can be seen in the spreading behaviour of a variety of surfactants and it is not limited to specific simple surfactants used previously. However, modifications will be needed due to the influence of surfactant-surfactant interactions in the droplet and the soap film. We will discuss this matter later in this chapter.

6.2.2 Effect of volume

Size of a droplet can play an important role in the spreading process. Large droplets tend to deform under the gravitational forces and take a pancake shape. For a droplet of liquid, the competition between the Laplace pressure caused by the surface tension and the hydrostatic pressure caused by gravity is well depicted in the capillary length[8]. If we put Laplace pressure ($\frac{\sigma}{L}$ where L is the relative length scale of the system) equal to the hydrostatic pressure

($\rho g L$ with ρ being the density of the liquid ang g the gravity constant) we will arrive at the relation for capillary length in a system as follows:

$$\frac{\sigma}{L} \sim \rho g L \qquad \rightarrow \qquad L_{ca} = \sqrt{\frac{\sigma}{\rho g}}$$

At length scales larger than the capillary length, the effect of gravity is no longer negligible. In **Chapter 2** we showed that the spreading exponent was similar for the spreading of droplets with characteristic size below and above the capillary length. However, the average velocity of the spreading increased by increasing the size of the droplet below the capillary length. Above L_{ca}, increasing the size of the droplet had neither significant effect on the average velocity nor on the spreading exponent.

6.2.3 Surfactant-surfactant interaction

In **Chapter 2** we focused on the influence of the surface tension gradient on the spreading, therefore, the type of the surfactants was kept similar in the soap film and the droplet. In **Chapter 3** we aimed to investigate the influence of surfactant-surfactant interaction on the spreading behaviour. To do so, while keeping the surface tension of the droplets similar we changed the type of the surfactant in the droplet to study how the interaction of the surfactants in the droplet and the soap film will affect the spreading dynamics. We used a broad variety of surfactants to cover different types of surfactants, especially, to compare those with the different ionic states.

The unexpected behaviour of surfactant solutions on different surfaces has been frequently addressed in the literature[4,9–11] in the past few years. For instance, the extraordinary rapid spreading of some super-spreaders such as AOT on solid surfaces is still not fully understood[12,13]. Another example is the exceptionally large contact angle of a number of surfactants (e.g. CTAB) on hydrophobic surfaces which Bera et. al[10] suggested a modification to the Zisman plot[14] is needed to correctly predict their contact angle. In the case of

liquid-liquid interfaces[15], with surfactants present in one[16] or both phases[17], conditions are even more complex since the diffusion and the adsorption kinetics of the surfactants[18] in both liquids are also needed to be taken into account. However, in our geometry (droplet on a soap film) the effect of diffusion can be neglected and the influence of adsorption kinetics can be decoupled from the effect of molecular interactions simply by looking at the dynamic surface tension of the solutions instead of the equilibrium surface tension.

Our findings in **Chapter 3** suggest that the changes in the spreading exponent upon varying $\Delta\sigma$ follow the same trend irrespective of the type of the surfactants. As we also observed in **Chapter 2**, almost in all cases, alpha stays approximately about 0.1 for $\Delta\sigma < 0$ and by increasing the surface tension difference between the droplet and the soap film to positive values, alpha increases and reaches above 1. Hence $\Delta\sigma$ remains a good indicator of the overall trend of alpha. The transition of exponent alpha from 0.1 to above 1 with increasing $\Delta\sigma$ has also been reported for spreading of oil droplets on a surfactant-laden deep pool[19]. However, we here observed a few exceptions; for example, the droplets of an aqueous solution of OTAB showed a rapid spreading on the soap film of SDS, with an exponent of 0.49 despite its large negative $\Delta\sigma$ of -38 mN/m. Another exception was the extraordinary rapid spreading of the solutions with high concentrations of AOT and Silwet-L77 with spreading exponents as high as 2 and 1.5, respectively.

Furthermore, near the region of $\Delta\sigma \sim 0$ the differentiation between slow (Laplace regime) and rapid (Marangoni regime) was not as clear as it was observed in **Chapter 2**. In a few cases, although the surface tension difference was not favouring the spreading, we observed rapid spreading, in contrast, for a few other cases we only observed slow spreading while $\Delta\sigma > 0$ and we expected a rapid spreading with an alpha larger than 0.1.

We have proposed in **Chapter 3** that for an accurate quantitative prediction of spreading exponent beside surface tensions of interfaces more understanding of the molecular level interaction of the surfactants at the contact areas is needed. The size of the surfactants, shape and length of their

hydrophobic tail, ionic state, and affinity of different surfactants to each other are among those parameters that might be influential.

6.2.4 Viscosity

In **Chapters 2** and **3** for the sake of simplicity, we studied the spreading of surfactant solutions with low viscosities (as low as the viscosity of water) thus the viscous effect could be neglected and the influence of surface tension gradient could be singled out. In **Chapter 4** we look at the role of the other crucial force involved in many spreading problems; viscous force. In order to investigate the role of the viscous effect, we added polymers to the droplets at different concentrations while the concentration of the surfactant was kept constant in the droplets. Therefore, we had droplets with similar surface tension and various viscosities.

We observed that droplets containing polymer spread in two regimes: an initial lag phase where the radius of the droplet grew very slowly in time followed by a fast regime leading to full spreading of the droplet. The duration of the lag phase increased by increasing the concentration of the polymer and reach to even more than 400 ms for the highest concentration of polymer in our experiments (70 gr/L PEO, Mw~ 3×10^5 amu). Interestingly, above a critical concentration of the polymer the spreading front was no longer stable, we will discuss these instabilities in detail later. For the stable cases, after the lag phase, the radius of the droplet grew linearly in time in the fast spreading regime resulting in $\alpha \sim 1$. By increasing the concentration of the polymer, α didn't change considerably and remained approximately 1.

As we explained in **Chapter 4**, since the droplet in our geometry is suspended in the air and is not in contact with any solid or liquid boundaries except for the soap film, the velocity gradient through the thickness of the droplet is nearly zero. Because of the symmetry, the fluid velocity at the centre of the droplet is zero and increases radially to reach its maximum at the spreading front. In this scenario the radial gradient of the velocity causes the viscous

force, resisting the spreading. The schematic in Fig. 6.3 illustrates how the spreading velocity changes along the radius of the droplet. By scaling surface tension gradient ($\Delta\sigma/_R$) as the driving force of the spreading with the viscous stress along the radius on the droplet ($\eta\frac{V}{R}$, η: viscosity of the spreading liquid) we will arrive at $\frac{\Delta\sigma}{R} \propto \eta\frac{V}{R}$ which results in $R{\sim}t$. Our experimental result in **chapter 4** showed a good agreement with the scaling argument. The exponent alpha we observed for the stable spreading fronts was approximately 1 for droplets with different polymer concentrations.

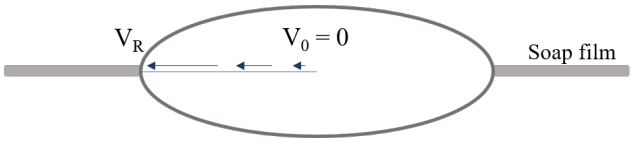

Fig 6.3: Schematic of the position of a spreading droplet in the center of a soap film. Because of the symmetry the spreading velocity is zero at the center of the droplet and it radially increases till it reaches its maximum at the spreading front.

One should note that although the exponent alpha we observed for highly viscous droplets in **Chapter 4** was similar to the spreading exponent of the fastest spreading we observed in **Chapter 2** and **3**, their dynamics are significantly slower with a very slow average front speed. This shows that considering solely the spreading exponent to evaluate the speed of spreading dynamics can be misleading and other factors such as time scales of the spreading or average velocity should be considered as well. In Fig. 6.4, we have provided an overview of all the spreading exponents we have experimentally observed throughout this thesis.

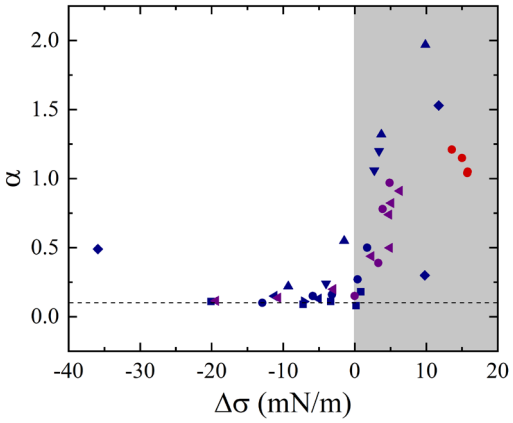

Fig 6.4: Spreading exponent (α) as function of surface tension difference between the droplet and the soap film for various spreading conditions discussed throughout the whole thesis. Symbols in purple represent the spreading exponents of droplet with different surface tension discussed in chapter 2, navy blue symbols show α of spreading solutions with different types of surfactants presented in chapter 3 and red symbols show the spreading exponents of droplet containing polymer which was investigated in chapter 4. For more details, see the corresponding chapters.

6.2.5 Rheology and elastic response

In **Chapter 4** we observed when the concentration of the polymer in the spreading droplet is increased, above a critical level, the spreading front destabilises into a daisy shape pattern. These instabilities were observed for different molecular weights of the polymer and various combinations of polymer-surfactants. However, the critical concentration varied for each case. Strikingly, we showed in **Chapter 4** that the critical concentration for the onset of the instabilities coincided precisely with the entanglement concentration of the polymers in that specific system.

The rheological characterisation of the samples indicated that the presence of the surfactants in the solution and the way they interact with the polymer strands at the molecular level, can strongly change the rheological properties

of the solutions[20]. For instance, it is well known that Sodium dodecyl sulphate (SDS) molecules tend to align next to the strands of polyethylene oxide and cause the increased viscosity of the polymer-surfactant ternary solutions[21–23]. In **Chapter 4** we focused on the entanglement concentration of such solutions and their viscous and elastic modulus behaviour below and above the entanglement concentration.

We introduced an elasto-capillary length scale as $l_{c-el} \sim \frac{\sigma}{G'(\omega)}$ where G' was the elastic modulus of the polymeric solution. As it can be seen l_{c-el} is inversely proportionate with G' and since G' decreases in time, consequently, l_{c-el} grows in time. We proved that the growth rate of the elasto-capillary length scale is an excellent measure to predict the onset of the instabilities. We showed that the enhanced elastic response of the polymer solution above the entanglement concentration dramatically influences the growth rate of l_{c-el} which leads to instability. Therefore, we suggest that beside the conventional parameters such as viscosity, surface tension gradient, etc., which we explained in **Chapter 2** and **3,** the growth rate of the elasto-capillary length scale also needs to be added to the parameter space of the spreading problem. This parameter can predict whether the spreading will take place stably or the spreading front will undergo instabilities.

As it was mentioned before, the molecular interactions between polymer and surfactants can have a detrimental influence on the rheological properties of polymer-surfactant solutions and consequently, on the spreading[24] or film formation behaviour of such solutions. In **Chapter 4** we observed that the entanglement concentration of polymer solutions[25] can be significantly different in the presence of different surfactants. For instance, in the solution of PEO and SDS, the entanglement of polymer strands was observed to occur at a much lower concentration of polymer (7gr/L) compared to the solutions of PEO and AOT (18gr/L of PEO). In **Chapter 5** we are taking a closer look at the macroscopic manifestation of these micro-scale interactions. We used a systematic approach to compare polymeric solutions with and without surfactants and also different combinations of polymer-surfactant. For polymer, we chose PEO because of its simple linear molecular structure[26] and

also because we had studied its spreading behaviour thoroughly earlier in this thesis. For surfactants, we chose SDS, Silwet L77 and DTAC (Dodecyltrimethylammonium) which are anionic, non-ionic and cationic surfactants, respectively. The aforementioned surfactants are widely used in industry, often in combination with organic or synthesized polymers.

As it was also proved by previous studies, SDS molecules interacts with PEO strands and form polymer-surfactant complexes which lead to an increase in the viscosity of the polymer-surfactant ternary solution[22,27,28]. On the contrary, non-ionic[29] and cationic surfactants have been shown to interact considerably less with PEO strands[30–32].

In **Chapter 5** we present a thorough rheological characterization of PEO with mentioned surfactants with different ionic states. Our results of viscosity and elastic and viscous modulus corroborate excellently with the previous works on similar systems[22,25,27]. We also reported the behaviour of PEO – surfactant solutions under large amplitude oscillatory shear (LAOS) tests which was not done before for such systems to the best of our knowledge. LAOS test was particularly selected since in the spreading scenario or many industrial applications, polymer-surfactant solutions undergo large deformations.

The presence of SDS has the strongest influence on the rheological behaviour of PEO solutions whereas all rheological aspects of PEO-DTAC and aqueous PEO solutions were identical. We used this opportunity to study also the tribological properties of these solutions. Polymer- surfactant solutions have been widely used for lubricating purposes in the industry. During the lubricating process, both rheological properties of a lubricant and its affinity to involved surfaces play important roles. We found this scenario intimately close to the spreading problem which in both, an interplay between the interfacial and rheological properties of a complex liquid governs the main dynamics. Earlier in this thesis, we have studied the spreading behaviour of liquids by changing the interfacial properties of the spreading liquid while keeping the rheological parameters intact (**Chapters 2 and 3**) or by keeping the interfacial properties the same and changing the rheological parameter (**Chapter4**). We took the same approach in **Chapter 5**.

Aqueous PEO solutions and PEO-DTAC solutions had identical rheological parameters at different concentrations of polymer, however, their surface properties were significantly different. The presence of DTAC molecules reduces the surface tension of the PEO-DTAC solutions and alter their surface chemistry. Strikingly, we noticed that the lubricating behaviour of these pairs can be drastically different. Our results suggest that the affinity of lubricating liquid to the surfaces involved in the tribology system can be as important as the rheological characteristics of the lubricant. Here we once again emphasize that for understanding and modelling the governing dynamics of the systems involving films of complex liquids, the rheological response of the liquid should be taken into account in close combination with the interfacial response of the liquid.

6.3 Conclusion and outlook:

Fluid mechanics problems are in essence, boundary condition problems. The experimental set-up we have used in this work (droplet on a soap film) provided us with a unique boundary condition to study the spreading behaviour of liquids. Throughout the thesis, we explained and modelled the role of various parameters on the spreading dynamics, however, there were challenges and limitations. For instance, we used only a high-speed camera with a conventional lens in a tilted angle to track the radius of the spreading front. Therefore, we were not able to measure the thickness of the spreading area at any location. We suggest using an interferometry setup to investigate the thickness of the droplet during the spreading which enables us to have a more accurate look into the flow profile of the spreading droplet. Additionally, such a setup can also be used to study the nature of the connection between the droplet and the soap film. Another suggestion is to increase the lifetime of the soap film by adding polymer and then study the influence of evaporation on the spreading droplet in such a system.

In conclusion, we have covered the influence of a few crucial parameters on the spreading of a droplet on the soap film in this thesis. For low viscous

liquids the effect of viscosity on spreading can be neglected. When surface tension gradient is not favouring the spreading we can still observe a slow-spreading which was driven by Laplace pressure. When the surface tension gradient was positively contributing to the spreading, it could be scaled with the inertial term which resulted in a power-law dependency of the radius of the spreading front on time with an exponent of 2/3.

For highly viscous liquids, however, the effect of viscosity was dominant and the inertia could be neglected. Scaling of the surface tension gradient with the viscous forces acting along the radius of the droplet results in a linear dependency of the R on time. It should be noted that although the spreading exponent in the viscous scaling is higher than the inertial scaling, the dynamics are much slower in the viscous regime. To predict the state of a spreading (viscous/inertial) we advise not only focusing on the value of the spreading exponent but also the average velocity and time scales of each spreading. Eventually, the emergence of instabilities in the viscous droplets containing high concentrations of the polymer shows the importance of elastic response in destabilising the spreading front.

Our results in this thesis can be pertinent to many industrial applications involving the rapid spreading of simply surfactant solutions or complex liquids containing polymers. The spreading geometry that we introduced here (drop on the soap) can be used to study the extensional behaviour of a variety of liquids as far as their surface tension allows for spreading. Furthermore, a soap film can be used to stretch liquids and form smooth liquid films with micrometer thickness. In particular for the formation of thin polymer films that can be used for instance in the coating industry. The current alternatives such as electrospinning usually involve high shear rates and large forces that can result in the breakage of polymer chains. One suggestion can be using relatively large soap films to control the final thickness of the deposited droplet.

References:

1. Hoult, D. P. Oil Spreading on the Sea. *Annu. Rev. Fluid Mech.* **4**, 341–368 (1972).

2. Fraaije, J. G. E. M. & Cazabat, A. M. Dynamics of spreading on a liquid substrate. *J. Colloid Interface Sci.* **133**, 452–460 (1989).

3. Camp, D. W. & Berg, J. C. The spreading of oil on water in the surface-tension regime. *J. Fluid Mech.* **184**, 445–462 (1987).

4. Jensen, O. E. & Grotberg, J. B. Insoluble surfactant spreading on a thin viscous film: Shock evolution and film rupture. *J. Fluid Mech.* **240**, 259–288 (1992).

5. Huh, C., Inoue, M. & Mason, S. G. Uni-directional spreading of one liquid on the surface of another. *Can. J. Chem. Eng.* **53**, 367–371 (1975).

6. Bergeron, V. & Langevin, D. Monolayer Spreading of Polydimethylsiloxane Oil on Surfactant Solutions. *Phys. Rev. Lett.* **76**, 3152–3155 (1996).

7. Koldeweij, R. B. J., van Capelleveen, B. F., Lohse, D. & Visser, C. W. Marangoni-driven spreading of miscible liquids in the binary pendant drop geometry. *Soft Matter* **15**, 8525–8531 (2019).

8. Widom, B. *Capillarity and Wetting Phenomena: Drops, Bubbles, Pearls, Waves* **Capillarity and Wetting Phenomena: Drops, Bubbles, Pearls, Waves** , Pierre-Gilles de Gennes , Françoise Brochard-Wyart , and David Quéré (translated from French by Axel Reisinger) Springer-Verlag, New York, 2004. $69.95 (291 pp.). ISBN 0-387-00592-7. *Phys. Today* **57**, 66–67 (2004).

9. Nikolov, A. D. *et al.* Superspreading driven by Marangoni flow. *Adv. Colloid Interface Sci.* **96**, 325–338 (2002).

10. Bera, B. *et al.* Antisurfactant (Autophobic) Behavior of Superspreader Surfactant Solutions. 13–17 (2021) doi:10.1021/acs.langmuir.1c00475.

11. Bera, B. *et al.* Counteracting Interfacial Energetics for Wetting of Hydrophobic Surfaces in the Presence of Surfactants. *Langmuir* **34**, 12344–12349 (2018).

12. Hoffman, H., Sijs, R., De Goede, T. & Bonn, D. Controlling droplet

deposition with surfactants. *Phys. Rev. Fluids* **6**, 1–12 (2021).

13. Aytouna, M., Bartolo, D., Wegdam, G., Bonn, D. & Rafaï, S. Impact dynamics of surfactant laden drops: Dynamic surface tension effects. *Exp. Fluids* **48**, 49–57 (2010).

14. Fox, H. W. & Zisman, W. A. The spreading of liquids on low energy surfaces. I. polytetrafluoroethylene. *J. Colloid Sci.* **5**, 514–531 (1950).

15. Iasella, S. V *et al.* Flow regime transitions and effects on solute transport in surfactant-driven Marangoni flows. *J. Colloid Interface Sci.* **553**, 136–147 (2019).

16. Clay, M. A. & Miksis, M. J. Effects of surfactant on droplet spreading. *Phys. Fluids* **16**, 3070–3078 (2004).

17. Matar, O. K. & Craster, R. V. Dynamics of surfactant-assisted spreading. *Soft Matter* **5**, 3801–3809 (2009).

18. Sharma, R. *et al.* Quasi-Immiscible Spreading of Aqueous Surfactant Solutions on Entangled Aqueous Polymer Solution Subphases. *ACS Appl. Mater. Interfaces* **5**, 5542–5549 (2013).

19. Deodhar, S., Thampi, S. P. & Basavaraj, M. G. Drops spreading on fluid surfaces: Transition from Laplace to Marangoni regime. *Phys. Rev. Fluids* **6**, 1–8 (2021).

20. Dastyar, P., Salehi, M. S., Firoozabadi, B. & Afshin, H. Influences of Polymer–Surfactant Interaction on the Drop Formation Process: An Experimental Study. *Langmuir* **37**, 1025–1036 (2021).

21. Chari, K., Antalek, B., Lin, M. Y. & Sinha, S. K. The viscosity of polymer–surfactant mixtures in water. *J. Chem. Phys.* **100**, 5294–5300 (1994).

22. Smitter, L. M., Guédez, J. F., Müller, A. J. & Sáez, A. E. Interactions between Poly(ethylene Oxide) and Sodium Dodecyl Sulfate in Elongational Flows. *J. Colloid Interface Sci.* **236**, 343–353 (2001).

23. Minatti, E. & Zanette, D. Salt effects on the interaction of poly(ethylene oxide) and sodium dodecyl sulfate measured by conductivity. *Colloids Surfaces A Physicochem. Eng. Asp.* **113**, 237–246 (1996).

24. Wang, X., Chen, L., Bonaccurso, E. & Venzmer, J. Dynamic wetting of hydrophobic polymers by aqueous surfactant and superspreader solutions. *Langmuir* **29**, 14855–14864 (2013).

25. Ebagninin, K. W., Benchabane, A. & Bekkour, K. Rheological characterization of poly(ethylene oxide) solutions of different molecular weights. *J. Colloid Interface Sci.* **336**, 360–367 (2009).

26. Tadokoro, H., Chatani, Y., Yoshihara, T., Tahara, S. & Murahashi, S. Structural studies on polyethers, [-(CH2)m-O-]n. II. Molecular structure of polyethylene oxide. *Die Makromol. Chemie* **73**, 109–127 (1964).

27. Martínez Narváez, C. D. V., Mazur, T. & Sharma, V. Dynamics and extensional rheology of polymer-surfactant association complexes. *Soft Matter* **17**, 6116–6126 (2021).

28. Nagarajan, R. Thermodynamics of nonionic polymer—micelle association. *Colloids and Surfaces* **13**, 1–17 (1985).

29. Sharma, R., Varade, D. & Bahadur, P. Mixed Micelles of Triton X-100 and Sodium Dodecyl Sulfate and Their Interaction with Polymers. *J. Dispers. Sci. Technol.* **24**, 53–61 (2003).

30. Bakshi, M. S., Sachar, S., Yoshimura, T. & Esumi, K. Association behavior of poly(ethylene oxide)–poly(propylene oxide)–poly(ethylene oxide) block copolymers with cationic surfactants in aqueous solution. *J. Colloid Interface Sci.* **278**, 224–233 (2004).

31. Sharma, S. & Kamil, M. Studies on the Interaction Between Polyethylene Oxide and Cationic Gemini/Conventional Surfactants. *Indian Chem. Eng.* **60**, 72–87 (2018).

32. Tajik, B., Sohrabi, B., Amani, R. & Hashemianzadeh, S. M. The study of polymer–surfactant interaction in catanionic surfactant mixtures. *Colloids Surfaces A Physicochem. Eng. Asp.* **436**, 890–897 (2013).

Appendix (A)

Determination of soap film thickness

When a droplet of ALS solution is deposited on a soap film of SDS solution, the coalescence of the droplet and soap film initially triggers a very fast mechanical wave. This propagating wave is different and much faster than the spreading front studied in detail in the main body of the paper. The latter one is a front of a stretching droplet while the first one is a propagating wave moving on the initial soap film. A sequence of images in Fig. A1 shows the mechanical wave propagating over the original soap film. The radius of the wave (R_W) was measured in time for four different experiments. Results are shown in Fig. A2. The average speed of the mechanical waves can be determined from the slopes of linear fits in Fig. A2.

The characteristic speed v of a mechanical wave on an elastic sheet under tension is defined by $v = \sqrt{\frac{\sigma}{\lambda}}$ where σ is the surface tension of the film and λ is the mass per unit area of the sheet, which can be defined as $\lambda=\rho h$, where ρ is the density and h is the thickness of the sheet. In our experiments, we have a fluid sheet (made of SDS 0.005 M) with a surface tension of σ~47 mN/m

and density of ρ=1000 kg/m^3 (i.e., the density of water). Substituting these parameters and the average speeds of the mechanical waves into the above equation results in a value of the thickness of the soap film for each experiment. The results for 4 different experiments are summarized in Table S1. The average thickness of the soap film is about 3.5 μm.

To check the accuracy of the soap film thickness measurements using the above method, we have also measured the thickness of the soap film using Taylor-Culick equation[1]. Taylor-Culick model is based on measuring the retraction speed of the soap film after bursting. When a suspended liquid film, bursts, based on its retraction speed, inertia dominated or viscous dominated regimes can explain the dynamics of the retracting film[2-4]. For liquids with low viscosity like the SDS solution used in our experiments, the inertial regime applies. In this regime after rupture, the liquid film retracts with a constant speed obtained by balancing the capillary and inertial terms and called Taylor-Culick speed ($U_T = \sqrt{\frac{2\sigma}{\rho h}}$) where σ, ρ and h are the surface tension, density and the thickness of the soap film respectively. Although this equation is very similar to the previous one but the mechanisms are different. Sequence of photos in Fig. S3 shows a soap film of 0.005 M SDS, 1, 2 and 3 ms after bursting. A retraction speed of 6.4 m/s was obtained by tracking the position of the edge using a high-speed imaging with 7000 frame per second. Taylor-Culick formula predicts a thickness of 2.5 μm, for this soap film in a good agreement with results of the previous method.

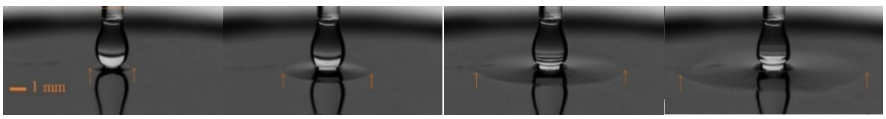

Fig A1: Immediately after coalescence of the droplet with the soap film a fast mechanical wave travels over the initial soap film. Images from left to right are captured at 1, 1.5, 2 and 2.5 ms after droplet touches the soap film.

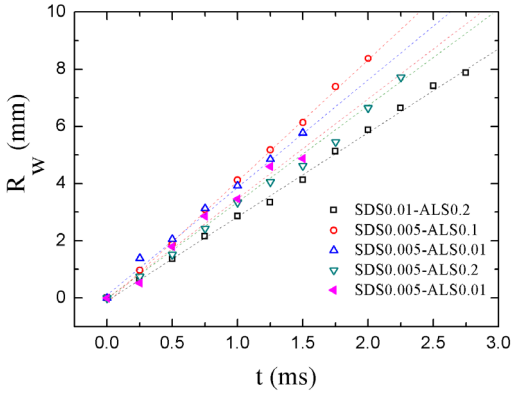

Fig. A2: Radius of the mechanical wave as a function of time for experiments with droplets of ALS solution with different concentrations on a soap film of SDS 0.005 M.

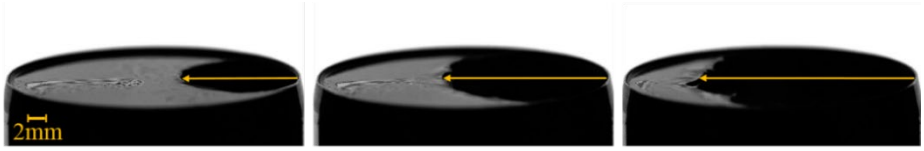

Fig. A3: Bursting of a soap film of 0.005 M SDS. From left to right the images are captured 1, 2 and 3 ms after bursting.

Table S1. Average velocity of the mechanical wave calculated by fitting lines to the data in Fig. A2, and thickness of the initial soap film for different experiments with ALS droplet of different concentrations.

Table A1: thickness of the soap film calculated from the speed on initial mechanical wave

ALS concentration (M)	**Speed of Mechanical wave (m/s)**	**Thickness of the soap film (µm)**
0.01	*3.73*	*3.4*
0.1	*4.23*	*2.6*
0.2	*3.34*	*4.2*
0.3	*3.49*	*3.9*

References

1. Taylor, G. I., The dynamics of thin sheets of fluid. III. Disintegration of fluid sheets. Proceedings of the Royal Society of London. Series A. Mathematical and Physical Sciences 1959, 253 (1274), 313-321.

2. Murano, M.; Okumura, K., Bursting dynamics of viscous film without circular symmetry: The effect of confinement. Phys. Rev. Fluids 2018, 3 (3), 031601.

3. Müller, F.; Kornek, U.; Stannarius, R., Experimental study of the bursting of inviscid bubbles. Phys. Rev. E 2007, 75 (6), 065302.

4. Savva, N.; Bush, J. W. M., Viscous sheet retraction. Journal of Fluid Mechanics 2009, 626, 211-240.

Appendix (B)

Sample preparation

We investigated the influence of three different parameters on the onset of instabilities: a) molecular weight of the polymer, b) type of the polymer and c) type of the surfactant. In order to study the effect of the molecular weight of the polymer, solutions of PEO with molecular weights of 3×10^5, 2×10^6, and 4×10^6amu were prepared with a series of concentrations for each molecular weight. In the table below the range of concentrations for each molecular weight is shown.

Table B1. Concentrations of PEO samples for different molecular weights of PEO

M_w (amu)	**Concentration (gr/L)**
PEO $3\times\mathbf{10^5}$	4, 6, 7, 8, 10, 30, 40, 50, 60, 70
PEO $2\times\mathbf{10^6}$	4, 6, 7, 8, 10, 12, 14
PEO $4\times\mathbf{10^6}$	1, 2 ,4, 6, 8, 10, 12

We used SDS as a reference surfactant for comparing solutions with the polymers of different molecular weights. solutions of 0.3 M SDS was prepared by adding SDS to Milli-Q water, then the powdered polymer was added slowly to the solution while it was mixed using a magnet stirrer at a very low rotation rate. After initial mixing, solutions were moved to a rotator at low rotating speed for a day to ensure that mixing was homogenous and polymer strands were not broken due to the high shear rates of mixing flows. Then droplets of solutions of PEO-SDS were gently deposited on the soap film of SDS 0.01. In the figure below (Fig. B1) the data for the spreading of different concentrations of PEO of 3×10^5, and 2×10^6 amu is presented (data for spreading of PEO 2×10^6 amu is presented in the article).

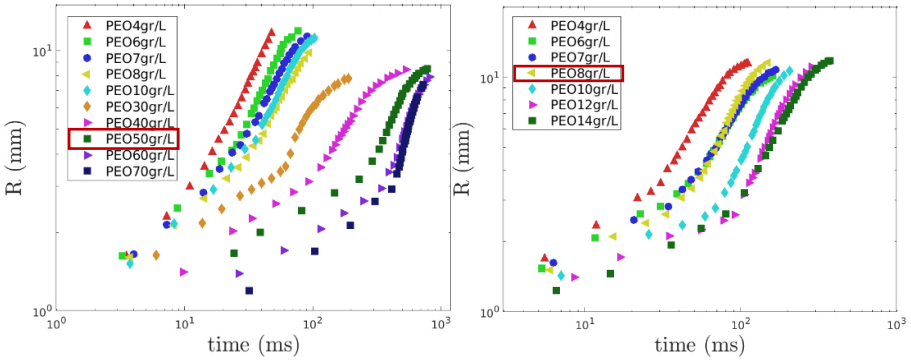

Fig. B1: Radius of the leading edge as a function of time for PEO of 3×10^5 amu (left), and 2×10^6 amu (right). The critical concentration above which the leading front destabilizes is indicated in the legend of the plots with red squares.

Polymer type

To study whether the type of the polymer can play a role in the triggering and evolution of instabilities in the spreading front, we also performed experiments with solutions of polyacrylamide (PAM) of molecular weight of 18×10^6 amu. Solutions with 0.3M SDS and varying concentrations of PAM were prepared (0.5, 1, 2, 3, 5, 10 gr/L). Droplets of PAM-SDS were deposited on a soap film of 0.01M SDS. At low concentrations, smooth spreading was

observed. However, at concentrations of 5 gr/L and higher, the spreading front destabilized into a daisy shape pattern similar to the PEO counterpart. In Fig. B2 radius of the leading edge is reported as a function of time for different concentrations of PAM.

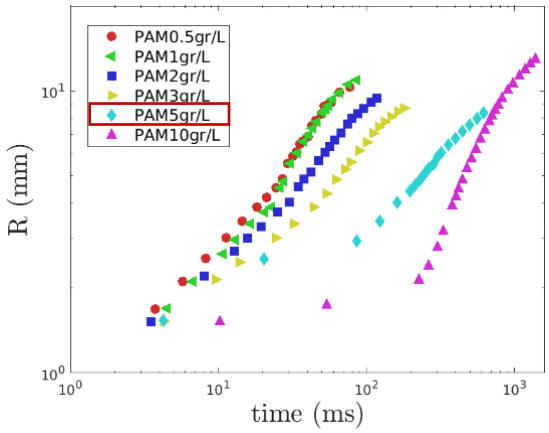

Fig. B2: Radius of the leading edge as a function of time for PAM 18×10^6 amu. The critical concentration above which the leading front destabilizes is indicated in the legend of the plot with

Type of Surfactant

In the figures below (Fig. B3) spreading of solutions with different concentrations of PEO 4×10^6 amu and 0.5 M ammonium lauryl sulphate (right) and 0.008 M dioctyl sulfosuccinate sodium salt (left) is presented. In all cases, the soap film is composed of 0.01 M SDS. Concentration of surfactants in both cases is several times of cmc. Both ammonium lauryl sulphate (ALS) and dioctyl sulfosuccinate sodium salt (AOT) are anionic surfactants. However, their molecular structures are significantly different. Solutions of PEO-ALS were considerably more viscous than the PEO-AOT solution with the same concentration of PEO (viscosities will be discussed in the next section). Instability was observed on the spreading front of PEO-ALS solutions with the concentration of 6 gr/L of PEO and higher. Nevertheless in

PEO-AOT samples, instability was observed only at a concentration of 18 gr/L of PEO and higher.

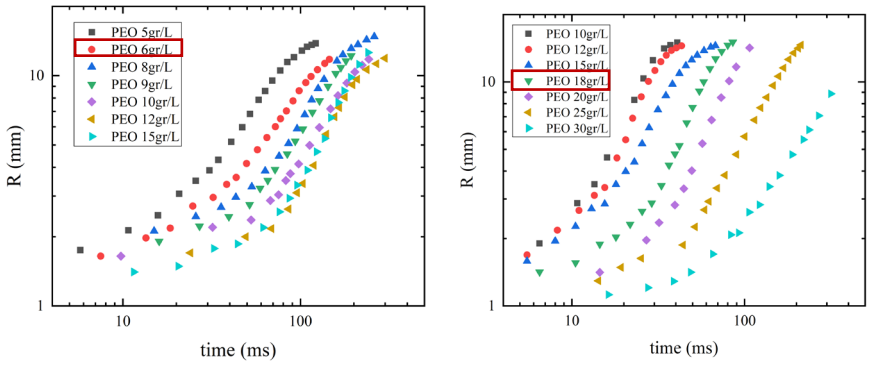

Fig B3: Radius of the leading edge as a function of time for various concentration of PEO 4×10^6 amu and 0.5M ALS(left) and 0.008M AOT (right). The critical concentration above which the leading front destabilizes is indicated in the legend of the plot with red squares.

Growth of the central region

Upon deposition of the droplet on the soap film, due to the lower surface tension of the droplet compared to the soap film, the droplet spreads rapidly. Behind the advancing front, a thin layer of the liquid is formed while the main body of the droplet rests in the centre where the thickness of the droplet is considerably larger. In the previous parts of this work we have studied the dynamics of the advancing front in detail, however, in this section, we look into the growth of the central region which is driven by the capillary pressure. In the series of images on the left side of Fig. B4, the diameter of the central region is depicted with red arrows. The radius of the central region over time was measured for all droplets where the central region could be distinguished from the rest of the spreading front. A power-law function ($R \propto t^{\alpha}$) was fitted to these data points and the resulting values for α are shown in Fig. B4 (right side).

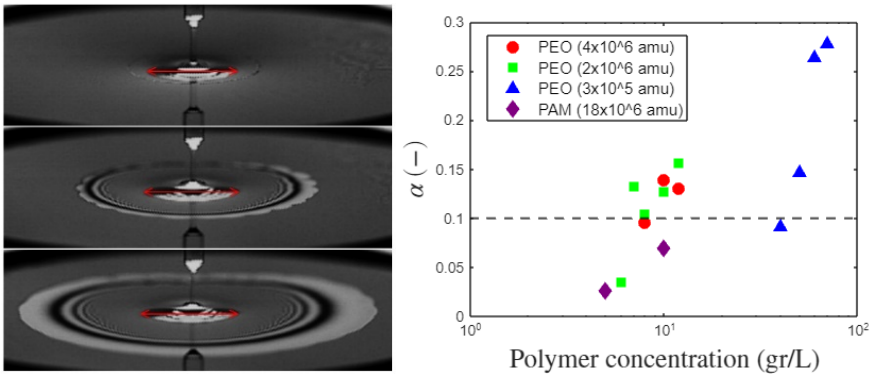

Fig. B4: Left: spreading of a droplet containing 8gr/L PEO (2×10^6 amu) and 0.3M SDS on a 0.01M SDS soap film. The growth of the central region is highlighted with the red arrows. Images from top to down were captured at 62, 87 and 147 ms after droplet deposition, respectively. Right: Power-law exponents for the evolution of R_c over time as function of polymer concentration for various spreading experiments. The dashed line represents Tanner's Law ($\alpha = 0.1$)

Rheological characterization and entanglement concentrations

Here, we investigate whether interactions between surfactant and polymer strands can influence the entanglement concentration of the polymers. Solutions of 0.5M ALS with different concentrations of PEO were prepared to compare with the solutions of AOT with various concentrations of PEO. In Fig. B5, zero shear viscosity as a function of polymer concentration is presented for ALS and AOT solutions.

The change in the slope of the fitted lines indicates a phase transition in the polymeric state of the solution. although the entanglement is considerably influenced by the type of the surfactant, precise correspondence of the entanglement concentration with the onset of instability for PEO-ALS and PEO-ALS proves that the onset of the instabilities depends on the entanglement concentration of the system.

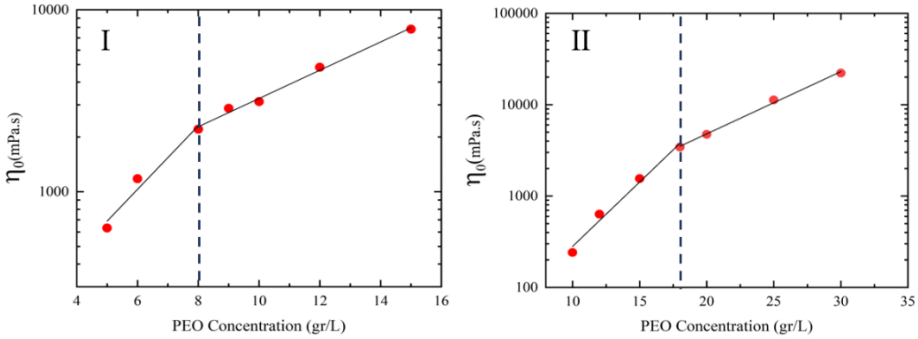

Fig. B5: Zero shear viscosity as function of polymer concentration I) solutions containing 0.5M ALS and various concentrations of PEO 4×10^6 amu. II) solutions containing 8 mM AOT and various concentrations of PEO 4×10^6 amu.

Amplitude sweep test to determine LVE region

Amplitude sweep measurements were performed to determine the range of linear viscoelastic regimes for one low and one high concentration of polymer (1 and 10gr/L respectively) (Fig. B6) . We selected 10% strain for the frequency sweep test as it is well within the LVE region and also for low concentration for polymer, the applied torque is high enough for accurate measurements.

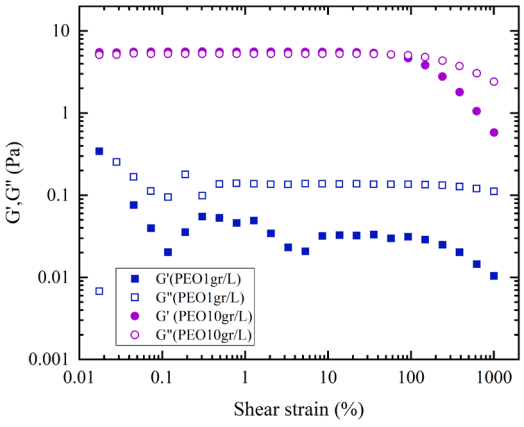

Fig. B6: Amplitude sweep test for two solutions of SDS 0.3 M, one with 1gr/L PEO and the other with 10 gr/L. 10% strain was selected within the linear viscoelastic regime to perform the frequency sweep measurements.

Spreading of ALS solution

Shear viscosity of a solution of 30 w% ALS in water (Sigma Aldrich) was measured within the shear rates of 0.01 to 1000 1/s (Fig. B7, left) it shows a clear shear thinning behaviour. A droplet of ALS solution was deposited on a soap film of 0.01M SDS. Despite the high viscosity and shear-thinning behaviour of the sample, the spreading front remained stable and perfectly circular during the course of spreading (Fig. B7, right).

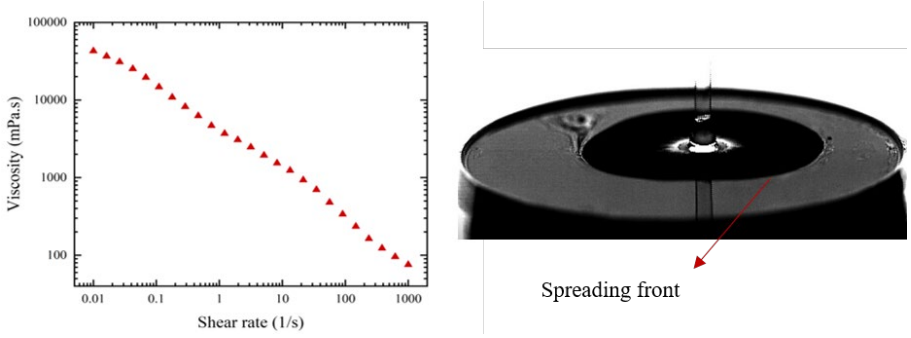

Fig. B7: (Left) shear viscosity of solution of 30 w% ALS in water. Right: image spreading front of ALS solution is depicted once it is deposited on a soap film of 0.01 M SDS.

Addition of microparticles

In order to investigate how large perturbations affect the stability of the spreading front, silica particles with a diameter of 500 μm were added to the mixture of PEO 2gr/L and 0.3M SDS. In the absence of silica particles, PEO-SDS solution spread with a stable front (Fig. B8, left), however, the presence of silica particles disturbed the spreading front and a similar daisy shape pattern emerged at concentrations below the entanglement concentration (Fig. B8, right).

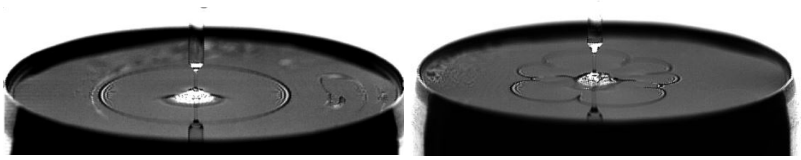

Fig. B8: Left: Stable spreading of PEO-SDS solution (PEO 2gr/L and 0.3M SDS) on a soap film of 0.01 M SDS without glass beads. Right: The same solution with glass beads shows unstable

Dynamic surface tension

Dynamic surface tensions of the solutions were measured using a Kruss bubble pressure surface tensiometer. In the following figure (Fig. SI 9) dynamic surface tension of the solutions containing various concentrations of PEO (4×10^6 amu) and 0.3 M SDS is presented. This method is most accurate for measuring the surface tension of low viscous liquids therefore for the two highest concentrations of PEO where the viscosity of the samples are considerably higher than water the data is less reliable.

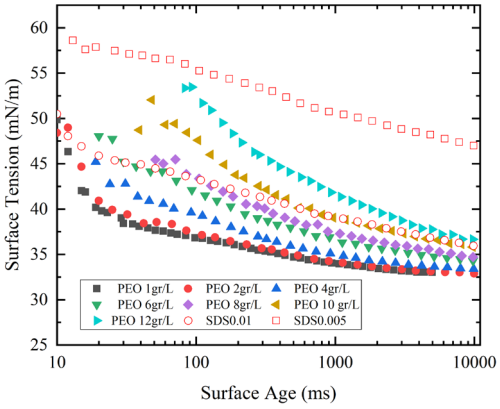

Fig. B9: Dynamic surface tension of the solutions containing 0.3 M SDS and different concentrations of PEO 4×10^6 (solid symbols). The hollow symbols represent dynamic surface tension of 0.01 M and 0.005 SDS which were used to generate soap films for spreading experiments.

Summary

One of the most important fluid dynamics challenges is to understand and model the flow behavior of liquids under complex boundary conditions. How fluids behave in the vicinity of a solid or another fluid surface can significantly influence their flow profile. In particular, spreading of liquids on different substrate can be greatly affected by boundary conditions and the interactions of the fluid with the neighbouring surfaces. When a droplet is deposited on a solid surface, depending on the surface energies of the droplet and the solid surface, it can slowly spread. Droplets of high surface energy, however, form a hemispherical cap with a stationary contact line and a finite contact angle.

Compared to solid surfaces, spreading on the liquid surfaces has exhibited faster dynamics. In this scenario, the viscosity of both liquids and the velocity profile in the viscous boundary layer in both liquids are influential in the spreading process. Furthermore, miscibility or immiscibility, diffusion, depth of the liquid substrate and the geometry of the spreading front can also affect the spreading dynamics. In general, the parameter space in the spreading problem is very broad and in each case based on the boundary conditions and the relevant time scale of the system a particular set of parameters should be taken into account. Many of these parameters are coupled and cannot be addressed separately. This adds to the complexity of the spreading problem and especially, modelling of the spreading liquids, independent of the major influences of the adjacent phases.

In this thesis, we employ a unique configuration of "a droplet on a soap film" to study the spreading behaviour of complex liquids. In this set-up since the droplet is suspended in the air and the contact area between the droplet and the soap film is very limited, the spreading behaviour of liquids can be studied in the absence of a solid or deep liquid boundary. We started our journey with this ambition to understand and model the governing dynamics of spreading of liquids under this boundary condition and even calibrate this set-up as a method to study the spreading behaviour for thin film formation of complex liquids. With 4 experimental chapters presented in this thesis, we succeeded to understand and model the role of some of the major governing parameters.

In **Chapter 1** we first provide a chronology of scientific efforts dedicated to the liquid spreading in the past decades. We discuss the scaling arguments commonly used to describe the dynamics in the spreading problem. Then we lay out our experimental configuration in the perspective of previous studies and explain the advantages and our motivations.

One of the most important forces in the liquid spreading phenomenon is the surface tension gradient. In **Chapter 2** we studied how the surface tension gradient between the droplet and soap film governs the spreading. We used a high-speed camera to record the spreading of the droplets once they are deposited on the soap film. We observed that the radius of the spreading area grew in time according to a power-law function. However, the exponent alpha varied from 0.1, for the cases that the surface tension difference was not favouring the spreading, to approximately 1 for cases that surface tension of the droplet was much smaller than that of the soap film. We also discussed the effect of volume of the droplet and the size of the soap film on the spreading dynamics in this chapter.

In **Chapter 3** we take a close look at the effect of surfactant-surfactant interactions on the spreading behavior of droplets on the soap film. In order to systematically investigate the effect of the molecular structure of the surfactants on the spreading we prepared an ensemble of surfactant solutions with similar macroscopic parameters such as viscosity (all similar to water) and surface tension and we only varied the type of the surfactant. Although

the spreading dynamics generally followed the same trend as we had observed in the previous chapter, there were a few considerable exceptions. We observed that when the surface tension difference between the droplet and the soap film is not significantly high, the effect of the molecular compositions of the surfactants becomes more pronounced. The surface tension difference between the droplet and the soap film in many cases failed to correctly predict the onset of a rapid or a slow spreading regime.

In the next step, we studied the spreading behavior of more complex liquids consisting a mixture of polymer and surfactants in **Chapter 4**. For low concentrations of polymer, we observed a viscous spreading regime. Scaling viscous forces acting along the radius of the droplet with the surface tension gradient resulted in a linear dependency of the radius of the spreading Film on time. Our experimental data showed an excellent agreement with the scaling argument.

However, the addition of polymer to a solution beside increasing the viscosity can induce viscoelastic properties. We observed that when the concentration of polymer in the droplet surpasses the entanglement concentration of the polymers, the spreading front was no longer stable. We showed the enhanced elastic response of the polymeric network above the entanglement concentration triggers the instabilities. We introduced an elasto-capillary length scale based on surface tension and elastic modulus of the solution. The comparison between the growth rate of the elasto-capillary length scale and the length scale of the system predicted perfectly the onset of the instabilities.

Although the instability was observed for various polymer-surfactant solutions, the critical concentration for the onset of the instability dramatically varied for different polymer-surfactant combinations. It indicates that the type of the surfactants and the interactions between surfactant molecules and the polymer strands can significantly influence the viscoelastic properties of the polymer-surfactant solutions. Therefore, in **Chapter 5**, we thoroughly investigated the rheological properties of polymer solutions in the presence of various surfactants. We used multiple rheological approaches to fully characterize the solutions, especially under large deformations. We also

performed tribology tests to study the frictional behavior of such solutions. Polymer-surfactant solutions are widely used as lubricants. During the lubrication process, such solutions are subject to large deformation. Their film formation properties and the stability of their film under large deformations are of great importance to many applications.

Eventually, in **Chapter 6**, we provided an over-view of all the influential parameters on the spreading of a droplet on a soap film that we discussed earlier in this thesis. We showed that there are two main regimes of spreading, namely slow and rapid. The surface tension difference between the droplet and the soap film could roughly predict the onset of each regime. However, there were many exceptions, especially when the surface tension difference was not considerably large. In the rapid spreading regime we observed a range of spreading exponents from 0.2 to approximately 2. The predicted spreading exponent using viscous or inertial scaling was within the range of our experimental exponents. Nevertheless to understand the exceptional behavior of some specific surfactants more investigations are needed.

Acknowledgement

I would like to greatly thank the ones who shared their passion for learning with me, inspired me, mentored me, supported me in the moments of darkness and confusion, celebrated with me the joy of achievements, and kindly helped me to reach to this place that I am now.
I hope one day I can pass the kindness to others.

About the author:

Melika was born on Aug 24, 1990, in Tehran, Iran. From 2008 to 2013, she studied physics for her bachelor's at the Iran university of science and technology (IUST), where she developed a keen interest in experimental soft matter and fluid mechanics.

During her master's studies between 2014 and 2016 at Sharif university of technology (SUT) in Tehran, she became aquatinted with optical trapping and micromanipulation. Her master thesis was dedicated to understanding the viscoelastic behavior of a single red blood cell using optical tweezers.

In December 2017, she moved to the Netherlands to start her PhD at Wageningen University and Research in the laboratory of Physics and Physical Chemistry of Foods. During her PhD, she conducted research on the spreading behavior of complex fluids, using a specific configuration of "droplet on a soap film." The main results of her study are presented in this thesis.

Contact:

Motaghian.Melika@gmail.com

Overview of completed training activities

Discipline specific courses

Rheology Course	FPH, the Netherlands	2018
CMIF summer school on Fluid mechanics	Denmark	2019
European summer school on rheology	KU Leuven, Belgium	2019

Conferences and symposia

Mini-Symposium Rheology	VLAG, the Netherlands	2018
Dutch soft matter day	UvA, the Netherlands	2019
Physics at Veldhoven	NWO, the Netherlands	2019
Physics at Veldhoven	NWO, the Netherlands	2020
Physics of fluids seminar	Twente, the Netherlands	2021
Dutch soft matter day	UvA, the Netherlands	2021
Physics at Veldhoven	NWO, the Netherlands	2021
APS March meeting	Chicago, USA	2022
AERC international conference of rheology	Sevilla, Spain	2022

General courses

Essentials of writing and presentation	WGS, the Netherlands	2019
Brain Friendly Working and Writing	WGS, the Netherlands	2019
Carousel Workshop	WGS, the Netherlands	2019
Adobe Indesign	WUR library, the Netherlands	2020
Scientific artwork, Adobe Illustrator	WUR library, the Netherlands	2020

PhD competence assessment	WGS, the Netherlands	2020
Effective and efficient communication in academia	WGS, the Netherlands	2021
Career Orientation	WGS, the Netherlands	2021
Entrepreneurship in and outside science	WGS, the Netherlands	2021

Other activities

Group meetings	FPH, the Netherlands	2017- 2022

Teaching and supervision

Supervision of 3 master's students	FPH, the Netherlands	2017-2022
Supervision of 2 bachelor's students	FPH, the Netherlands	2017-2022
Teaching assistant for the course of Physical chemistry for food scientists	FPH, the Netherlands	2018-2022

List of publications

This thesis:

Motaghian, Melika, Shirsavar, Reza, Erfanifam, Mehran, Sabouhi, Mahsa, van der Linden, Erik, Stone, Howard A., Bonn, Daniel, and Habibi, Mehdi. 2019. "Rapid Spreading of a Droplet on a Thin Soap Film." Langmuir 35 (46): 14855–60. https://doi.org/10.1021/acs.langmuir.9b02274.

Motaghian, Melika, van Esbroeck, Thiemo, van der Linden, Erik, and Habibi, Mehdi. "Interfacial Instabilities in Marangoni-Driven Spreading of Polymer Solutions on Soap Films." Journal of Colloid and Interface Science 612 (2021): 261–66. https://doi.org/10.1016/j.jcis.2021.12.168

Motaghian, Melika, van der Linden, Erik, and Habibi, Mehdi. "Surfactant-surfactant interactions govern unusual Marangoni spreading on a soap film." Journal of colloids and surfaces A. (Submitted)

Motaghian. Melika, Gimenez-Ribes, Gerard, Ji, Lei, van der Linden, Erik, Scholten, Elke, and Habibi, Mehdi. "Polymer-surfactant mixtures: Rheology and tribology" (Manuscript in preparation)

Other work:

Gimenez-Ribes, Gerard, Motaghian, Melika, van der Linden, Erik, and Habibi, Mehdi. "Crumpled structures as robust disordered mechanical metamaterials." (Manuscript in preparation)

The research described in this thesis has been funded by the Netherlands Organization for Scientific Research through NWO-VIDI grant No. 680-47-548/983.

The financial support from Wageningen University for printing this thesis is gratefully acknowledged.

Cover design and layout by Melika Motaghian and Iliana Boshoven-Gkini.

Printed by Proefschriftmaken.nl